THE UNIVERSITY OF CHICAGO

TOUCH SPANNING SPATIAL SCALES:

TEXTURE CODING ALONG THE SOMATOSENSORY NEURAXIS

A DISSERTATION SUBMITTED TO

THE FACULTY OF THE DIVISION OF THE BIOLOGICAL SCIENCES

AND THE PRITZKER SCHOOL OF MEDICINE

IN CANDIDACY FOR THE DEGREE OF

DOCTOR OF PHILOSOPHY

INTERDISCIPLINARY SCIENTIST TRAINING PROGRAM:

COMPUTATIONAL NEUROSCIENCE

BY

KATIE LONG

CHICAGO, ILLINOIS

AUGUST 2021

TABLE OF CONTENTS

TABLE OF FIGURES

TABLE OF SUPPLEMENTARY FIGURES

TABLE OF TABLES

ACKNOWLEDGMENTS

Bensmaia Lab members:

Sliman Bensmaia, without whom none of this would be possible.
Benoit Delhaye
Ashley van Driesche
James Goodman
Charles Greenspon
Justin Lieber
Aneesha Suresh Sahu
Jeremy Winberry

Thesis Committee:

Wim van Drongelen
Leah A Krubitzer
John HR Maunsell

Family:

Mom, for emphasizing the value of discipline, and for teaching me to push through every barrier.
Dad, for always encouraging curiosity and instilling in me an unshakable sense of wonder.
Jon, for being my role model and a consistent source of laughter and perspective.
And Michael, my husband and best friend, for celebrating every victory and helping me through every challenge. You are forever my inspiration and oasis. Love is both.

ABSTRACT

We are exquisitely sensitive to textures: our sense of touch provides us with a sensitivity that spans six orders in magnitude in spatial scale, from tens of nanometers to tens of millimeters. Here, we characterize neural representations of texture across the somatosensory neuraxis, from responses in the peripheral nerve and early stages of cortical processing, up through higher-order areas of cortex whose responses to natural texture have never before been evaluated. We monitor single-unit activity of peripheral afferents and cortical neurons in the macaque, and we relate these neural patterns of activity to perceptual features of texture evaluated by human subjects. This allows us to assess how the neural coding of texture is maintained and transformed across multiple stages of processing, as well as how it gives rise to our perceptual experience of texture.

The first major focus of this work was to evaluate the role of precise temporal patterning of texture responses in somatosensory cortex. We find that finely timed patterns of activity, on the order of just a few milliseconds, are highly informative about texture. Individual cells vary in their temporal precision, and this heterogeneity can be explained, at least in part, by the inputs a cell receives: those cells that receive temporally precise inputs (from Pacinian-corpuscle associated peripheral afferents) are, themselves, temporally precise. Finally, while identifying a role for precise timing in perception had been elusive, we find that a combination of rate and timing is best for predicting the perceptual features of texture.

The second focus of this work was to characterize natural texture representations in higher-order somatosensory cortex, including secondary somatosensory cortex (S2) and the

parietal ventral area (PV). We find that cells in S2/PV convey information about texture, but this representation is sparser, higher-dimensional, and less driven by a shared response to low-level features. Furthermore, we find a portion of cells that are modulated by the behavioral task. Some cells are sensitive to trial type (same vs different), and other cells' activity correlates with the animal's decision, regardless of the actual trial type. Altogether, these findings provide for a more holistic view of texture coding and how it evolves across various stages of cortical processing in the somatosensory neuraxis.

CHAPTER 1 | NEURAL BASIS OF TOUCH AND PROPRIOCEPTION IN PRIMATE CORTEX[1]

The sense of proprioception allows us to keep track of our limb posture and movements and the sense of touch provides us with information about objects with which we come into contact. In both senses, mechanoreceptors convert the deformation of tissues - skin, muscles, tendons, ligaments, or joints – into neural signals. Tactile and proprioceptive signals are then relayed by the peripheral nerves to the central nervous system, where they are processed to give rise to percepts of objects and of the state of our body. In this review, we first examine briefly the receptors that mediate touch and proprioception, their associated nerve fibers, and pathways they follow to the cerebral cortex. We then provide an overview of the different cortical areas that process tactile and proprioceptive information. Next, we discuss how various features of objects – their shape, motion, and texture, e.g. – are encoded in the various cortical fields, and the susceptibility of these neural codes to attention and other forms of higher-order modulation. Finally, we summarize recent efforts to restore the senses of touch and proprioception by electrically stimulating somatosensory cortex.

1.1 | INTRODUCTION

How do we distinguish our body from the rest of the world? How do we keep track of its posture and movements? How do we sense objects or other organisms that we come into contact with? These abilities rely on somatosensation, a collection of senses that convey information about the state of the body and its physical interactions with the environment. Here, we examine in detail

[1] This chapter is published: Delhaye BP, Long KH, Bensmaia SJ (2018) Neural Basis of Touch and Proprioception in Primate Cortex. *Compr Physiol* 8:1575-1602 and is available at https://doi.org/10.1002/cphy.c170033

two of these senses: Proprioception – the sense of the posture and movements of our body in space – and touch – the sense originating from our skin when we make contact with objects, with a specific focus on the hands. Proprioception and touch are critical for our ability to plan and execute movements and manipulate objects. Indeed, the elimination of proprioception results in severe movement deficits (3 25), and the elimination of touch severely impairs our ability to grasp and manipulate objects (8, 184, 386). The sense of touch is also critical to our sense of embodiment: in fact, an extracorporeal device, like a robotic arm, can be made to feel like part of our body if it is endowed with a sense of touch (236). Moreover, touch plays a key role in emotional communication (153): we touch the people we love, and the absence of normal affective touch in childhood has devastating consequences on emotional development (147, 148, 379). Touch is also essential to sexual function, as evidenced by the severe sexual dysfunction that follows sensory loss in erogenous zones (121, 263, 318).

Touch and proprioception rely on a variety of different mechanoreceptors embedded in the skin, muscles, tendons, joints, and ligaments. These receptors are activated any time the skin is deformed or the limb moves. Primary afferents carry signals from these receptors to the spinal cord, brain stem, and ultimately to the neocortex, where information about contacted objects and about the state of the limb is elaborated. Here, we first provide a brief overview of the receptors that mediate touch and proprioception and of the nerve fibers that innervate these receptors. We then summarize the various pathways that carry somatosensory information to the central nervous system. Finally, we discuss the processing of tactile and proprioceptive

information in the somatosensory cortex of primates, focusing on work conducted over the last 30 years (intended to complement ref. (250), which covers earlier findings in greater detail).

1.2 | THE SOMATOSENSORY PERIPHERY

The senses of touch and proprioception involve mechanotransduction, the conversion of mechanical deformations of tissues (skin, muscles, tendons, ligaments) into neural signals. Cutaneous mechanoreceptors (from cutis, latin for skin), located in the skin, signal contact with objects. Proprioceptors (from proprius, latin for one's own) – located in the muscles, tendons, and ligaments (but also in the skin) – convey information about the position and movement of the limbs and about the forces they exert. The different types of receptors are innervated by nerve fibers or afferents that carry tactile and proprioceptive signals to the brain. Most tactile and proprioceptive fibers are large and myelinated, and thus exhibit high conduction velocities (60-100m/s for Group I proprioceptive fibers and 30-80m/s for Aβ tactile fibers and Group II proprioceptive fibers) with one exception, C-tactile fibers (see affective touch section below). Different types of cutaneous mechanoreceptors and proprioceptors respond in different ways to mechanical deformations, and therefore convey complementary information about the state of the limbs or about contacted objects. Signals from these different receptors are integrated to yield a rich neural image of the state of our bodies and of our immediate surroundings.

The following section briefly describes the neural basis of touch and proprioception at the somatosensory periphery to help frame the subsequent sections on central processing. For more detailed and complete reviews of the structure, physiology, and function of mechanoreceptors and their associated neurites, see refs (73, 184, 189, 370).

1.2.1 | CUTANEOUS INNERVATION OF THE HAND

Cutaneous mechanoreceptors, which convert skin deformations into electrical signals, are located in the skin throughout the body, but their density differs across body regions. In primates, the hands and lips contain the highest densities of mechanoreceptors, the legs and back the lowest. Approximately 17,000 afferents innervate the human hand, with densities peaking around 240 units/cm^2 at the fingertips (187).

1.2.2 | GLABROUS SKIN

The cutaneous afferents of the glabrous skin are categorized into four classes, each exhibiting different response properties (Figure 1.1). These four classes can be split into two categories according to their responses to skin indentations: slowly adapting afferents produce a sustained response to a static indentation of the skin, one that declines (adapts) slowly over time, whereas rapidly adapting afferents respond only at the onset and offset of the indentation. These classes can also be distinguished based on the size of their receptive fields (RFs): mechanoreceptors innervated by type I afferents lie close to the surface of the skin and have small and clearly defined RFs, whereas mechanoreceptors innervated by type II afferents are deeper in the skin and have large RFs with ill-defined boundaries. The four different classes of afferents innervate different types of mechanoreceptors.

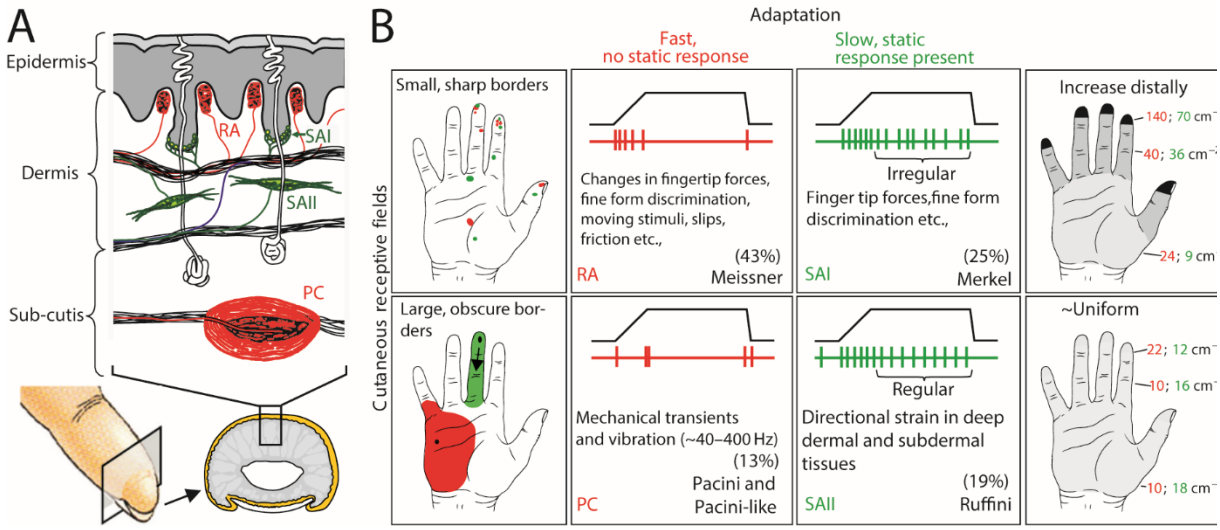

Figure 1.1. The four classes of cutaneous afferents of the glabrous skin. Al Morphology of the different mechanoreceptors and their respective locations in the skin. Bl Adaptation properties and receptive field (RF) size of the four classes of cutaneous afferents. Rapidly adapting (sometimes referred to as fast adapting, particularly for humans) vs. slowly adapting refers to responses to indentations (transient vs. sustained, respectively). Type I vs. type II refers to the size of the RFs, determined in part by the depth of the mechanoreceptors in the skin: Type I fibers have small RFs whereas type II fibers have large ones. The density of innervation depends on the fiber type: Type I fibers innervate the skin more densely than do type II fibers. For example, rapidly adapting afferent type II (PC) afferents show rapidly adapting responses with large RFs and relatively low innervation density (type II). Adapted from (183).

While all afferents respond to most contact events, different afferent fibers exhibit different response properties, conferred to them by the mechanoreceptors they innervate. Single afferents, and even single classes of afferents, convey ambiguous information, and signals from the different afferent populations are integrated to give rise to tactile percepts of objects (322, 380).

SLOWLY ADAPTING TYPE I (SA1) AFFERENTS

SA1 fibers, which constitute about 25% of all tactile fibers that innervate the hand, split into multiple branches near the skin surface to impinge upon multiple clusters of Merkel receptors (258), distributed over different fingerprint ridges; this branching results in RFs with multiple "hot spots," each corresponding to an individual cluster, spanning an average of 10 mm^2 (47, 182, 188, 293). Most Merkel cell clusters are found at the base of dermal papillae close to sweat ducts (Figure 1.1A). In response to a skin indentation, SA1 fibers produce a sustained response which slowly decreases over time, a property to which they owe their appellation (Figure 1.1B) (211). SA1 fibers are most sensitive to static indentations (374) and to slow skin deformations (112, 253), responding to a combination of absolute skin displacement and rate of displacement (211). SA1 fibers respond preferentially to local spatial discontinuities of a stimulus (185, 282) and convey, as a population, a neural image of spatially patterned skin indentations (282), with a peak spatial resolution (at the fingertips) of about 1 mm.

RAPIDLY ADAPTING TYPE I (RA) AFFERENTS

RA fibers account for around 40% of all tactile fibers innervating the hand. Each RA fiber innervates multiple Meissner corpuscles (and Meissner corpuscles are typically innervated by more than one fiber) (46, 48, 265), which results in complex RFs whose size is similar to that of SA1 fibers. Meissner corpuscles are regularly distributed at the apex of dermal papillae (Figure 1.1A). RA afferents respond to dynamic skin deformation at intermediate frequencies (5-50Hz) (112, 186, 253), are silent when the skin is not moving (210), and produce a characteristic off response when a skin indentation is removed (Figure 1.1B). Similarly to their SA1 counterparts,

RA fibers convey a spatial image of indented patterns, but this image tends to be more poorly defined (281).

SLOWLY ADAPTING TYPE II (SA2) AFFERENTS

SA2 fibers, which account for about 20% of the tactile fibers from the hand, are thought to each innervate an individual Ruffini corpuscle but have large RFs (with a mean of 50 mm^2), presumably due to the depth of the mechanoreceptor in the skin. SA2 fibers primarily respond to tension and stretch in skin and sub-cutaneous tissues (211). SA2 units densely innervate the skin around the nails, an arrangement that is well suited to convey information about forces applied on and by the fingertips (20).

RAPIDLY ADAPTING TYPE II (PC OR RA2) AFFERENTS

PC fibers, which account for about 15% of tactile fibers from the hand, each innervate a single Pacinian corpuscle, hence their name, and have large RFs due to the depth of the corpuscle in the skin and its high sensitivity to mechanical deformations propagating across the skin. The characteristic onion-like structure of the corpuscle confers to the fiber an exquisite sensitivity to rapid transients (9) and submicron-scale vibrations at high frequencies (40-400Hz) (112, 186, 253). PC fibers respond strongly to textured surfaces scanned across the skin (380) and to vibrations transmitted through objects held in the hand (27).

1.2.3 | HAIRY SKIN

The four afferent types described above are also found in the hairy skin (at lower densities). However, afferents having RA-I type response, called "field units", have larger receptive fields and have not been associated with Meissner corpuscles (372). Other types of hair follicle afferents

signal deformations of hairs with rapidly adapting responses, often with large receptive fields that include at least twenty hairs (372). Also present are C-tactile fibers (371), which are thought to play a role in affective touch (see affective touch section below) (1, 229). Cutaneous afferents that innervate the hairy skin, particularly those with RFs over or near joints (for instance those on the dorsal surface of the hand), are sensitive to skin stretch (92, 94) and may also contribute to proprioception (93).

1.2.4 | Sensory innervation of muscles and joints

Proprioceptive afferents – sometimes referred to as "deep" afferents – respond to deep palpation of the muscles and to joint movements, but not to light touch, and can be divided into three groups: muscle spindle afferents, Golgi tendon organs (GTOs), and joint receptors. These afferents can further be divided according to the size of their axons into type I and type II fibers: type I fibers are larger and therefore conduct signals faster than type II fibers.

Primary and secondary spindle afferents

Primary and secondary spindle afferents (also known as type Ia and type II fibers, respectively) innervate the muscle spindles, which consist of a bundle of intrafusal muscle fibers contained within a spindle-shaped capsule and are innervated by one type Ia afferent and a few type II afferents (160). Afferents branch when entering the spindle and each innervate several fibers. Each afferent innervates a combination of intrafusal fibers in the spindles (nuclear bag 1 and 2, nuclear chain fiber), and the different combinations lead to different response properties. The responses of spindle fibers to passive movements depend on both the length of the muscle and the rate at which length changes. Primary spindle fibers are more sensitive to the dynamic

components (rate of length change) than are secondary spindle fibers (58, 95) (Figure 1.2A). Importantly, muscle spindles are also innervated by gamma motor fibers that can contract intrafusal fibers thereby tuning the sensitivity of spindle afferents. The response properties of spindle afferents during active movements are therefore more complex (compared to the passive case) and poorly understood (83, 84).

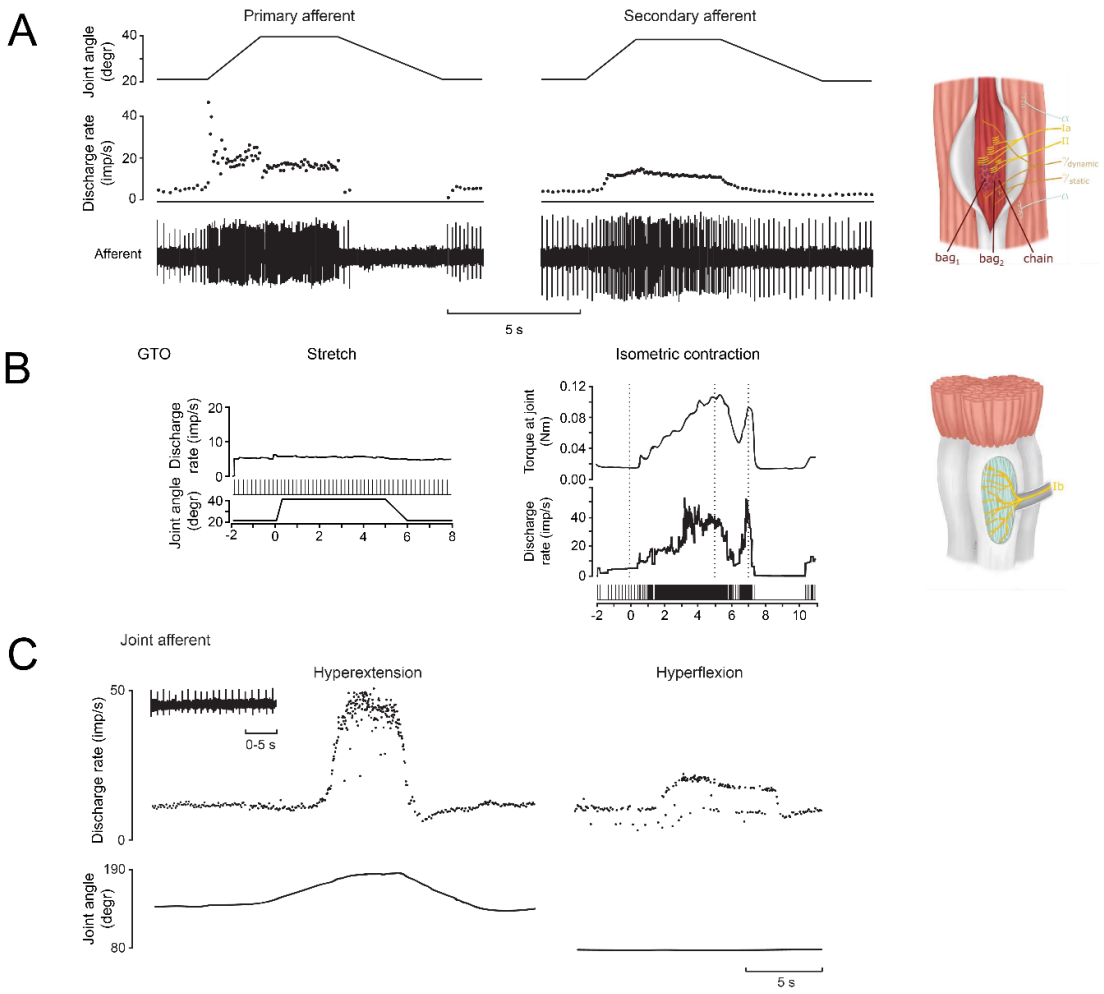

Figure 1.2. Typical responses of proprioceptive afferents. Al Responses of a primary (left) and secondary (right) spindle afferent from the finger extensors muscles to passive ramp and hold stretches applied to the metacarpophalangeal (MCP) joint. Primary afferents tend to be more sensitive to changes in length than secondary ones. Adapted from (95). Bl Golgi Tendon Organ (GTO) do not respond to passive ramp and hold stretches (left) but respond robustly to isometric contraction (right). Adapted from (96). Cl Responses of a joint afferent associated with the proximal interphalangeal joint of the index finger during passive manipulations. Joint receptors tend to only respond at the extrema of joint movements, perhaps to signal the threat of injury. Adapted from (30).

GOLGI TENDON ORGAN AFFERENTS

GTOs (also known as type Ib fibers) innervate thin capsules that envelop collagenous fascicles at the muscle-tendon junctions. GTO afferents are exquisitely sensitive to tension on the tendon and respond vigorously during isometric contractions (Figure 1.2B). They also show some sensitivity to muscle stretch, most likely because muscle stretch results in small level of tension in the tendons (95, 96, 238).

JOINT RECEPTOR AFFERENTS

As their name indicates, these fibers innervate receptors located in the joint capsules, but also nearby ligaments. Joint receptor afferents are not sensitive to cutaneous or muscle stimulation, but respond to moderate pressure applied directly over the joint, to joint movements, and to contraction of muscles inserting into the capsule (145). Three types of receptors are found in the joints: Ruffini-like corpuscles, Pacinian-like corpuscles, and Golgi organs located in the ligaments (396). Most joint afferents exhibit slowly adapting responses when the joint is near one of its extrema – hyperflexion and hyperextension (30, 145) – suggesting that these fibers play a limited role in proprioception under most circumstances and are involved primarily in signaling the potential for joint damage (Figure 1.2B).

1.3 | SOMATOSENSORY PATHWAYS

Afferents that innervate nearby receptors bundle into fascicles that successively join other fascicles to ultimately unite into nerves, together with efferent (motor) fibers (Figure 1.3). Three nerves innervate the hands: the median and ulnar nerves innervate the palmar side of the hand and arm, and the radial nerve innervates the dorsal side of the hand and arm. As it approaches

the vertebral column, the nerve segregates into dorsal and ventral roots, with the former carrying sensory fibers and the latter motor ones. The cell bodies of the sensory neurons are located in the dorsal root ganglia (DRG).

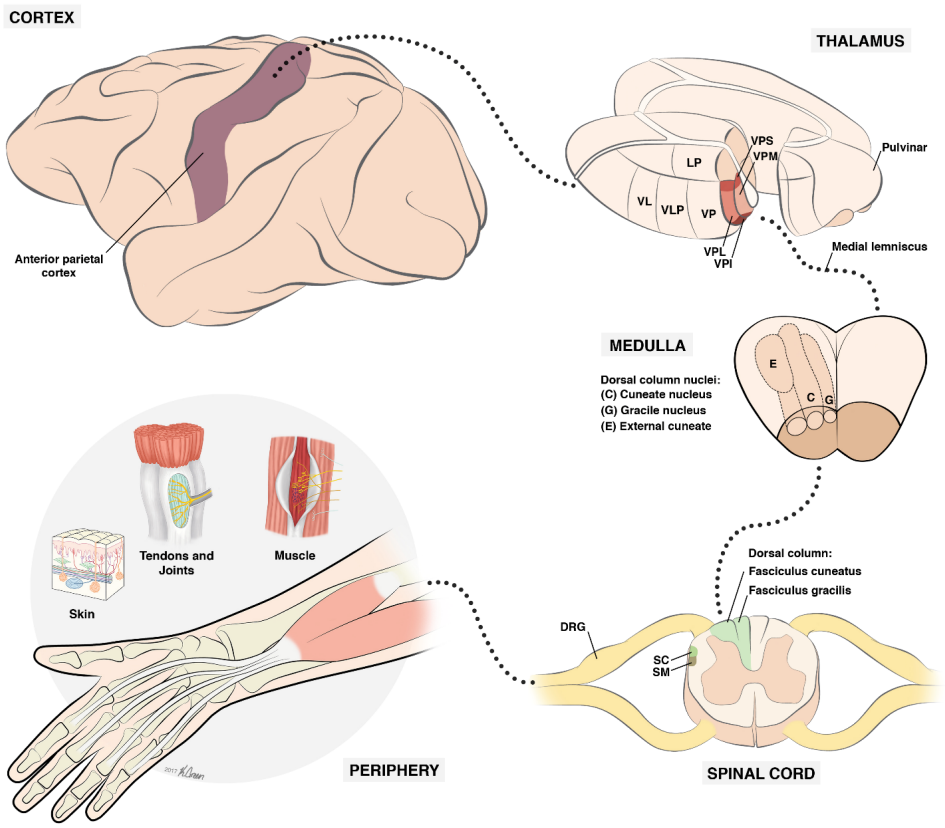

Figure 1.3. Pathways from somatosensory periphery to cortex. Afferent fibers at the periphery bundle in fascicles that join to form the nerves. Afferent cell bodies are gathered in the dorsal root ganglia (DRG). When entering the spinal cord through the dorsal root, afferent axons branch, sending one projection to the dorsal horn and one projection to the dorsal column nuclei (DCN) through the dorsal column. The DCN projects contralaterally through the medial lemniscus to the ventroposterior complex of the thalamus, which in turns relays the information to cortex. Abbreviations: dorsal root ganglion (DRG); spinomedullothalamic (SM) and spinocervicothalamic (SC) tracts. Thalamus: ventral posterior (VP), posterolateral (VPL), posteromedial (VPM), posterior inferior (VPI) and posterior superior (VPS) nuclei, posterior division (VLp) of the ventral lateral nucleus (VL), lateral posterior nucleus (LP).

1.3.1 | SPINAL CORD: DORSAL COLUMN

Axons of afferent fibers in the DRG terminate in several different locations. First, they can project directly onto alpha motor neurons or interneurons at the same level of the spinal cord. Second, they can ascend or descend and project onto either interneurons or alpha motor neurons at nearby levels of the spinal cord. Finally, they can ascend (forming the dorsal column tract) and synapse onto neurons in the dorsal column nuclei (DCN) of the brainstem. Some second order neurons in the spinal cord follow the same tract to the DCN in the medulla while others follow the dorso-lateral tracts (spinomedullothalamic and spinocervicothalamic tracts, see Figure 1.3, Spinal Cord) to reach the same complex. Within the dorsal columns, fibers are grossly organized somatotopically (339); that is, afferents that innervate adjacent parts of the body tend to be near one another, thereby forming a structured map of the body, with the lower body located medially and the upper body located laterally. However, recent findings in multiple mammalian species, including monkeys and humans, suggest that the main organizing principle in the dorsal column is modality: cutaneous fibers tend to cluster medially while deep neurons are found mostly laterally (264). Somatotopy is therefore a secondary organization principle, within modality. The dorsal columns contain all of the inputs that ultimately activate primary somatosensory cortex (S1) as evidenced by the abolition of S1 activation following complete lesions of the dorsal columns (177, 234).

1.3.2 | MEDULLA: DORSAL COLUMN NUCLEI (DCN)

The dorsal column nuclei (DCN) comprise three nuclei, which mainly receive input from first order neurons. Signals from the upper body project to the cuneate and external cuneate nuclei and

signals from the lower body to the gracile nucleus (Figure 1.3, Medulla). Note that the mechanoreceptive fibers from the head and face are supplied by the trigeminal nerve to the principal division of the trigeminal nucleus. The cuneate nucleus receives input primarily from cutaneous afferents while the external cuneate nucleus receives primarily proprioceptive or deep input (91, 122, 161). The DCN are somatotopically organized proceeding from the lower limb to the head along the mediolateral axis (388, 389). Response properties of neurons in the DCN seem to be very similar to those of their afferent inputs, but most studies have been carried out in cats and careful characterization in primate is lacking. The DCN also receive descending input from sensorimotor cortices (17, 54) which may modulate sensory signals before they are relayed to higher processing structures. The projection neurons of the DCN send axons contralaterally to the ventroposterior complex of the thalamus (298), forming the medial lemniscal pathway. The external cuneate also projects to the cerebellum (307). The DCN have long been thought to be relay stations for somatosensory signals, simply transmitting sensory information without processing it. However, recent work reveals that individual neurons in cuneate are dominated by the input of a few afferents (4 to 8) and may carry out some degree of feature extraction (10, 150, 196), but most of this work has been carried out in cats. Not much is known about the response properties of DCN neurons in primates except that they relay sensory information with high temporal fidelity (385). Recent advances in chronic implants will likely lead to insights about neural coding in the DCN (305, 351).

1.3.3 | Thalamus: Ventro-posterior complex

The somatosensory thalamus receives inputs from the contralateral dorsal column nuclei via the medial lemniscal pathway (and the trigeminal lemniscus). The ventroposterior complex has been subdivided into three major regions, the ventroposterior nucleus (VP, also known as the ventrocaudalis region, or Vc, in humans, see Figure 1.3, Thalamus), the ventroposterior superior nucleus (VPS), and the ventroposterior inferior nucleus (VPI) (217). VP is further subdivided into a lateral compartment (VPL) and a medial compartment (VPM). Different parts of the ventroposterior complex receive different sensory inputs: VPL receives cutaneous inputs from the DCN and VPM from the trigeminal nucleus; VPS receives input from proprioceptive fibers; VPI receives major input from the spinothalamic tract and is associated with thermoreception and nociception (6, 67, 204, 225). Each of three main divisions of the ventroposterior complex (VP, VPS and VPI) is somatotopically organized and contains a complete map of the contralateral body (270). This organization is also reflected in the cytoarchitecture of these structures: single digit representations are separated by cell-poor septa (294). The response properties of somatosensory neurons in the thalamus have been described as similar to those of primary afferent fibers, suggesting that there is little processing of sensory information before cortex, but this assertion is based on scant evidence. Finally, neurons in the thalamus do not seem to be modulated by attention or cognitive tasks in contrast to their counterparts in the somatosensory cortices (40, 41, 51, 373).

Thalamic projections to cortex are highly divergent and convergent (71, 193, 270): while the bulk of VP neurons project to areas 3b and 1, they also sparsely project to areas 3a, 2, and 5 (115, 192, 195, 270). Thalamic projections have different layer targets in different areas: projections in

areas 3a and 3b reach layer 4 and deep part of layer 3 while projection to area 1 and 2 reach layer 3 (192). The most anterior part of VPL, VLp (also termed VPLo previously), relays deep inputs to area 3a (270). The bulk of VPS neurons project densely to areas 2 and 5 and less so to areas 3a, 3b, and 1. Individual thalamic neurons can sometimes branch over distributed regions of the anterior parietal cortex, sometimes spanning multiple cortical fields (133, 270).

1.4 | CORTEX

The principal cortical recipient of tactile and proprioceptive signals from the periphery is the anterior parietal cortex (APC) – often referred to as primary somatosensory cortex – located along the anterior border of the parietal lobe (Figure 1.4A). APC comprises four cytoarchitectonically defined areas – Brodmann's areas 3a, 3b, 1 and 2 – only one of which can be considered primary somatosensory cortex proper based on the prominence and laminar targeting of its thalamocortical input, namely area 3b (197, 212). Areas 1 and 2 are generally considered to be higher cortical areas as evidenced by larger RFs and more complex response properties (104, 169, 218, 269). APC, in turn, sends projections along two parallel streams (Figure 1.5), which have drawn analogies to the ventral and dorsal streams described for the visual system (123, 246). The ventral stream, in the lateral parietal cortex (LPC), includes the secondary somatosensory cortex (S2) and the parietal ventral area (PV), where neurons have even larger RFs and more complex response properties than do their counterparts in APC. This somatosensory pathway is linked to higher level feature extraction (106) and to cognitive functions such as attention and decision-making (181, 218, 245, 312). The dorsal stream in the posterior parietal cortex (PPC) includes areas 5 and 7, where neurons have large and often bilateral RFs (223, 326,

333), and is more tightly linked to motor behavior, such as reach and grasp (5, 109, 123, 138, 180, 254).

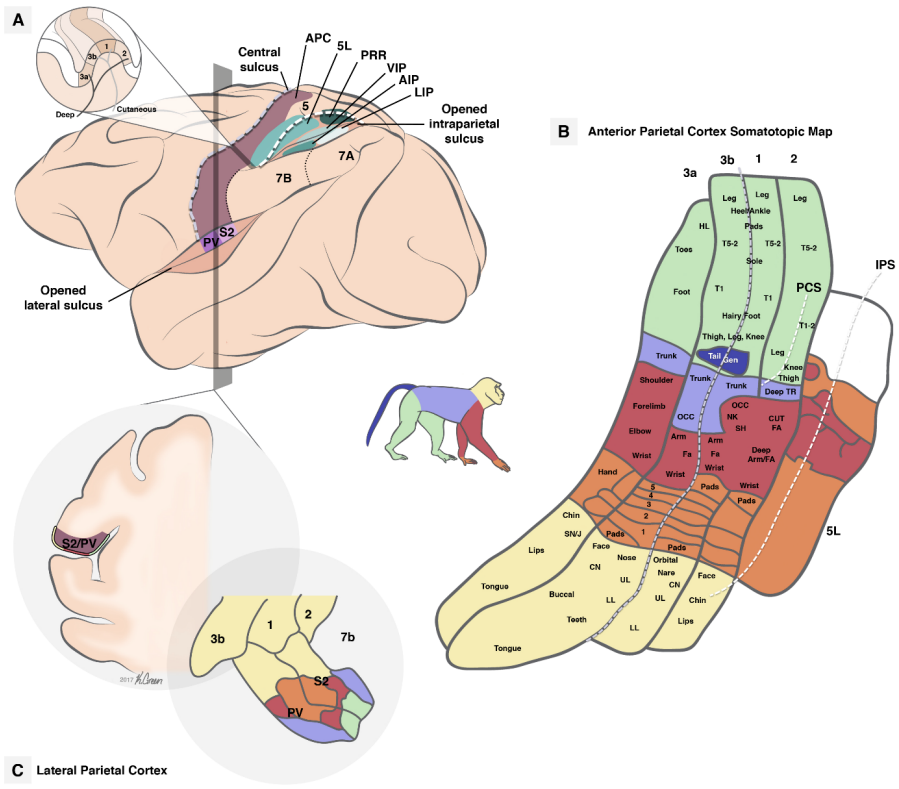

Figure 1.4. Organization of somatosensory cortical areas. Al A lateral view of the brain showing the different somatosensory areas in macaque monkey cortex (Adapted from (198)). Inset: Horizontal section of the postcentral gyrus at the level of the hand representation, showing the position of the different APC modules relative to the central and the intraparietal sulci. Bl Detailed view of the somatotopic representation of the body in the four fields of APC (areas 3a, 3b, 1 and 2) and in area 5L (Adapted from (262, 333)). Cl Coronal section showing the location of LPC in the lateral sulcus (Adapted from (214)). Abbreviations: Anterior parietal cortex (APC); second somatosensory area (S2); parietal ventral area (PV); parietal reaching region (PRR); anterior (AIP), ventral (VIP) and lateral (LIP) intraparietal areas; post central sulcus (PCS); intraparietal sulcus (IPS). Somatotopic map: Upper lip (UL); lower lip (LL); chin (CN); snout/jaw (SN/J); digits of the hand (1-5); (cutaneous) forearm ((CUT) FA); occiput (OCC); trunk (TR); toes (T1-5); hindlimb (HL).

The hierarchical organization of somatosensory cortex draws strong parallels with that observed in other sensory modalities and is supported by several lines of evidence. First, lesions in early somatosensory areas abolish or nearly abolish activation of higher areas, but the reverse is not true (130, 285). Second, responses begin later (36) and last longer (256) as one ascends the somatosensory neuraxis. Third, as further described below, the size of RFs increases and response properties become increasingly complex and selective. That is, neurons in the early stages of processing respond to most stimuli impinging upon their RFs whereas neurons downstream respond only when a preferred feature is present in their RFs. Finally, while the APC and LPC of mammals receive parallel projections from the VP nucleus of the thalamus (90, 131, 317), LPC receive only very sparse input from VP in monkeys and other higher primates (VPL or VPM, not VPI) (116, 216). These four lines of evidence all point to a hierarchical structure in somatosensory cortex with APC as an earlier stage of processing than LPC.

In the next section, we describe the overall organization and structure of the somatosensory areas, beginning with APC. Then, we describe higher cortical areas, first the ventral stream (lateral parietal cortex) then the dorsal one (posterior parietal cortex). Next, we present in more detail the neural computations performed in APC and LPC along several stimulus continua that have been extensively studied. Most of the referenced studies involve single-unit or multi-unit recordings in macaque monkeys, but recent imaging studies carried out in humans confirm many findings from the animal work and are highlighted when helpful.

1.4.1 | ANTERIOR PARIETAL CORTEX (APC)

The anterior parietal cortex consists of four distinct cortical fields that form parallel bands along the central sulcus: areas 3a, 3b, 1 and 2 (199). A major feature of APC is its somatotopic organization: nearby APC neurons respond to stimulation of nearby and partially overlapping patches of skin on the body or to nearby combinations of joints (Figure 1.4B). As a result, APC comprises four complete maps of the contralateral side of the body – one in each area – with the foot representations near the midline and the face and tongue representations at the lateral end. Body regions that are more densely innervated (such as the fingers and the lips) occupy more cortical area than do less innervated regions (such as the proximal arms or the back), a phenomenon referred to as cortical magnification (348). At the same time, RF size is inversely proportional to neural magnification: for example, neurons with RFs on fingers have much smaller RFs than do neurons with RFs on the back (348).

The body maps in each area of APC are organized systematically with respect to one another (see Figure 1.4B). That is, the representation of each body part in each area is approximately aligned along central sulcus and the organization along the axis perpendicular to the sulcus is also predictable and systematic. For instance, proceeding caudally along the axis orthogonal to the central sulcus, RFs in area 3b shift from the digit tips, down the digits, to the palm, and there the transition with area 1 occurs. In turn, RFs in area 1 shift back towards the fingertips as one continues to proceed caudally to area 2. The RFs of area 2 then shift back from the fingertips down the finger as one maintains course (284). The somatotopy in area 2 is cruder than that in areas 3b and 1 (170).

The four APC areas are also histologically distinct, differing in laminar morphology and overall cell density (197). Within each area, sub-regions representing different parts of the body are also histologically distinguishable: Subdivisions of area 3b related to different body parts form myelin-dense ovals separated by myelin-light septa (178). The representations of individual digits, and even of individual fingerpads, are isolated from each other by cell-poor septa (295). These histologically observed boundaries appear to be immutable even after de-afferentation (179). While the general organization of APC is consistent across individuals, the precise locations of the boundaries between areas along the rostral-caudal axis are not (159, 331). Recent studies in humans corroborate findings in primates (23, 135, 136).

The following sections describe the major patterns of connections between areas (summarized in Figure 1.5). Note, however, that other relatively sparse connections exist.

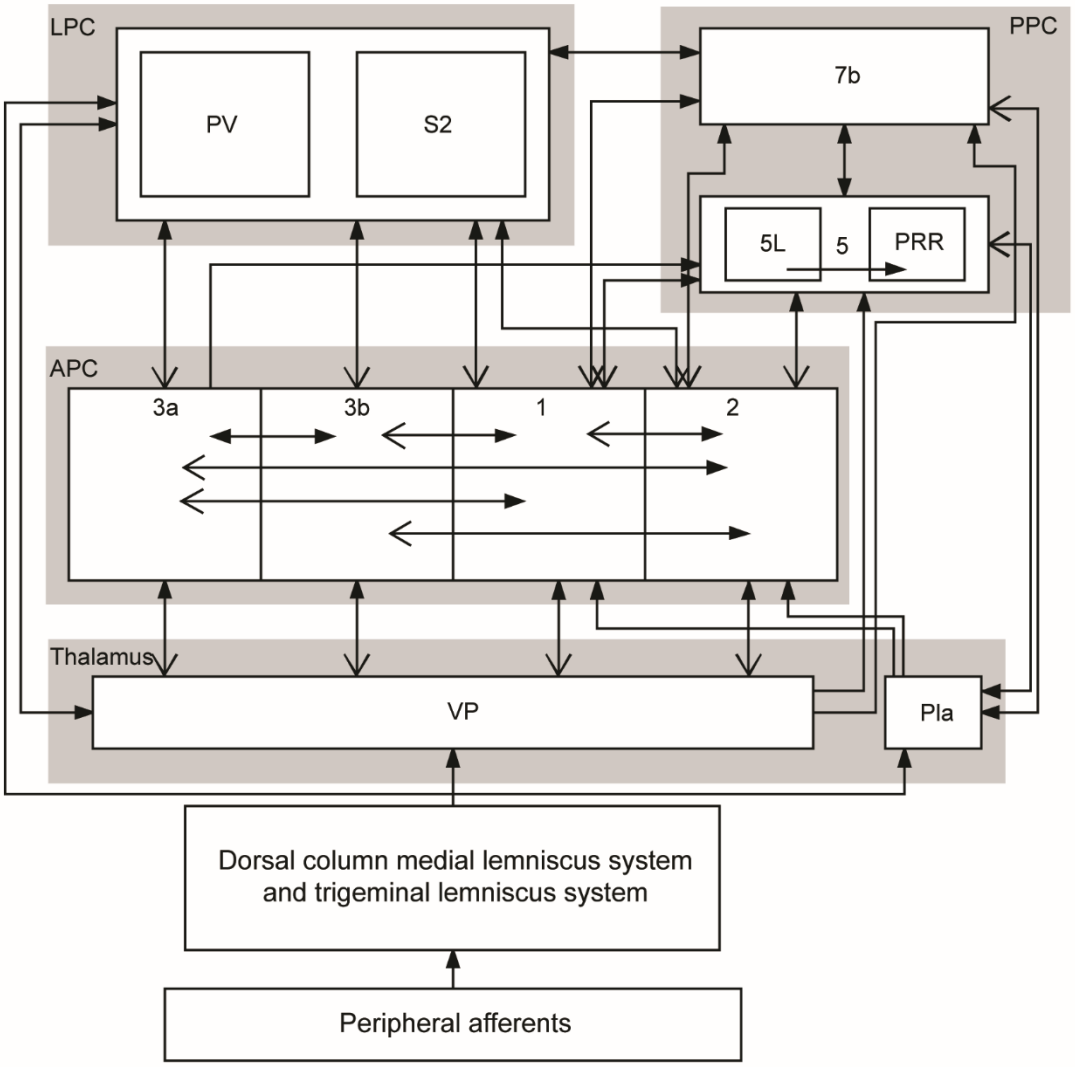

Figure 1.5. Major connections between somatosensory areas. Schematic representation of the major connections between somatosensory areas in the central nervous system, split into four major regions: the thalamus, the anterior parietal cortex (APC), the lateral parietal cortex (LPC) and the posterior parietal cortex (PPC). Abbreviations: ventral posterior nucleus (VP), anterior pulvinar nucleus (Pla), secondary somatoensory cortex (S2), parietal ventral area (PV), parietal reach region (PRR). Area 5 also receive input from the lateral posterior nucleus in thalamus (LP, not shown in the chart). Updated from (249).

AREA 3B

Area 3b is homologous to primary somatosensory cortex described in other mammals (197). The vast majority of neurons in area 3b respond to cutaneous stimulation (165, 176, 333, 357) and are organized in cortical columns: neurons in a given column exhibit similar RF properties (including almost complete spatial overlap) and are thought to be involved in a common sensory computation (56, 118, 349, 350, 366). Most neurons in area 3b exhibit responses that imply input from multiple tactile submodalities (SA1, RA, PC) (see below) (275). RFs on the hand are small (10-60 mm^2, (82)), typically limited to a single digit or even a single finger pad, and tend to be smallest for neurons in layer 4, intermediate for neurons in the subgranular layers, and largest for neurons in the supragranular ones, a size progression that is also observed in area 1 (347). Lesions in area 3b result in a nearly complete abolition of tactile abilities, including texture and shape discrimination and haptic object recognition. Neurons in area 3b are strongly interconnected and reciprocally connected to neurons in areas 3a, 1, and 2, and in lateral parietal cortex (33, 194, 216).

AREA 1

Similarly to their counterparts in area 3b, nearly all neurons in area 1 respond to cutaneous stimulation (90% or more) (165, 172, 174, 176, 333, 357). A small proportion of neurons in area 1 have Pacinian-like response properties (5%), which are even rarer in area 3b. Neurons in area 1 tend to have larger RFs than their counterparts in area 3b, sometimes spanning multiple digits (7, 172). Lesions of area 1 selectively impair the tactile discrimination of texture while preserving shape discrimination (44, 297). Ablation of area 3b abolishes cutaneous responsivity in area 1,

consistent with the aforementioned hierarchical relationship between these two areas. Area 1 has reciprocal connections with areas 3a, 3b, and 2, primary motor cortex (M1), lateral parietal cortex, and posterior parietal area 5 (33, 194, 216, 287, 346) and also receives thalamic input from anterior pulvinar area (Pla) (270).

AREA 3A

Located in or near the fundus of the central sulcus, neurons in area 3a exhibit primarily proprioceptive responses, i.e. respond to joint manipulations and muscle stretch (173, 174, 176, 215, 357), and perhaps also heat-induced pain (363, 364). RFs in the hand representation of area 3a sometimes include a single digit, sometimes multiple digits, and sometimes the entire hand (215). Whether RFs spanning multiple digits result from convergent input from multiple afferents or from single afferents innervating multi-joint muscles remains unknown. Area 3a has dense intrinsic connections and makes reciprocal connections with area 2, M1, and supplementary motor area (SMA) and also receives input from area 1 (70, 158, 159, 194, 346). Interestingly, area 3a also contains 15% of the cortico-motoneuronal (CM) cells that monosynaptically drive motoneurons of the hand in the spinal cord (300).

AREA 2

Neurons in area 2 exhibit both cutaneous and proprioceptive responses (55% deep, 45% cutaneous in the hand representation) (165, 176, 333, 357), and the submodality composition follows a gradient across its extent: neurons near the boundary with area 1 tend to be more cutaneous, neurons near the caudal boundary tend to be more proprioceptive (176, 284). The hand representation is especially rich in cutaneous input but also includes neurons that exhibit

both proprioceptive and cutaneous responses (165, 171, 172, 206), which may constitute an initial step towards stereognosis, i.e. three dimensional haptic representations of objects (see stereognosis section). Neurons in area 2 typically have large RFs, comprising multiple fingers, and may even occasionally have bilateral receptive fields, at least on the hind limb (357). Large RFs lead to a more blurred somatotopy than that observed in the three other anterior parietal fields (284). Lesions of area 2 impair the coordination of finger movements and the ability to discriminate the shape and size of grasped objects. Area 2 makes reciprocal connections with areas 3a, 3b, and 1 (287), with M1 (194, 287, 346), and with anterior pulvinar area in thalamus (270). Area 2 projects to lateral parietal cortex (S2 and PV) and to posterior parietal cortex (area 5) (287).

CORTICO-THALAMIC FEEDBACK FROM APC

In cats, cortico-thalamic feedback projections are more numerous than thalamo-cortical feedforward projections (228), but little is known about the cortico-thalamic projections from area 3b of primates. Convergent evidence in primates and other mammals suggests that area 3b sends feedback projection to the somatosensory thalamus (72, 316) and that these feedback projections exert a powerful influence on the response properties of thalamic neurons. Indeed, suppression of neuronal activity in area 3b results in a striking enlargement of thalamic RFs (99).

1.4.2 | RESPONSE PROPERTIES OF CUTANEOUS NEURONS IN APC

SUBMODALITY CONVERGENCE

As briefly summarized above, touch in the glabrous skin is mediated by four classes of nerve fibers which each respond to different aspects of skin deformation. These different sensory

channels were initially thought to serve different sensory functions (shape perception, motion perception, etc.) and remain relatively segregated along the somatosensory neuraxis (189, 349). However, recent studies suggest that neurons in APC – including in area 3b, the first cortical target for tactile input – exhibit response properties that imply convergent input from multiple afferent classes. For example, a large proportion of APC neurons (51% in area 3b and 40% in area 1) produce a sustained response during the static phase of a skin indentation – which implies input from SA1 fibers – but also an off response during the offset of the indentation – which implies input from RA and/or PC fibers (275) (Figure 1.6). Indeed, RA and PC fibers do not respond during the static phase of a skin indentation, and SA1 fibers do not produce a phasic response at its offset. The presence of both features in the majority of APC neurons strongly suggests that convergent input is the rule rather than the exception. Furthermore, the time varying firing rates of APC neurons to simple and complex vibrations are better predicted from the combined responses of multiple afferent classes than from those of a single class (323). These observations indicate that touch does not comprise distinct sensory channels, each serving a different function, but rather relies on the integration of sensory signals across tactile submodalities to extract behaviorally relevant information during manual interactions with objects (322).

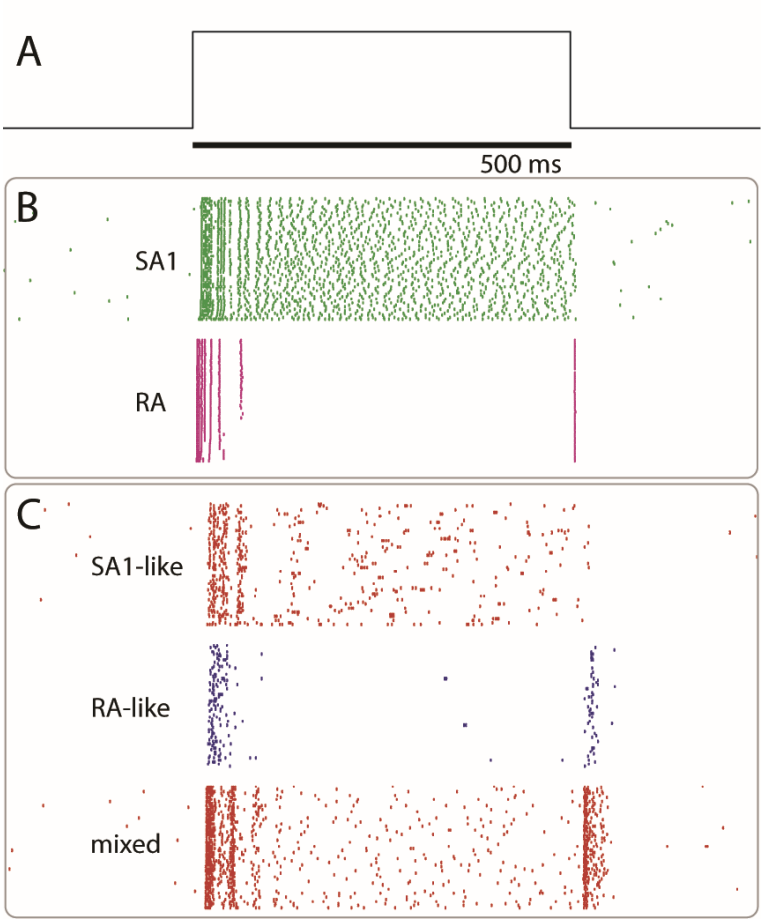

Figure 1.6. Sub-modality convergence in APC. Al Trajectory of a punctate stimulus indented 2mm into the center of a neuron's receptive field. Bl Typical response of a slowly adapting type 1 (SA1) and rapidly adapting (RA) afferent to 60 repeated presentations of the stimulus. Cl Response of typical neurons in area 3b. Some neurons respond throughout the stimulation interval and do not show phasic off responses, similar to SA1 fibers; others respond with phasic on-off responses, similar to RA1 fibers, but the majority respond with a mixture of sustained and phasic responses, implying input from both fiber types. Adapted from ref. (275).

SPATIAL STRUCTURE OF RECEPTIVE FIELDS

The receptive fields of many neurons in area 3b comprise excitatory subfields flanked by inhibitory ones and can often be well approximated by linear spatial filters (Gabor functions, see Figure 1.7). That is, stimulation of excitatory patches of skin sum to create an excitatory drive to

the neuron; stimulation of the inhibitory patches sum to create an inhibitory drive, and the overall activity of the neuron is well approximated by the linear combination of these excitatory and inhibitory drives. The inhibitory surround is distinct from the surround suppression observed in the receptive fields of tactile fibers, which reflects skin mechanical effects (344). In addition to inhibitory components flanking the excitatory one, RFs tend to also comprise an inhibitory component co-localized with the excitatory field but delayed by 20-30 ms (81, 125). This RF structure results in an initial excitatory drive that is followed by an inhibitory one, rendering the neuron less excitable for a period of time. As mentioned above, excitatory and inhibitory inputs are combined in an approximately linear fashion (11, 81) and their interplay yields RFs whose spatial structure is relatively consistent across scanning speeds (80) (Figure 1.7). Importantly, neurons in area 3b tend to have elongated RFs (with a mean aspect ratio of 1.7), which confers orientation tuning to these neurons (see shape section below) (11, 82). The RF structure of neurons in area 3b thus draws a strong analogy to that of simple cells in primary visual cortex.

In contrast to their counterparts in area 3b, neurons in areas 1 and 2 tend to have larger, more complex RFs, that are poorly approximated using linear spatial filters (11, 166, 171, 172, 175). That is, RFs often do not comprise distinct excitatory and inhibitory fields, and to the extent that they do, these fields are poor predictors of the neurons' response properties. Rather, neurons in these higher processing areas within somatosensory cortex tend to exhibit more complex feature selectivity, such as a selectivity for curvature or a shape-invariant selectivity for direction of

motion, neither of which are reflected in the spatial structure of their RFs.

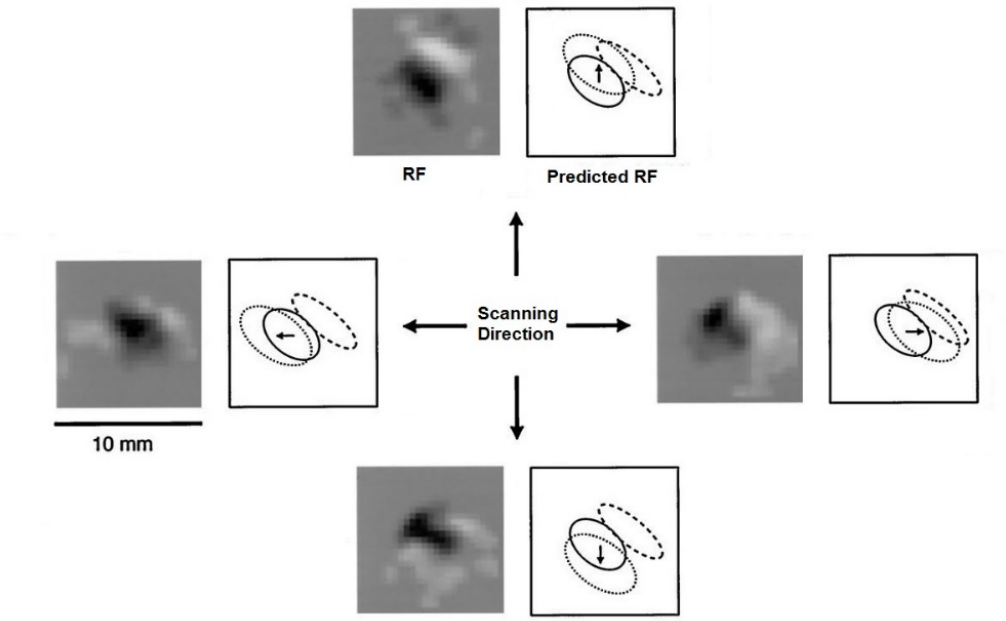

Figure 1.7. Spatial structure of receptive fields of a neuron in area 3b. The two squares in each group display the RF estimated from the raw data (left) and the positions of the modeled Gaussian representations (right). Leftl The experimental RF was obtained by continuously scanning the finger with a random pattern of raised dots, and then computing an RF map using reverse correlation (see (82)). Dark regions are excitatory, white regions are inhibitory. Rightl The locations of the excitatory (solid ellipse) and fixed inhibitory components are unaffected by scanning direction and the lagged inhibitory component (dotted ellipse) trails the center by a fixed distance in each direction. Reproduced from (81).

RECEPTIVE FIELD INTERACTIONS

Touch involves the integration of information stemming from hundreds or thousands of tactile fibers, each innervating a small patch of skin, and this integration occurs gradually as signals ascend the neuraxis through subcortex and cortex. Interestingly, while S1 neurons (area 3b) are characterized by relatively small RFs, seemingly reflecting only weak integration from periphery to the cortex, thalamo-cortical projections have been shown in anatomical studies to branch

extensively over wide spatial areas (133), as have cortico-cortical connections (33). While widespread branching and lateral connectivity is obscured when RFs are mapped using sequential application of well-controlled indentations, these connections manifest themselves as modulatory influences on APC responses when stimuli are simultaneously applied to a neuron's RF and outside of it. Indeed, a stimulus applied outside a neuron's classical RF results in a decrease in sensitivity for a period of about 100 ms (303, 304). In fact, this suppression is sometimes observed when the conditioning stimulus is applied to the contralateral hand (302), an observation also made using optimal intrinsic signal (OIS) imaging (362). Paired stimulation of multiple digits also produces a reduced spatial pattern of activation compared to what would be expected based on the stimulation of each digit individually, suggesting lateral inhibition (119). Such spatial interactions can also account for the tactile funneling illusion, referring to the phenomenon in which the simultaneous presentation of brief tactile stimuli at two skin locations evokes a sensation localized between the two sites where no stimulus is present. Indeed, simultaneous stimulation of two adjacent digits produces a single patch of activation in cortex located between the activation sites of the individual digits (57). Some of these second order properties can be described mathematically using models in which the primary receptive field is captured by a linear filter (as described above, see Figure 1.7) and the inter-digit interactions are captured by non-linear components (360). Another manifestation of long-distance spatial interactions is the increased synchronous firing over the entire hand representation when a fingertip is touched (301). Taken together, these results suggest that, even at the earliest stage

of cortical processing (area 3b), tactile signals from large swaths of skin are integrated in complex ways.

TEMPORAL RESPONSE PROPERTIES

As summarized above, the different classes of tactile fibers differ in their frequency sensitivity profiles. SA1 fibers are most sensitive to low-frequency vibrations, below about 10 Hz, while PC fibers peak in sensitivity at around 250Hz, and RA fibers exhibit intermediate frequency sensitivity. APC neurons also differ in their frequency sensitivity profiles (252, 330) but these tend to be much more idiosyncratic, in part because individual neurons receive input from multiple classes of afferents. Indeed, the frequency sensitivity profile of the afferent input will shape the frequency profile of its target and so APC neurons will differ in their spectral sensitivity because they differ in the relative strength of the input from each of the tactile modalities. Moreover, the frequency profile of APC neurons is shaped by how this input is processed. Indeed, APC responses to vibrations – particularly those of neurons in area 3b – can be well approximated as a linear function of the afferent input passed through a temporal filter and these filters vary from neuron to neuron (323). Interestingly, filters tend to differ systematically depending on the input modality: RA input tends to be excitatory whereas PC input tends to be balanced or inhibitory. In other words, RA signals tend to be integrated over time whereas PC signals tend to be differentiated. As a result, the strength of APC responses to skin vibrations is determined largely by the RA (and probably SA1) input, whereas the precise timing of the responses is shaped primarily by the PC input (323). These finding are in line with those from OIS imaging studies which showed that 25-Hz vibrations (which excite primarily SA1 and RA fibers) produce strong

localized excitation, whereas 200-Hz vibrations (which excite primarily PC fibers) produce a short excitatory transient followed by strong, spatially extended inhibition (365, 367). Thus, while input from the different tactile channels converges onto individual APC neurons, their impact is highly channel-dependent. Because vibratory sensitivity depends on the submodality composition of the input (which varies from neuron to neuron) and on the way that submodality specific input is integrated (which also varies from neuron to neuron), APC neurons exhibit a wide array of frequency response properties.

RESPONSE PROPERTIES OF PROPRIOCEPTIVE NEURONS IN APC

As mentioned earlier, proprioceptive signals from the periphery – signals originating from muscle, joint, ligament, and skin afferents that provide information about time varying muscle length and joint position – target primarily areas 3a and 2 in APC. Much less is known about the RFs and response properties of these so-called "deep" neurons compared to their cutaneous counterparts. As mentioned previously, a striking observation at the periphery is that afferent responses to passive and active movements elicit very different responses, because muscle spindle discharge is powerfully affected by fusimotor activity and because many muscle and joint receptors are sensitive to the level of tension or contraction in the muscle. Such differences between active and passive movement are also a hallmark of proprioceptive responses in cortex. Some neurons respond only to passive movements or only to active moments, while others respond to both (231, 342). During passive movements, responses have been classified as phasic, thus encoding movement, tonic, thus encoding posture, or a combination of both (127, 342). Phasic neurons typically respond to either flexion or extension, but not both (394).

Individual neurons exhibit different combinations of tonic and phasic responses, forming a continuum from purely phasic to purely tonic (290). As shown during an active reaching task, proprioceptive neurons from the arm typically exhibit a unimodal and broad tuning for reach direction (290). The preferred direction is generally similar during the phasic and tonic components of the response, and consistent for active and passive movements (231, 290). Moreover, imposing a load on the arm affects responses, but less so in APC than in M1. A subset of proprioceptive neurons exhibit RFs that include multiple joints which are not necessarily adjacent to each other (66). The responses of some neurons with multi-joint RFs are a simple summation of their single-joint activations. Others neurons show complex interaction between joints, with their response peaking at a preferred combination of joint postures. Some neurons discharge before the onset of voluntary movement, an observation that has been attributed to efference copy (231, 261). Note that cutaneous units also discharge during arm movements, although more weakly than during direct touch (16), and some of these exhibit the same kind of direction tuning observed in deep neurons (59, 289). These neurons may thus also contribute to kinesthetic sensations. Interestingly, a sub-region of area 3a, in the representation of the head, provide proprioceptive signals to encode eye position in the head (376): These neurons are tuned for the direction of gaze and their responses increase with increasing orbital eccentricity. Little is known about how hand movements and postures are encoded in somatosensory cortex.

1.4.3 | LATERAL PARIETAL CORTEX (LPC)

The second somatosensory area (S2) and the parietal ventral area (PV) sit within the upper bank of the lateral sulcus, just lateral to the tongue representation of APC (Figure 1.4B-C). The border

between APC and LPC is medial to the lateral sulcus and splits the head representations of the two regions (32). S2 and PV contain mirrored body maps that meet at the digits, lips, and mouth (32, 87, 214) and have been characterized in both macaques and humans (87, 88, 97, 98, 214). In primates, S2 and PV have only been clearly identified and separated relatively recently (213, 214, 216) so earlier reports often confuse or combine the two areas (309, 384).

Over the years, different groups have published seemingly conflicting reports of the properties of neurons in LPC. These discrepancies are likely due to several factors, including the precise locations of recording sites, the behavioral relevance and complexity of the stimuli, and the attentional state of the animal. When somatosensory properties were reported in the upper bank of the lateral sulcus in the 1940s, only one area was described (387). Later, when two mirror-reflected body maps were observed in this region and histological differences were characterized, the terminology expanded to two regions, S2 and PV, the latter located anterior to the former (214). Neurons in the central region that spans the boundary between PV and S2 exhibit primarily cutaneous responses, whereas neurons in the outer regions tend to exhibit proprioceptive responses (105, 214). In macaques, the hand representation within the central region spans 10 mm along the anterior posterior axis (105) and is relatively well defined and consistent across animals (32). The face region is rostral, medial, and superficial, while the tail and sacrum are caudal, lateral, and deep in the sulcus.

Receptive fields in LPC tend to be larger and more diffuse than those in earlier stages of processing. RFs encompass multiple finger pads, span multiple digits, and respond bilaterally to stimuli applied to either hand (32, 106, 170, 288, 321, 337) or to multiple regions of the body

(356) or even the entire body. Indeed, while both areas primarily receive input from the contralateral side of the body, bilateral RFs have also been reported. For neurons with bilateral RFs, stimulation of the ipsilateral side typically exerts a modulatory effect on the response evoked by contralateral stimulation (87, 88). About half of LPC neurons respond to cutaneous stimulation and half to deep stimulation (356). Both S2 and PV receive projections from all four APC areas (34, 216, 296) as evidenced by the fact that lesioning individual areas reduces the responsiveness of their downstream targets (35, 132, 285): selective removal of proprioceptive input (areas 3a and 2) or cutaneous input (areas 3b et 1) selectively reduces proprioceptive and cutaneous responses in LPC, respectively (286) (Figure 1.5). LPC receives input from area 5 (287) and area 7b (86). LPC also receives direct inputs from the thalamus (85, 116): PV from ventroposterior inferior nucleus (VPI) and Pla; S2 from VPI, ventroposterior superior nucleus (VPS), and Pla. Thus, LPC integrates proprioceptive, and thermoreceptive/nociceptive signals directly from thalamus (85). LPC in turn projects densely to ipsilateral APC, particularly areas 3b and 1, and area 7b (117), with connections between S2 and PV, as well as contralaterally to LPC, area 7b, and area 3b (86). LPC is also reciprocally connected with multiple insular areas (117), and sends cortico-thalamic feedback projections to the VPL and the anterior pulvinar (31, 375). PV projects to areas 3b and 7b, premotor cortex, and other posterior parietal areas (86). Lesions of LPC severely impair the ability of monkeys to perform texture and shape discrimination tasks (255, 352).

RESPONSE PROPERTIES OF NEURONS IN LPC

LPC neurons tend to exhibit more complex response properties; for example, some orientation-tuned neurons in LPC have the same preferred orientation over large swaths of skin on the hand,

an extent of positional invariance not seen in APC (106). When RFs are mapped using passive presentation of behaviorally irrelevant stimuli, modality is difficult to identify and tends to vary over time (337), a property that can be attributed to the strong susceptibility of LPC responses to changes in attentional state (39, 52, 157, 244, 330). Not only do the responses of LPC neurons depend on the attentional state of the animal, they also depend on the behavioral task and its demands. Indeed, while APC neurons faithfully encode the stimulus, irrespective of the task, LPC neurons exhibit a tendency to encode both the stimulus and the behavioral outcome in a task-dependent way (Figure 1.8), a hallmark of higher cortical processing (151, 181, 218, 312, 330). This task-dependent modulation and the correlation of neural activity with perceptual reports suggest a role of LPC in sensory decision making (312, 314).

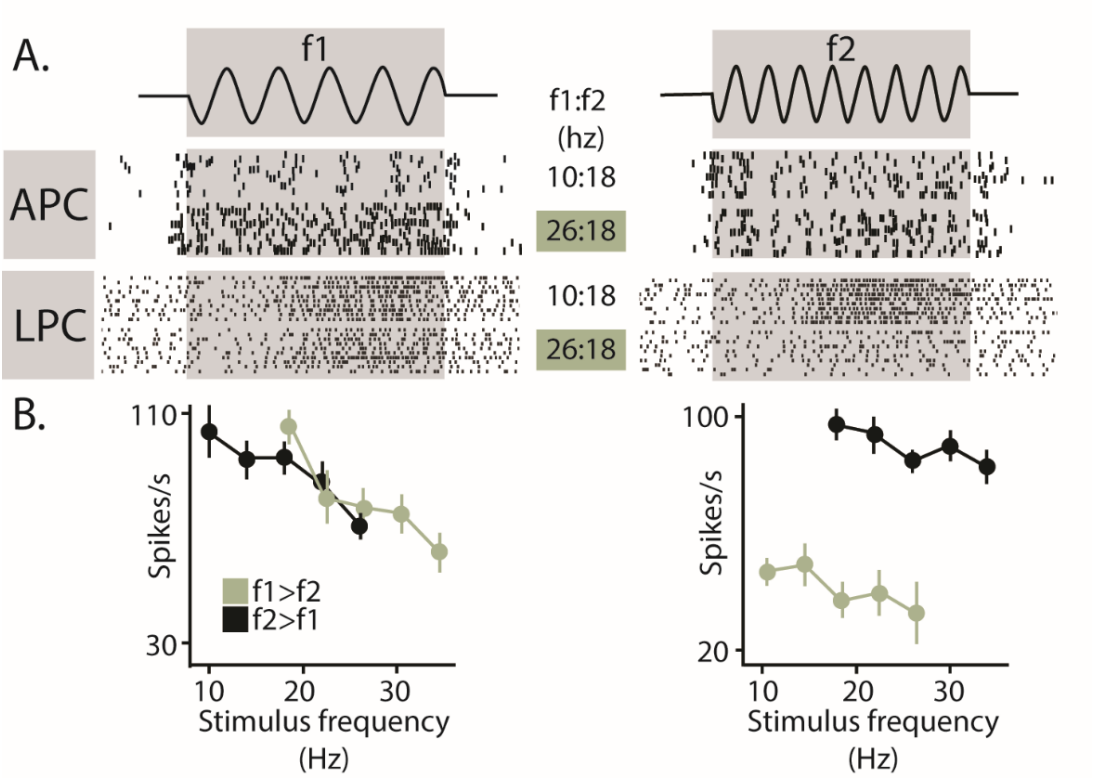

Figure 1.8. In contrast to their counterparts in primary somatosensory cortex, neurons in secondary somatosensory cortex exhibit task-dependent modulation in their responses to identical vibratory stimuli. Al Spiking responses recorded from one neuron in APC and one in LPC (adapted from (152) and from (312) respectively). Each row shows the response to a pair of stimuli: 10 or 26 Hz in the first stimulus period (f1) and 18Hz in the second (f2). In APC, the response to f2 is independent of f1, while in LPC, the response to f2 is greater when f2 > f1. Bl LPC firing rates as a function of the frequency of vibration in the tactile stimulus. During the first stimulation period (f1), rates decrease monotonically as stimulus frequency increases. During the comparison period (f2), neurons respond preferentially when f2 > f1 (shown here) or vice versa (black points show trials on which f2 > f1; green traces denote trials on which f2 < f1).

Visually (3, 203) and acoustically (103, 308) evoked responses in LPC have long been reported in human imaging studies, but had not been observed in single unit recordings from non-human primates until recently (154, 243), a discrepancy that may be attributable to particular stimuli used in early neurophysiological studies. Indeed, sounds and images that have no tactile

correlate, like pure tones or speech, do not drive neurons in LPC (154, 311), but the sound of hands rubbing together does. These multisensory responses may underlie a phenomenon documented in humans: modifying the sound that hands makes while rubbing against one another influences how moist or dry the skin feels (146, 352). Additionally, about a third of neurons exhibiting somatosensory responses also respond to visual stimuli and sometimes to auditory stimuli (154), and these neurons, interspersed throughout LPC among a majority of unimodal somatosensory neurons, may play an important role in multisensory integration.

1.4.4 | POSTERIOR PARIETAL CORTEX (PPC)

The posterior parietal cortex (PPC) is caudal to APC and straddles the intraparietal sulcus (IPS) (164). PPC comprises two major architectonical areas originally described by Brodmann: area 5, located on the rostral side of the IPS, and area 7, located between the IPS and the lateral sulcus (Figure 1.4A). Both areas have been divided into multiple distinct cortical fields based on a variety of criteria including cytoarchitecture, patterns of connectivity with other areas, and neural response properties. The names and boundaries of these sub-regions are a matter of ongoing debate (144, 226, 272, 333), probably because different studies have used different criteria. Area 5 can be split into two major parts — a lateral region, presently referred to as 5L (previously 5a, 5v/d or PE) (333), and a medial region dubbed the parietal reaching region (PRR)(5). Area 7 is traditionally split into two major regions—a rostral, mostly somatosensory region 7b, and a caudal, mostly visual region 7a. However, some histological and physiological evidence suggests that area 7 actually comprises three separate fields, PF, PFG, and PG (272, 320). Other cortical fields have also been identified within the IPS (namely AIP, LIP and VIP, see Figure 1.4A), but are

mostly visual or visuo-motor areas, and will not be discussed here. The pattern of cortical connections suggests two major streams in PPC, both originating in area 2 and progressing rostral-to-caudal, one along the superior lobule (area 5) and the other along the inferior lobule (area 7) (272). Connections and the response properties of PPC neurons also suggest that area 5 precedes area 7 in the processing hierarchy (see below). PPC comprises strong interhemispheric connections as well as many connections with pre-motor areas (49, 50, 170, 357). The correspondence between macaque and human PPC, both in terms of location in cortex and functional properties, is not straightforward and remains poorly characterized (143).

Most PPC areas contain neurons that respond to cutaneous stimulation and joint movements, but PPC, unlike APC and LPC, is not a somatosensory region per se. First, neurons in PPC respond to other sensory modalities, mainly visual, but also auditory (60) and vestibular (341). Second, a large subset of neurons responds most strongly when the animal is awake and behaving, and many sites are unresponsive during anesthesia (251, 333). Third, cortical fields in PPC are known to be involved in motor functions such as planning reaching and grasping movements, as indicated by dense, reciprocal connections to pre-frontal and motor areas (42, 280) and by the fact that neurons seem to encode not just limb position but also target locations and motor intent (202). Fourth, lesioning or ablating areas within the PPC does not strongly impact passive tactile discrimination but does affect animals' ability to reach and grasp objects or to recognize an object's shape through haptic exploration (stereognosis) (114). For all of these reasons, the PPC is thought to play a critical role in both multisensory integration and

sensorimotor planning and guidance, especially for the upper limbs (340). In the following sections, we describe the properties of PPC areas that exhibit somatosensory responses.

AREA 5L

The lateral aspect of area 5, called 5L (333), borders the hand and arm representations of area 2 and is partially buried in the IPS. The somatosensory RFs of neurons in area 5L span only the shoulders, forelimbs, and hands with a somatotopic organization that roughly follows that in area 2 (under anesthesia , 333). RFs tend to be larger than those in APC, often containing multiple joints and digits, can be bilateral (358), and typically exhibit proprioceptive responses (~90%). Only a small fraction of area 5L neurons maintain activity during anesthesia and most respond best while animals make voluntary movements (251, 326). Area 5L receives the majority of its inputs from APC (137), especially area 2 (274, 287). Area 5L also receives direct input from the thalamus: Pla, lateral posterior (LP) nucleus (393), and VP (287). Area 5L projects ipsilaterally and bilaterally to other parts of area 5, area 7, LPC, motor cortices, and superior temporal gyrus (164). Neurons in area 5L have been shown to encode texture and object shape (2, 171) but lesions in this area have only modest effects on animals' ability to discriminate passively presented textures (255, 271), consistent with its putative role in the planning of grasping and other manual behaviors that require information about shape and texture (124, 128, 129, 299). During a grasp, neurons in area 5L respond strongly during the approach, their response peaks during the grasp, and then drops during the lift, with a majority inhibited during hold (124). Neurons in area 5L show evidence for synergies between reaching and grasping that may facilitate smooth, coordinated actions of the arm and hand (55). Ablation or lesions of area 5L interferes with the

ability to orient the hand to grasp (271). Interestingly, area 5L neurons respond during reaching even if the animal is de-afferented, showing again the tight interplay between area 5L and motor areas (332).

PARIETAL REACH REGION

The parietal reach region (PRR) is found in the medial aspect of area 5 (Figure 1.4A), located in part in the convexity of the superior parietal lobule (region also named PEc) and partially buried in the IPS (a region also named MIP). PRR probably contains multiple fields, the precise boundaries and locations of which remain vague. PRR receives major input from area 5L, as well as inputs from other parietal visual areas (areas 7a and V6A, just caudal to it). PRR projects to areas 7a and 7b and is strongly reciprocally connected with the dorsal premotor cortex (227, 237, 272). Neurons in PRR respond to passive somatosensory stimulation, in particular movements of the joints (26) with RFs located on the arm. PRR neurons also respond to visual stimuli (343) and most are multisensory (visual and somatosensory). In active reaching tasks, PRR cells are strongly activated before and during reaching movements and their responses are typically tuned for movement direction (200, 201). In light of these observations, PRR is thought to encode cognitive signals related to the direction of intended arm movement (5, 340) and movement-related sensory feedback. Ablation of PRR only has only modest effects on tactile discrimination (255) and inactivation of PRR causes impairments in reaching (162).

AREA 7B

Area 7b is located in the lateral aspect of area 7 (Figure 1.4A), in part on the convexity of the inferior parietal lobule, caudal to area 2, and in part buried in the lateral sulcus (a region also

denoted 7op), adjacent to LPC (214). Area 7b is strongly and reciprocally connected with area 5 and LPC (259, 260). The rostral part of area 7b (PF) is primarily connected with somatosensory areas while the caudal part (PFG) also receives inputs from multiple visual areas (MST, temporal visual areas and lateral intraparietal area) (4, 320). Area 7b also receives input from thalamic pulvinar areas (116, 273, 381) and projects to frontal and pre-motor areas as well as caudal PPC (144). While some neurons only respond during voluntary movements, the majority of neurons in area 7b also respond to imposed movements of the joints and to tactile stimuli, some respond to visual stimuli, and some to both (4, 89, 223, 251, 311). Furthermore, some neurons respond to both tactile and thermal or nociceptive stimuli, and a few to only nociceptive stimuli (89, 310). RFs in area 7b are generally large but vary greatly in size (from single digit to whole hand or even whole arm). The RFs follow a crude somatotopic organization, with the head represented in the anterior portion of area 7b, aligned with the head representation of area 2, and the hand, arm, and trunk representations further posterior (163, 223, 224). Little is known about the functional properties of neurons in area 7b, though some qualitative similarities have been reported in the response properties of areas 7b and 5L (124).

1.4.4 | TOP-DOWN MODULATION OF APC

As mentioned above, APC projections to thalamus exert a strong influence on the response properties of thalamic neurons. Such top-down modulation is also observed from PPC to APC. In fact, PPC sends cortico-cortical projections to APC (33) and cortico-thalamic projections to Pla of the thalamus (43, 381, 393), which in turn projects back to APC (areas 1 and 2)(68, 217) and these feedback loops between PPC and APC exert a strong influence on the response properties

of APC neurons. Indeed, reversible inactivation of areas 5L or 7b results in an expansion of RFs in areas 1 and 2 (64) and can increase or decrease the cutaneous sensitivity of individual APC neurons (140). This powerful top down effect from PPC to APC stands in contrast to that from LPC to APC: LPC lesions seem to have negligible effects on APC responses (285, 395).

1.5 | Sensory Coding in Somatosensory Cortex

1.5.1 | Vibration

Frequency

Vibratory stimuli – mechanical sinusoids in particular – have been used extensively to probe tactile sensibility, inspired by the use of auditory pure tones to probe hearing. As summarized above, the different classes of tactile nerve fibers have different sensitivity profiles, with SA1 fibers tending to be more sensitive at the low frequencies (~5Hz), PC fibers peaking in sensitivity at around 250 Hz, and RA fibers preferring intermediate frequencies (355). A striking aspect of afferent responses to skin vibrations is that they exhibit phase locked responses to periodic vibratory stimuli – that is, they produce one spike or burst of spikes within a restricted portion of each stimulus cycle – as do their counterparts in the auditory nerve (112, 113, 355) (Figure 1.9A). This temporal patterning in afferent responses carries information about the frequency composition of vibratory stimuli applied to the skin (21, 233).

APC neurons also exhibit phase locking to low-frequency sinusoids (Figure 1.9B), but the fidelity of the phase locking decreases rapidly as vibratory frequency increases: the vast majority of APC neurons entrain at 1 Hz, but only a small proportion of them is capable of following a 300 Hz

stimulus (152, 252). Surprisingly, a small fraction of neurons (4%) can phase lock to vibrations with frequencies up to 800 Hz (149). For low-frequency stimuli, the spike rates of individual APC neurons increase or decrease monotonically with frequency and the inter-spike or inter-burst intervals decrease systematically, so frequency information is conveyed in the strength of the response (firing rate) as well as in its temporal patterning (phase locking) (152, 330) (Figure 1.9B). At high frequencies, on the other hand, firing rates become frequency independent while the patterning is preserved in a subpopulation of neurons, which carries information about stimulus frequency. The ability of human and monkeys to perceive stimulus frequency above 100 Hz is thus mediated by the temporally patterned responses of this subpopulation of phase-locking neurons (149), a range of frequencies that may be implicated in the perception of texture (12, 380).

The responses of LPC neurons to mechanical sinusoids also exhibit phase locking, though weaker than that observed in APC. Indeed, vibration-sensitive LPC neurons phase lock to sinusoids with frequencies below 10 Hz, though some can follow frequencies up to 50-75 Hz, and fewer still up to 300 Hz (36). On the other hand, frequency is robustly encoded in the firing rates of LPC neurons, with rates either monotonically increasing or decreasing with increases in frequency (312), at least in the flutter range (< 50 Hz). The weak phase locking and strong rate coding of frequency in LPC has been interpreted as implying that frequency is encoded entirely in neuronal firing rates (330), which implies a progressive conversion from a temporal to rate code as one ascends the somatosensory neuraxis. This progression of neural codes has also been observed along the auditory neuraxis and may reflect a general principle of sensory processing (324).

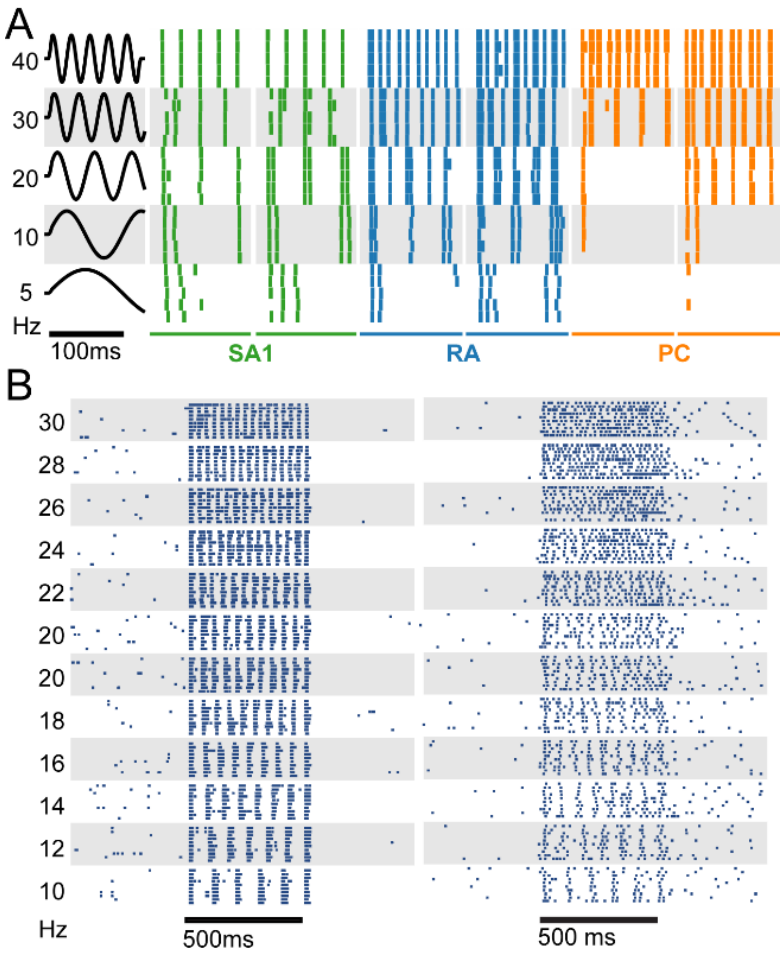

Figure 1.9. Temporal patterning in peripheral and cortical responses to sinusoidal vibrations applied to the skin Al Typical response of peripheral afferents (two SAI in green, two RA in blue and two PC in orange) to sinusoidal vibrations (amplitude = 250 microns) of different frequencies applied in the center of their RF. The responses of tactile fibers are strongly phase-locked to the stimulus and highly repeatable. Data from (253) Bl Responses of two typical APC neurons to sinusoidal vibrations. APC neurons show various degrees of phase-locking and greater trial-to-trial variability. Within this low-frequency range, the frequency of the stimulus can be extracted from both the temporal patterning of the response and the mean firing rate. Reproduced from (152, 315).

AMPLITUDE

At the somatosensory periphery, the strength of the response of most tactile fibers to a vibration is dependent not only on its amplitude but also on its frequency, so the amplitude information

carried in the firing rates of any one population of tactile fibers is ambiguous. Rather, the intensity of skin vibrations is encoded in the firing rate evoked in all tactile nerve fibers, weighted by fiber type (253). In APC, neuronal responses to skin vibrations are also frequency-dependent up to about 50 Hz. Over this frequency range, firing rates are modulated by stimulus amplitude, but also by stimulus frequency, as discussed above (152, 330) so it is unclear how these two stimulus dimensions can be independently decoded by downstream structures. In contrast, the firing rates of APC neurons evoked by high-frequency skin vibrations (above 50 Hz) increase with vibratory amplitude – with rate intensity functions well approximated using a rectified logarithmic function – but do not depend on stimulus frequency (149). Therefore, spike count (at the single unit or population level) faithfully encodes vibratory amplitude independent of frequency at frequencies above about 50 Hz.

1.5.2 | TANGENTIAL/SHEAR FORCES

When we manipulate objects, forces are not just exerted normal to the surface of the skin but also parallel to it. The normal force – which corresponds to grip force in object grasping – is the force applied perpendicularly to the object surface. The tangential force – corresponding to load force –, is the reaction force acting parallel to the object's surface and often exerted by gravity (184). The responses of tactile afferents to tangential forces are in part dependent on the direction in which the tangential forces are exerted: Afferents respond maximally to forces exerted in a specific direction and less so to forces exerted in other directions (19, 382), and their responses are also modulated by the magnitude of the tangential force (382). The majority of APC neurons (85%) produce responses that are dependent on the magnitude and direction of

shear forces applied on or near their RFs (110). In the context of active movements, some neurons encode normal forces, others tangential forces, and some both (327–329). Interestingly, some neurons seem to carry information about friction, the ratio between tangential and normal force needed to achieve movement (111).

1.5.3 | SHAPE

When we grasp an object, we can sense its three dimensional structure based on somatosensory signals from the hand (391). Stereognosis relies on the integration of cutaneous information about local shape at each point of contact between skin and object and proprioceptive information about global shape from the relative position of these different contact points. In this section, we examine how information about local shape – stemming from local deformations of the skin – is processed in somatosensory cortex. In the stereognosis section below, we discuss what little is known about stereognosis.

In both vision and touch, the shape of objects is reflected in a spatial pattern of activation across the receptor sheet, in the retina and in the skin, respectively (142, 190) (Figure 1.10A). In primary visual cortex, a preponderance of neurons respond preferentially to the presence of an edge at a specific orientation in their RF, with a smooth drop off in response strength when the orientation of the bar deviates from this preferred orientation. In other words, the visual scene is parsed into a set of oriented contours, which forms the basis for downstream processing, a representation that is thought to be optimal given the statistics of the visual world and sparseness constraints (268). Similarly, a large fraction of APC neurons (40 to 60%) exhibit orientation tuning for edges indented into the skin (Figure 1.10B), with a slightly larger fraction

in area 1 than area 3b (11). As the tuning width of V1 neurons is invariant with respect to contrast, the tuning width of APC neurons is invariant with respect to depth of indentation, the tactile equivalent of visual contrast. The two sensory systems thus seem to implement similar mechanisms to extract orientation information, a phenomenon that can be at least in part attributed to the RF structure of APC and V1 neurons: RFs consist of excitatory regions flanked by inhibitory ones (or vice versa) and can be approximated using Gabor filters. Orientation tuning is somewhat broader in APC than in V1 and, perceptually, angular acuity is coarser in touch than vision for stimuli of comparable size presented passively (4- vs. 20-degree angular threshold in vision and touch, respectively) (14). Interestingly, tactile orientation acuity is much higher when measured in the context of an active orienting task (292).

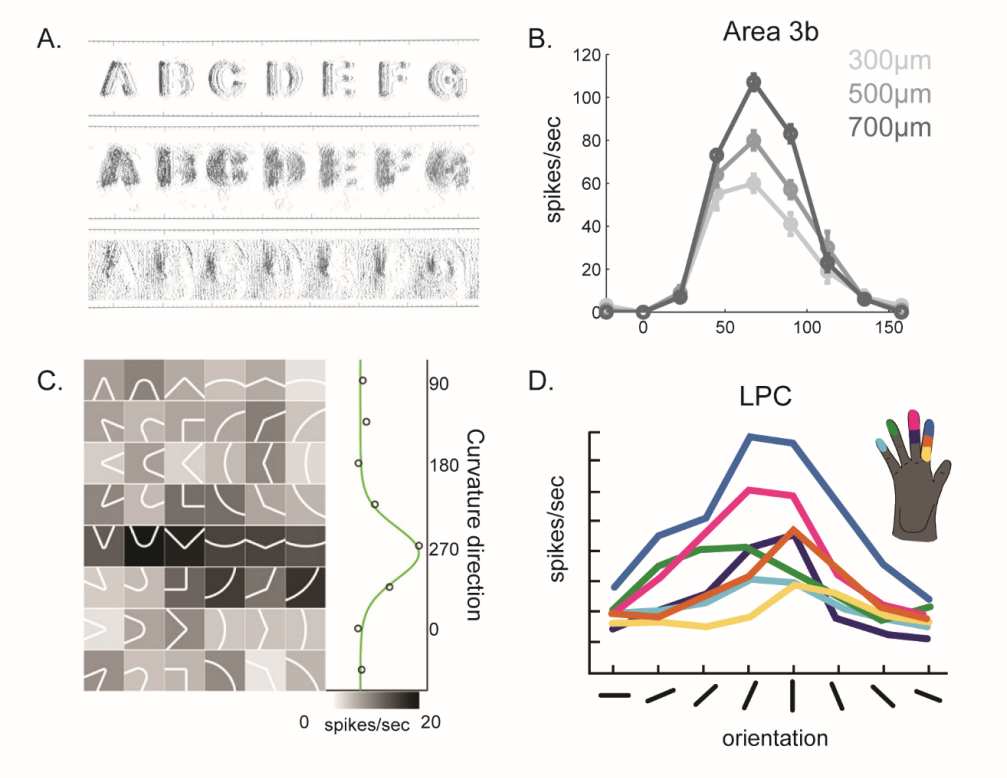

Figure 1.10. Spatial processing in the somatosensory system. Al Reconstructed response of tactile nerve fibers to embossed letters scanned across the skin. As in the retina, the spatial configuration of the stimulus is reflected in the spatial pattern of activation it evokes in SA1 and RA populations. Reproduced from ref. (283) Bl Responses of a neuron in area 3b to oriented edges indented into the skin (8 orientations, three indentation depths). This neuron is strongly tuned for edge orientation, as are neurons in primary visual cortex. Reproduced from ref. (11) Cl Responses of an LPC neuron to curvatures indented into the skin. This neuron prefers intermediate curvatures with the convex end pointing proximally. This type of feature selectivity is not observed in early stages of cortical processing (e.g., in area 3b). Reproduced from (392) Dl Responses of an LPC neuron to bars indented into the skin. This neuron exhibits the similar preferred orientation over large swaths of skin (position-invariant orientation tuning). Reproduced from (107).

One of the well-known principles that governs the processing of visual shape is that of hierarchical processing: Neurons at successive layers of processing have progressively larger RFs and progressively more complex feature selectivity that is progressively more invariant with

respect to other stimulus features. The same principle operates in the processing of tactile shape along the somatosensory neuraxis. Indeed, neurons in area 2 exhibit tuning for curved shapes – comprising multiple orientations – a complex selectivity that is not observed in areas 3b and 1 and is even more pronounced in LPC (390, 392)(Figure 1.10C). Furthermore, neurons in LPC exhibit orientation tuning over wide swaths of skin, with a consistent orientation preference across their RFs, reflecting increased position-invariance with respect to their APC counterparts (107) (Figure 1.10D). Lesions of LPC lead to an impairment in shape discrimination, as do lesions in area 2 (255), confirming that these two areas are part of a tactile shape processing pathway.

1.5.4 | MOTION

Tool use and, more generally, object interactions often involve motion between skin and object. Furthermore, to sense the shape of an object or its texture requires movement between skin and object (221). Not surprisingly, then, cutaneous cues convey information about the velocity of relative movement between skin and surface. Indeed, human subjects can discriminate the direction (100, 102, 278) or the speed (15, 101, 383) of movement across the skin.

As is the case with shape perception, the neural mechanisms underlying motion perception are remarkably analogous in vision and touch (269, 276). Indeed, a subpopulation of APC neurons is tuned for motion direction (65, 126, 277, 377), as are many V1 neurons (Figure 1.11A). In area 3b, direction-selective neurons are maximally sensitive to oriented bars moving across their RFs but these neurons cannot signal the direction of a stimulus comprising multiple orientations. Indeed, given their small RFs, they are subject to the aperture problem (Figure 1.11B). That is, any one straight edge of a moving object conveys information only about the motion component

perpendicular to that edge's orientation. Due to its small RF, a single neuron in area 3b will respond to only one of an object's many edges, and will therefore convey erroneous information about the object's global direction of motion (Figure 1.11C). Most direction selective neurons in primary visual cortex are subject to the same limitation.

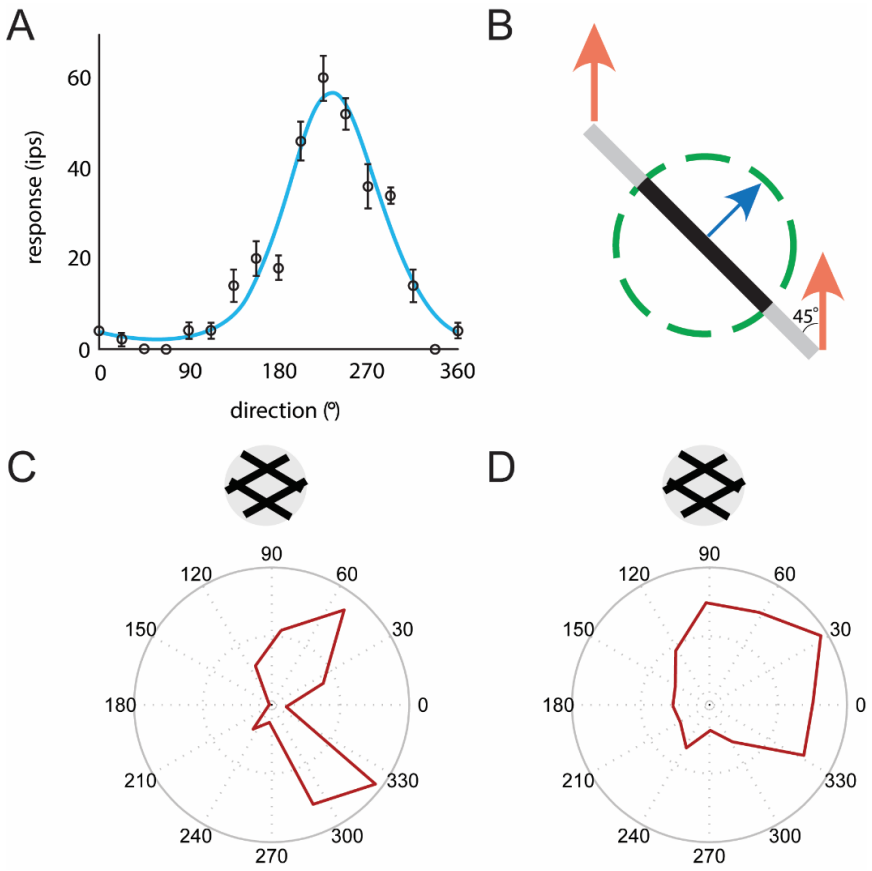

Figure 1.11. Motion coding in APC. Al Direction tuning of a neuron in area 3b to bars scanned across its receptive field. Adapted from (277). Bl The geometry of the aperture problem. The orange arrows show the actual motion of the bar; the blue arrow shows the motion of the bar as observed through the circular aperture (dashed circle). When an edge is observed through a circular aperture, the only available information about its direction of motion is along the axis perpendicular to its orientation. In other words, no time-varying information is conveyed along the parallel axis. In the example, a bar oriented at 45° and moving upwards at speed s seems to be moving up and to the right with speed s = sin(45°). Neurons in early stages of processing (APC or V1) experience the portion of a stimulus that impinges upon their small RFs, so through the equivalent of an aperture. Cl Response of a neuron in area 1 that responds to the motion of the component gratings but not to the global motion of the plaid. This neuron will respond if either of the component gratings is moving in its preferred direction. Dl Response of a neuron in area 1 that responds to the global motion of the plaid. This neuron's response reflects the integration of local motion cues, each subject to the aperture problem, except those emanating from intersections, which convey unambiguous information about motion direction. Reproduced from (278).

In contrast, some neurons in area 1 integrate information across locally ambiguous motion cues and therefore carry a global motion signal (277) (Figure 1.11D). This ability to recover global motion is analogous to that of direction selective neurons in medial temporal cortex, a brain region specialized for visual motion processing. In fact, the algorithm that is implemented in somatosensory cortex to compute the global direction of tactile motion seems to be identical to its visual counterpart: Motion signals from edges, subject to the aperture problem, and motion signals from terminators (intersections, corners), which convey more reliable information about motion, are integrated using a vector average computation to estimate the global direction of motion. Finally, the responses of APC neurons can account for the ability of human observers to judge the direction of movement across a variety of psychophysical paradigms (276, 277), as has been found with MT neurons (28, 29).

APC neurons are sensitive not only to motion direction but also to motion speed. Indeed, the responses of a large fraction of neurons increase as the speed at which a textured surface is scanned across the skin increases (78). Most of these speed-sensitive neurons also modulate their response to surface texture so the speed signal is confounded by a texture one, particularly in area 3b. This ambiguity between speed and texture is also reflected in psychophysical judgments of speed, which are also influenced by texture (77). Interestingly, judgments of texture are largely independent of speed (24, 220, 242).

1.5.5 | TEXTURE

Our sense of touch endows us with an exquisite sensitivity to surface microstructure which allows us to distinguish satin, from silk, from sandpaper. In fact, we can discriminate textures with

element sizes differing in the tens of nanometers or with spatial periods differing in the hundreds of nanometers (338). Tangible textures thus span a huge range of spatial scales from tens of nanometers to about a centimeter—almost six orders of magnitude. This wide dynamic range is possible because texture perception relies on two distinct mechanisms, each best suited to encode texture over a subrange. The coarse features of a texture produce millimeter-scale deformations in the skin, which evoke a spatial pattern of activation in SA1 (and perhaps RA) fibers. This spatial code can account for the roughness of surfaces that comprise only such features, for example gratings and Braille-like embossed dot patterns (62, 63, 141). However, SA1 fibers are almost completely insensitive to finer textural elements. The perception of these fine features requires movement between skin and surface (155), which in turn elicits texture- and speed-dependent vibrations in the skin (12, 13, 75, 235). These texture-elicited vibrations evoke temporal spiking patterns in mechanoreceptive afferents, particularly RA and PC fibers, which carry information about fine texture at millisecond time scales (233, 380). This combination of spatial coding for coarse textural features and temporal coding for fine ones accounts for the wide dynamic range of tangible textures.

The cortical mechanisms that mediate tactile texture perception have not been conclusively elucidated. To date, experiments investigating texture coding in cortex used gratings (37, 74, 336, 378) and Braille-like embossed dot patterns (25, 53) as stimuli, which robustly engage SA1 fibers and discount the contribution of signals from other nerve fibers (380). With this caveat, the responses of APC neurons to gratings and dot patterns have been shown to be modulated by the spatial period of the stimuli. However, a subset of these neurons seems to track the perceived

roughness of such textures (25, 53), consistent with the hypothesis that they are causally implicated in texture perception. Furthermore, lesions of area 1 result in pronounced deficits in texture discrimination (297, 334, 335), so this area may be part of a pathway specialized for texture processing.

The RF structure of cortical neurons may provide clues as to how texture information is encoded in cortex. As mentioned above, many neurons in APC have RFs comprising excitatory subfields flanked by inhibitory ones (82). The precise structure and scale of these RFs varies from neuron to neuron, so APC neurons can be thought of as spatial filters, each differentially sensitive to a textured surface depending on its spatial properties. This category of neurons is well suited to encode coarse spatial features. Some APC neurons integrate signals from RA and PC fibers and do so in different ways (323). These neurons can be thought of as temporal filters, which each respond to skin vibrations, and by extension textures comprising fine features, in different ways. Neurons with idiosyncratic spatial or temporal RF properties thus respond idiosyncratically to a textured surface depending on the spatial scale of its coarse features and on the properties of the vibrations that are elicited in the skin by its fine features, respectively.

LPC responses to gratings are modulated by groove width as well as contact force, and/or scanning speed (291). An individual neuron is likely to respond to two or even three of these parameters, sometimes in an additive manner, and sometimes in more complex ways. LPC is implicated in texture perception as evidenced by the modulation of LPC responses by both groove width and contact force, two parameters known to determine the perceived roughness of gratings (219, 222, 359), and by the impairment in roughness discrimination caused by lesions

of LPC (255). Furthermore, some LPC neurons encode the presence, but not magnitude, of a change in the spatial pattern of a texture, in a same/different task, another example of task-specific modulation (181).

1.5.6 | STEREOGNOSIS

A fascinating aspect of somatosensation is that it comprises a deformable sensory sheet: changes in hand posture reconfigure the positions of cutaneous mechanoreceptors with respect to one another. To interpret signals from cutaneous mechanoreceptors thus requires taking into account their positions relative to one another (156, 306). This integration of touch and proprioception is particularly critical for stereognosis, the ability to sense the three dimensional structure of objects grasped in the hand: Cutaneous input from each fingertip contacting the object provides a snapshot of its shape at each contact point (local edge orientation or surface curvature, e.g.), and the relative position of the fingertips conveys information of the size and global shape of the object, as well as about the relative position of the local features relative to one another.

Virtually nothing is known about how this takes place in the somatosensory system. However, area 2 is the first location along the somatosensory neuraxis where neurons exhibit both cutaneous and proprioceptive responses (165, 171, 172, 206). That is, their firing rates are modulated both by light touch and joint configuration (Figure 1.12) so the process of constructing a three dimensional representation of objects likely begins there. Some evidence suggests that cutaneous and proprioceptive inputs interact in complex ways in area 2, and the temporal progression of these interactions may reflect the dynamics of a circuit involved in stereognosis (206). However, stereognosis requires active movements (221) but the challenges

associated with tracking both hand postures and contact events have, to date, precluded the study of active stereognosis.

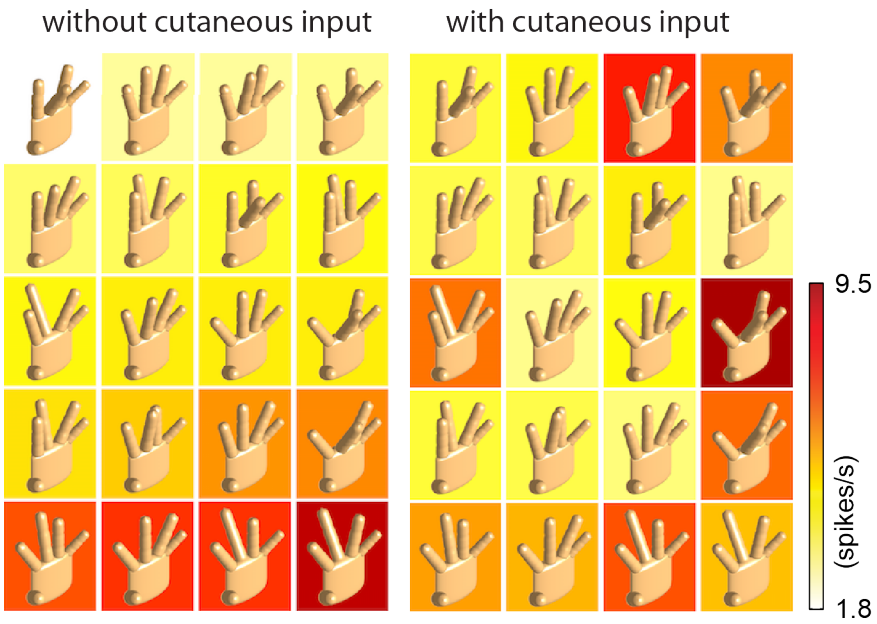

Figure 1.12. Neuron in area 2 that exhibits both tactile and proprioceptive responses (courtesy of Sung Soo Kim, see (206)). This neuron's activity is modulated when the hand is placed in different configurations using a motorized apparatus (left panel). However, responses are further modulated by cutaneous stimulation, consisting of edges indented into the skin (right panel). The neuron's response is a complex function of hand conformation and cutaneous input.

1.6 | ATTENTION AND DECISION MAKING IN THE SOMATOSENSORY SYSTEM

Our bodies are constantly and simultaneously touched in many ways – through contact with our clothes, the ground, grasped objects, etc. – most of which are of little relevance at any given time. As is the case in other sensory modalities, certain sources of sensory input can be magnified relative to others through the deployment of attention. The consequences of attention on neuronal responses are typically probed by presenting a stimulus that is relevant to the performance of a task (and so attention is deployed towards it) or that is not (and so attention is

diverted away from it, to another sensory stimulus for example). Comparison of responses to the same stimulus in the attended vs. unattended conditions, then, reveals the effects of attention. In visual cortex, for example, responses to the attended stimulus have been shown to be enhanced relative to those to the same stimulus, unattended (232, 247, 369).

Attention is thought to enhance the contrast of behaviorally relevant inputs by increasing the gain for cells that play a role in detecting a stimulus at a particular location on the skin (52). Responses of neurons in the early stages of somatosensory processing to a stimulus are relatively impervious to modulations by behavioral relevance. Indeed, responses to a stimulus in VP (VPL and VPM, thalamus) are equivalent whether the animal is attending to it or not (41, 368, 373). As few as 16% and as many 50% of APC neurons have been reported to show attentional modulation (38, 157, 244). Caudal APC exhibits a greater degree of attentional modulation than does rostral APC, again consistent with their respective positions along the somatosensory hierarchy (167, 168, 244) as attentional effects tend to be stronger in higher sensory areas (239). The type and magnitude of these effects varies across studies, with some reporting that nearly all attentionally modulated neurons show enhanced activity (157, 244) and others observing mostly suppressed activity (38). The proportion of attention-sensitive cells is greater in LPC than in APC, ranging from 60-80% (39, 157, 244) and the magnitude of the attentional effects are greater in LPC. Enhancement of activity seen in LPC seems to target neurons that encode behaviorally relevant stimulus features, e.g. texture, while attentional gain increases in APC neurons are less stimulus dependent (244), perhaps reflecting the weaker feature selectivity at earlier stages of cortical processing.

Increases in neural synchrony constitute another neural correlate of attention in the sensory cortices (319, 345). That is, the degree to which nearby neurons fire in synchrony increases with selective attention. Such observations have been made in APC (257), in LPC (319, 345), in posterior parietal cortex (79), and in other sensory modalities (e.g. visual cortex , 120).

1.7 | AFFECTIVE TOUCH

Touch plays a critical role in emotion and affective communication: we touch the people we care about and derive comfort from the touch of a loved one (153). The importance of touch is highlighted in studies showing that the texture of a mother surrogate has a major impact on its effectiveness as a surrogate, and deprivation of affective touch during development leads to severe emotional problems (147, 148, 379). Affective touch is mediated by fundamentally different neural mechanisms than is discriminative touch (241). First, affective touch may rely, at least in part, on different receptors. Indeed, C-tactile afferents, which innervate the hairy skin, respond most strongly to stimuli brushed across the skin that are experienced as pleasant (229), suggesting that these nerve fibers convey information about the affective quality of a stimulus rather than its physical properties. Second, signals from these fibers have been shown to bypass APC (45, 266, 267) and instead target the insula, which is associated with affective coding (22, 248). While C-tactile afferent fibers do not innervate the glabrous skin, it is commonly observed that touch with the glabrous skin can also be perceived as pleasant (208, 209). Pleasant touch involving the glabrous skin may thus be processed separately from its hairy skin counterpart, the former by somatosensory cortex, the latter by the limbic system (134, 240). Affective touch with the glabrous skin typically involves self-generated movement while affective touch with the hairy

skin results from external stimulation, which may explain why the two categories of touch are processed separately.

1.8 | ARTIFICIAL SOMATOSENSATION THROUGH INTRACORTICAL MICROSTIMUTION IN APC

When Wilder Penfield and colleagues applied electrical stimuli to the surface of APC searching for epileptic foci, patients reported tactile sensations, the location of which depended systematically on where the stimulus was delivered (279). Later, Romo and colleagues showed that monkeys could learn to distinguish the frequency of low-amplitude electrical pulse trains delivered to APC (313). In other words, changes in one stimulation parameter – frequency – systematically changed the evoked sensory experience. While this work had important scientific implications about how stimulus information is encoded in the nervous system, it also laid the foundation for somatosensory neuroprostheses. Indeed, one approach to restoring some independence to tetraplegic patients – who are paralyzed and insensate from the neck down – is to equip them with prosthetic arms that they can control by thought alone. The development of anthropomorphic robotic limbs and of algorithms to decode intended movements from brain signals led to a much more sophisticated movement repertoire (61). This newfound function established the need to restore somatosensation, without which movements are slow, clumsy, and effortful (139, 325).

In experiments with monkeys (353), intracortical microstimulation (ICMS) was shown to elicit percepts that are highly localized – to a single fingerpad or palmar whorl – much more so than are percepts evoked by electrical stimulation of the surface of APC, as in Penfield's experiments (191, 353). The somatotopic map within APC can thus be exploited to intuitively convey

information about the points of contact between prosthetic hand and object. Furthermore, changes in ICMS amplitude produce systematic changes in the magnitude of the evoked sensation, a phenomenon that can be used to intuitively convey information about contact pressure (18, 205, 353, 354). The success of primate studies has led to the deployment of this approach in human patients, who report tactile sensations that are nearly natural (108, 207).

The development of artificial proprioception is more challenging because much less is known about the cortical basis for natural proprioception. However, monkeys are able to detect and discriminate different patterns of electrical stimulation applied to area 3a (230), and some evidence even suggests that stimulation of neurons that are selective for a particular direction of limb movement biases the monkeys' perceived limb movement towards that direction of movement (361). This latter finding suggests that it may be possible to create sensations of directed limb movement by stimulating populations of APC neurons with consistent preferred directions to track the movements of the prosthesis. If tapping into natural proprioceptive representations proves too challenging, it may be possible to develop novel but systematic mappings between limb state and ICMS-evoked patterns of neuronal activation that the patients would have to learn (69). Whether learning-based approaches will scale to accommodate the complexity of a limb remains to be seen (76).

The inclusion of artificial touch and proprioception in brain-controlled prostheses will be an important step in improving the dexterity conferred to their users.

1.9 | References

1. Ackerley R, Backlund Wasling H, Liljencrantz J, Olausson H, Johnson RD, Wessberg J. Human C-tactile afferents are tuned to the temperature of a skin-stroking caress. J Neurosci 34: 2879–83, 2014.

2. Ageranioti-Bélanger SA, Chapman CE. Discharge properties of neurones in the hand area of primary somatosensory cortex in monkeys in relation to the performance of an active tactile discrimination task. II. Area 2 as compared to areas 3b and 1. Exp brain Res 91: 207–28, 1992.

3. Agnew Z, Wise RJS. Separate Areas for Mirror Responses and Agency within the Parietal Operculum. J Neurosci 28, 2008.

4. Andersen RA, Asanuma C, Essick GK, Siegel RM. Corticocortical connections of anatomically and physiologically defined subdivisions within the inferior parietal lobule. J Comp Neurol 296: 65–113, 1990.

5. Andersen RA, Buneo CA. Intentional maps in posterior parietal cortex. Annu Rev Neurosci 25: 189–220, 2002.

6. Apkarian AV, Shi T. Squirrel monkey lateral thalamus. I. Somatic nociresponsive neurons and their relation to spinothalamic terminals. J Neurosci 14: 6779–6795, 1994.

7. Ashaber M, Pálfi E, Friedman RM, Palmer C, Jákli B, Chen LM, Kántor O, Roe AW, Négyessy L. Connectivity of somatosensory cortical area 1 forms an anatomical substrate for the emergence of multifinger receptive fields and complex feature selectivity in the squirrel monkey (Saimiri sciureus). J Comp Neurol 522: 1769–1785, 2014.

8. Augurelle A-S, Smith AM, Lejeune T, Thonnard J-L. Importance of cutaneous feedback in maintaining a secure grip during manipulation of hand-held objects. J Neurophysiol 89: 665–671, 2003.

9. Bell J, Bolanowski SJ, Holmes MH. The structure and function of Pacinian corpuscles: a review. Prog Neurobiol 42: 79–128, 1994.

10. Bengtsson F, Brasselet R, Johansson RS, Arleo A, Jörntell H. Integration of sensory quanta in cuneate nucleus neurons in vivo. PLoS One 8: e56630, 2013.

11. Bensmaia SJ, Denchev PVP V, Dammann 3rd JF, Craig JC, Hsiao SS, Dammann JF. The representation of stimulus orientation in the early stages of somatosensory processing. J Neurosci 28: 776–86, 2008.

12. Bensmaia SJ, Hollins M. The vibrations of texture. Somatosens Mot Res 20: 33–43, 2003.

13. Bensmaia SJ, Hollins M. Pacinian representations of fine surface texture. Percept Psychophys 67: 842–854, 2005.

14. Bensmaia SJ, Hsiao SS, Denchev P V, Killebrew JH, Craig JC. The tactile perception of stimulus orientation. Somatosens Mot Res 25: 49–59, 2008.

15. Bensmaia SJ, Killebrew JH, Craig JC. Influence of visual motion on tactile motion perception. J Neurophysiol 96: 1625–37, 2006.

16. Bensmaia SJ, Tillery SIH. Tactile feedback from the hand. Springer Tracts Adv Robot 95: 143–157, 2014.

17. Bentivoglio M, Rustioni A. Corticospinal neurons with branching axons to the dorsal column nuclei in the monkey. J Comp Neurol 253: 260–276, 1986.

18. Berg JA, Dammann JF, Tenore F V., Tabot GA, Boback JL, Manfredi LR, Peterson ML, Katyal KD, Johannes MS, Makhlin A, Wilcox R, Franklin RK, Vogelstein RJ, Hatsopoulos NG, Bensmaia SJ. Behavioral demonstration of a somatosensory neuroprosthesis. IEEE Trans Neural Syst Rehabil Eng 21: 500–7, 2013.

19. Birznieks I, Jenmalm P, Goodwin AW, Johansson RS. Encoding of direction of fingertip forces by human tactile afferents. J Neurosci 21: 8222–37, 2001.

20. Birznieks I, Macefield VG, Westling G, Johansson RS. Slowly adapting mechanoreceptors in the borders of the human fingernail encode fingertip forces. J Neurosci 29: 9370–9, 2009.

21. Birznieks I, Vickery RM. Spike Timing Matters in Novel Neuronal Code Involved in Vibrotactile Frequency Perception. Curr. Biol. (2017). doi: 10.1016/j.cub.2017.04.011.

22. Björnsdotter M, Löken L, Olausson H, Vallbo AB, Wessberg J. Somatotopic organization of gentle touch processing in the posterior insular cortex. J Neurosci 29: 9314–9320, 2009.

23. Blankenburg F. Evidence for a Rostral-to-Caudal Somatotopic Organization in Human Primary Somatosensory Cortex with Mirror-reversal in Areas 3b and 1. Cereb Cortex 13: 987–993, 2003.

24. Boundy-Singer ZMZM, Saal HP, Bensmaia SJ. Speed Invariance of Tactile Texture Perception. J Neurophysiol 118: jn.00161.2017, 2017.

25. Bourgeon S, Dépeault A, Meftah E-M, Chapman CE. Tactile texture signals in primate primary somatosensory cortex and their relation to subjective roughness intensity. J Neurophysiol 115: 1767–1785, 2016.

26. Breveglieri R. Somatosensory Cells in Area PEc of Macaque Posterior Parietal Cortex. J Neurosci 26: 3679–3684, 2006.

27. Brisben AJ, Hsiao SS, Johnson KO. Detection of vibration transmitted through an object grasped in the hand. J Neurophysiol 81: 1548–58, 1999.

28. Britten KH, Newsome WT, Shadlen MN, Celebrini S, Movshon JA. A relationship between behavioral choice and the visual responses of neurons in macaque MT. Vis Neurosci 13: 87–100, 1996.

29. Britten KH, Shadlen MN, Newsome WT, Movshon JA. The analysis of visual motion: a comparison of neuronal and psychophysical performance. J Neurosci 12: 4745–65, 1992.

30. Burke D, Gandevia SC, Macefield G. Responses to passive movement of receptors in joint, skin and muscle of the human hand. J Physiol 402: 347–361, 1988.

31. Burton H. Corticothalamic connections from the second somatosensory area and neighboring regions in the lateral sulcus of macaque monkeys. Brain Res 309: 367–372, 1984.

32. Burton H, Carlson M. Second somatic sensory cortical area (sii) in a prosimian primate,galago crassicaudatus. J Comp Neurol 247: 200–220, 1986.

33. Burton H, Fabri M. Ipsilateral intracortical connections of physiologically defined cutaneous representations in areas 3b and 1 of macaque monkeys: Projections in the vicinity of the central sulcus. J Comp Neurol 355: 508–538, 1995.

34. Burton H, Fabri M, Alloway K. Cortical areas within the lateral sulcus connected to cutaneous representations in areas 3b and 1: A revised interpretation of the second somatosensory area in macaque monkeys. J Comp Neurol 355: 539–562, 1995.

35. Burton H, Sinclair RJ. Second somatosensory cortical areas in macaque monkeys. 1. Neuronal response to controlled, punctate indentations of glabrous skin on the hand. Brain Res 520: 262–271, 1990.

36. Burton H, Sinclair RJ. Second somatosensory cortical area in macaque monkeys: 2. Neuronal responses to punctate vibrotactile stimulation of glabrous skin on the hand. Brain Res 538: 127–35, 1991.

37. Burton H, Sinclair RJ. Representation of tactile roughness in thalamus and somatosensory cortex. Can J Physiol Pharmacol 72: 546–57, 1994.

38. Burton H, Sinclair RJ. Tactile-spatial and cross-modal attention effects in the primary somatosensory cortical areas 3b and 1-2 of rhesus monkeys. Somatosens Mot Res 17: 213–28, 2000.

39. Burton H, Sinclair RJ, Hong SY, Pruett JR, Whang KC. Tactile-spatial and cross-modal attention effects in the second somatosensory and 7b cortical areas of rhesus monkeys. Somatosens Mot

Res 14: 237–67, 1997.

40. Bushnell MC, Duncan GH. Mechanical response properties of ventroposterior medial thalamic neurons in the alert monkey. Exp Brain Res 67: 4–7, 1987.

41. Camarillo L, Luna R, Nácher V, Romo R. Coding perceptual discrimination in the somatosensory thalamus. Proc Natl Acad Sci Unites States Am 109: 21093–8, 2012.

42. Caminiti R, Borra E, Visco-Comandini F, Battaglia-Mayer A, Averbeck BB, Luppino G. Computational Architecture of the Parieto-Frontal Network Underlying Cognitive-Motor Control in Monkeys. Eneuro 4: ENEURO.0306-16.2017, 2017.

43. Cappe C, Morel A, Rouiller EM. Thalamocortical and the dual pattern of corticothalamic projections of the posterior parietal cortex in macaque monkeys. Neuroscience 146: 1371–1387, 2007.

44. Carlson M. Characteristics of sensory deficits following lesions of Brodmann's areas 1 and 2 in the postcentral gyrus of Mococo mulatto. Brain Res 204: 424–430, 1981.

45. Case LK, Laubacher CM, Olausson H, Wang B, Spagnolo PA, Bushnell MC. Encoding of Touch Intensity But Not Pleasantness in Human Primary Somatosensory Cortex. J Neurosci 36: 5850–5860, 2016.

46. Cauna N. Nerve supply and nerve endings in Meissner's corpuscles. Am J Anat 99: 315–350, 1956.

47. Cauna N. The mode of termination of the sensory nerves and its significance. J Comp Neurol 113: 169–209, 1959.

48. Cauna N, ROSS LL. The fine structure of Meissner's touch corpuscles of human fingers. J Biophys Biochem Cytol 8: 467–82, 1960.

49. Cavada C, Goldman-Rakic PS. Posterior parietal cortex in rhesus monkey: II. Evidence for segregated corticocortical networks linking sensory and limbic areas with the frontal lobe. J Comp Neurol 287: 422–45, 1989.

50. Cavada C, Goldman-Rakic PS. Posterior parietal cortex in rhesus monkey: I. Parcellation of areas based on distinctive limbic and sensory corticocortical connections. J Comp Neurol 287: 393–421, 1989.

51. Chapman CE, Bushnell MC, Miron D, Duncan GH, Lund JP. Sensory perception during movement in man. Exp Brain Res 68: 516–524, 1987.

52. Chapman CE, Meftah E-M. Independent Controls of Attentional Influences in Primary and

Secondary Somatosensory Cortex. J Neurophysiol 94: 4094–4107, 2005.

53. Chapman CE, Tremblay F, Jiang W, Belingard L, Meftah E-M. Central neural mechanisms contributing to the perception of tactile roughness. Behav Brain Res 135: 225–33, 2002.

54. Cheema S, Whitsel BL, Rustioni A. The corticocuneate pathway in the cat: relations among terminal distribution patterns, cytoarchitecture, and single neuron functional properties. Somatosens Res 1: 169–205, 1983.

55. Chen J, Reitzen SD, Kohlenstein JB, Gardner EP. Neural representation of hand kinematics during prehension in posterior parietal cortex of the macaque monkey. J Neurophysiol 102: 3310–3328, 2009.

56. Chen LM, Friedman RM, Ramsden BM, LaMotte RH, Roe AW. Fine-scale organization of SI (area 3b) in the squirrel monkey revealed with intrinsic optical imaging. J Neurophysiol 86: 3011–29, 2001.

57. Chen LM, Friedman RM, Roe AW. Optical imaging of a tactile illusion in area 3b of the primary somatosensory cortex. Science 302: 881–5, 2003.

58. Cheney PD, Preston JB. Classification and response characteristics of muscle spindle afferents in the primate. J Neurophysiol 39: 1–8, 1976.

59. Cohen DA, Prud'homme MJ, Kalaska JF. Tactile activity in primate primary somatosensory cortex during active arm movements: correlation with receptive field properties. J Neurophysiol 71: 161–72, 1994.

60. Cohen YE, Cohen IS, Gifford GW. Modulation of LIP activity by predictive auditory and visual cues. Cereb Cortex 14: 1287–1301, 2004.

61. Collinger JL, Wodlinger B, Downey JE, Wang W, Tyler-Kabara EC, Weber DJ, McMorland AJC, Velliste M, Boninger ML, Schwartz AB. High-performance neuroprosthetic control by an individual with tetraplegia. Lancet 381: 557–564, 2013.

62. Connor CE, Hsiao SS, Phillips JR, Johnson KO. Tactile roughness: neural codes that account for psychophysical magnitude estimates. J Neurosci 10: 3823–36, 1990.

63. Connor CE, Johnson KO. Neural coding of tactile texture: comparison of spatial and temporal mechanisms for roughness perception. J Neurosci 12: 3414–26, 1992.

64. Cooke DF, Goldring AB, Baldwin MKL, Recanzone GH, Chen A, Pan T, Simon SI, Krubitzer LA. Reversible deactivation of higher-order posterior parietal areas. I. Alterations of receptive field characteristics in early stages of neocortical processing. J Neurophysiol 112: 2529–2544, 2014.

65. Costanzo RM, Gardner EP. A quantitative analysis of responses of direction-sensitive neurons in somatosensory cortex of awake monkeys. J Neurophysiol 43: 1319–1341, 1980.

66. Costanzo RM, Gardner EP. Multiple-joint neurons in somatosensory cortex of awake monkeys. Brain Res 214: 321–333, 1981.

67. Craig AD. Retrograde analyses of spinothalamic projections in the macaque monkey: input to ventral posterior nuclei. J Comp Neurol 499: 965–78, 2006.

68. Cusick CG, Gould HJ. Connections between area 3b of the somatosensory cortex and subdivisions of the ventroposterior nuclear complex and the anterior pulvinar nucleus in squirrel monkeys. J Comp Neurol 292: 83–102, 1990.

69. Dadarlat MC, O'Doherty JE, Sabes PN. A learning-based approach to artificial sensory feedback leads to optimal integration. Nat Neurosci 18: 138–44, 2015.

70. Darian-Smith C, Darian-Smith I, Burman K, Ratcliffe N. Ipsilateral cortical projections to areas 3a, 3b, and 4 in the macaque monkey. J Comp Neurol 335: 200–213, 1993.

71. Darian-Smith C, Darian-Smith I, Cheema SS. Thalamic projections to sensorimotor cortex in the macaque monkey: use of multiple retrograde fluorescent tracers. J Comp Neurol 299: 17–46, 1990.

72. Darian-Smith C, Tan A, Edwards S. Comparing thalamocortical and corticothalamic microstructure and spatial reciprocity in the macaque ventral posterolateral nucleus (VPLc) and medial pulvinar. J Comp Neurol 410: 211–234, 1999.

73. Darian-Smith I. The Sense of Touch: Performance and Peripheral Neural Processes. In: Comprehensive Physiology. Hoboken, NJ, USA: John Wiley & Sons, Inc., 2011.

74. Darian-Smith I, Sugitani M, Heywood J, Karita K, Goodwin AW. Touching textured surfaces: cells in somatosensory cortex respond both to finger movement and to surface features. Science 218: 906–9, 1982.

75. Delhaye BP, Hayward V, Lefèvre P, Thonnard J-L. Texture-induced vibrations in the forearm during tactile exploration. Front Behav Neurosci 6: 37, 2012.

76. Delhaye BP, Saal HP, Bensmaia SJ. Key considerations in designing a somatosensory neuroprosthesis. J Physiol 110: 402–408, 2016.

77. Dépeault A, Meftah E-M, Chapman CE. Tactile speed scaling: contributions of time and space. J Neurophysiol 99: 1422–34, 2008.

78. Dépeault A, Meftah E-M, Chapman CE. Neuronal correlates of tactile speed in primary

somatosensory cortex. J. Neurophysiol. (July 10, 2013). doi: 10.1152/jn.00675.2012.

79. Desmedt JE, Tomberg C. Transient phase-locking of 40 Hz electrical oscillations in prefrontal and parietal human cortex reflects the process of conscious somatic perception. Neurosci Lett 168: 126–129, 1994.

80. DiCarlo JJ, Johnson KO. Velocity invariance of receptive field structure in somatosensory cortical area 3b of the alert monkey. J Neurosci 19: 401–19, 1999.

81. DiCarlo JJ, Johnson KO. Spatial and temporal structure of receptive fields in primate somatosensory area 3b: effects of stimulus scanning direction and orientation. J Neurosci 20: 495–510, 2000.

82. DiCarlo JJ, Johnson KO, Hsiao SS. Structure of receptive fields in area 3b of primary somatosensory cortex in the alert monkey. J Neurosci 18: 2626–45, 1998.

83. Dimitriou M, Edin BB. Discharges in human muscle spindle afferents during a key-pressing task. J Physiol 586: 5455–70, 2008.

84. Dimitriou M, Edin BB. Discharges in human muscle receptor afferents during block grasping. J Neurosci 28: 12632–42, 2008.

85. Disbrow E. Thalamocortical connections of the parietal ventral area (PV) and the second somatosensory area (S2) in macaque monkeys. Thalamus Relat Syst 1: 289–302, 2002.

86. Disbrow E, Litinas E, Recanzone GH, Padberg J, Krubitzer LA. Cortical connections of the second somatosensory area and the parietal ventral area in macaque monkeys. J Comp Neurol 462: 382–399, 2003.

87. Disbrow E, Roberts T, Krubitzer LA. Somatotopic organization of cortical fields in the lateral sulcus of Homo sapiens: Evidence for SII and PV. J Comp Neurol 418: 1–21, 2000.

88. Disbrow E, Roberts T, Poeppel D, Krubitzer LA. Evidence for interhemispheric processing of inputs from the hands in human S2 and PV. J Neurophysiol 85: 2236–44, 2001.

89. Dong WK, Chudler EH, Sugiyama K, Roberts VJ, Hayashi T. Somatosensory, multisensory, and task-related neurons in cortical area 7b (PF) of unanesthetized monkeys. J Neurophysiol 72: 542–564, 1994.

90. Dykes RW. Parallel processing of somatosensory information: A theory. Brain Res Rev 6: 47–115, 1983.

91. Dykes RW, Rasmusson DD, Sretavan D, Rehman NB. Submodality segregation and receptive-field sequences in cuneate, gracile, and external cuneate nuclei of the cat. J Neurophysiol 47:

389–416, 1982.

92. Edin BB. Quantitative analysis of static strain sensitivity in human mechanoreceptors from hairy skin. J Neurophysiol 67: 1105–13, 1992.

93. Edin BB. Cutaneous afferents provide information about knee joint movements in humans. J Physiol 531: 289–97, 2001.

94. Edin BB. Quantitative analyses of dynamic strain sensitivity in human skin mechanoreceptors. J Neurophysiol 92: 3233–43, 2004.

95. Edin BB, Vallbo AB. Dynamic response of human muscle spindle afferents to stretch. J Neurophysiol 63: 1297–306, 1990.

96. Edin BB, Vallbo AB. Muscle afferent responses to isometric contractions and relaxations in humans. J Neurophysiol 63: 1307–13, 1990.

97. Eickhoff SB, Amunts K, Mohlberg H, Zilles K. The human parietal operculum. II. Stereotaxic maps and correlation with functional imaging results. Cereb Cortex 16: 268–279, 2006.

98. Eickhoff SB, Schleicher A, Zilles K, Amunts K. The human parietal operculum. I. Cytoarchitectonic mapping of subdivisions. Cereb Cortex 16: 254–267, 2006.

99. Ergenzinger ER, Glasier MM, Hahm JO, Pons TP. Cortically induced thalamic plasticity in the primate somatosensory system. Nat Neurosci 1: 226–229, 1998.

100. Essick GK, Bredehoeft KR, McLaughlin DF, Szaniszlo J a. Directional sensitivity along the upper limb in humans. Somatosens Mot Res 8: 13–22, 1991.

101. Essick GK, Franzén O, Whitsel BL, Franzen O, Whitsel BL. Discrimination and scaling of velocity of stimulus motion across the skin. Somatosens Mot Res 6: 21–40, 1988.

102. Essick GK, Whitsel BL. Assessment of the capacity of human subjects and S-I neurons to distinguish opposing directions of stimulus motion across the skin. Brain Res Rev 10: 187–212, 1985.

103. Etzel JA, Gazzola V, Keysers C, Rotte M, Drescher D. Testing Simulation Theory with Cross-Modal Multivariate Classification of fMRI Data. PLoS One 3: e3690, 2008.

104. Felleman DJ, Van Essen DC. Distributed hierarchical processing in the primate cerebral cortex. Cereb Cortex 1: 1–47, 1991.

105. Fitzgerald PJ, Lane JW, Thakur PH, Hsiao SS. Receptive field properties of the macaque second somatosensory cortex: evidence for multiple functional representations. J Neurosci 24: 11193–

204, 2004.

106. Fitzgerald PJ, Lane JW, Thakur PH, Hsiao SS. Receptive field (RF) properties of the macaque second somatosensory cortex: RF size, shape, and somatotopic organization. J Neurosci 26: 6485–95, 2006.

107. Fitzgerald PJ, Lane JW, Thakur PH, Hsiao SS. Receptive field properties of the macaque second somatosensory cortex: representation of orientation on different finger pads. J Neurosci 26: 6473–84, 2006.

108. Flesher SN, Collinger JL, Foldes ST, Weiss JM, Downey JE, Tyler-Kabara EC, Bensmaia SJ, Schwartz AB, Boninger ML, Gaunt RA. Intracortical microstimulation of human somatosensory cortex. Sci Transl Med 8: 361ra141-361ra141, 2016.

109. Fogassi L, Luppino G. Motor functions of the parietal lobe. Curr Opin Neurobiol 15: 626–631, 2005.

110. Fortier-Poisson P, Langlais J-S, Smith AM. Correlation of fingertip shear force direction with somatosensory cortical activity in monkey. J Neurophysiol 115: jn.00749.2014, 2015.

111. Fortier-Poisson P, Smith AM. Neuronal activity in somatosensory cortex related to tactile exploration. J Neurophysiol 115: jn.00747.2014, 2015.

112. Freeman AW, Johnson KO. A model accounting for effects of vibratory amplitude on responses of cutaneous mechanoreceptors in macaque monkey. J Physiol 323: 43–64, 1982.

113. Freeman AW, Johnson KO. Cutaneous mechanoreceptors in macaque monkey: temporal discharge patterns evoked by vibration, and a receptor model. J Physiol 323: 21–41, 1982.

114. Freund HJ. The parietal lobe as a sensorimotor interface: a perspective from clinical and neuroimaging data. Neuroimage 14: S142–S146, 2001.

115. Friedman DP, Jones EG. Thalamic input to areas 3a and 2 in monkeys. J Neurophysiol 45: 59–85, 1981.

116. Friedman DP, Murray EA. Thalamic connectivity of the second somatosensory area and neighboring somatosensory fields of the lateral sulcus of the macaque. J Comp Neurol 252: 348–373, 1986.

117. Friedman DP, Murray EA, O'Neill JB, Mishkin M. Cortical connections of the somatosensory fields of the lateral sulcus of macaques: Evidence for a corticolimbic pathway for touch. J Comp Neurol 252: 323–347, 1986.

118. Friedman RM, Chen LM, Roe AW. Modality maps within primate somatosensory cortex. Proc

Natl Acad Sci U S A 101: 12724–9, 2004.

119. Friedman RM, Chen LM, Roe AW. Responses of areas 3b and 1 in anesthetized squirrel monkeys to single- and dual-site stimulation of the digits. J Neurophysiol 100: 3185–3196, 2008.

120. Fries P, Reynolds JH, Rorie AE, Desimone R. Modulation of oscillatory neuronal synchronization by selective visual attention. Science 291: 1560–3, 2001.

121. Frohlich PF, Meston CM. Tactile Sensitivity in Women with Sexual Arousal Disorder. Arch Sex Behav 34: 207–217, 2005.

122. Fyffe RE, Cheema SS, Rustioni A. Intracellular staining study of the feline cuneate nucleus. I. Terminal patterns of primary afferent fibers. J Neurophysiol 56: 1268–1283, 1986.

123. Gardner EP. Dorsal and Ventral Streams in the Sense of Touch. Senses A Compr Ref 6: 233–258, 2010.

124. Gardner EP, Babu KS, Reitzen SD, Ghosh S, Brown AS, Chen J, Hall AL, Herzlinger MD, Kohlenstein JB, Ro JY. Neurophysiology of Prehension. I. Posterior Parietal Cortex and Object-Oriented Hand Behaviors. J Neurophysiol 97: 387–406, 2007.

125. Gardner EP, Costanzo RM. Temporal integration of multiple-point stimuli in primary somatosensory cortical receptive fields of alert monkeys. J Neurophysiol 43: 444–68, 1980.

126. Gardner EP, Costanzo RM. Neuronal mechanisms underlying direction sensitivity of somatosensory cortical neurons in awake monkeys. J Neurophysiol 43: 1342–54, 1980.

127. Gardner EP, Costanzo RM. Properties of kinesthetic neurons in somatosensory cortex of awake monkeys. Brain Res 214: 301–319, 1981.

128. Gardner EP, Debowy DJ, Ro JY, Ghosh S, Srinivasa Babu K. Sensory monitoring of prehension in the parietal lobe: A study using digital video. Behav Brain Res 135: 213–224, 2002.

129. Gardner EP, Ro JY, Debowy D, Ghosh S. Facilitation of neuronal activity in somatosensory and posterior parietal cortex during prehension. Exp Brain Res 127: 329–354, 1999.

130. Garraghty PE, Florence SL, Kaas JH. Ablations of areas 3a and 3b of monkey somatosensory cortex abolish cutaneous responsivity in area 1. Brain Res 528: 165–169, 1990.

131. Garraghty PE, Florence SL, Tenhula WN, Kaas JH. Parallel thalamic activation of the first and second somatosensory areas in prosimian primates and tree shrews. J Comp Neurol 311: 289–299, 1991.

132. Garraghty PE, Pons TP, Kaas JH. Ablations of areas 3b (SI proper) and 3a of somatosensory cortex in marmosets deactivate the second and parietal ventral somatosensory areas. Somat Mot Res 7: 125–135, 1990.

133. Garraghty PE, Pons TP, Sur M, Kaas JH. The arbors of axons terminating in middle cortical layers of somatosensory area 3b in owl monkeys. Somatosens Mot Res 6: 401–11, 1989.

134. Gazzola V, Spezio ML, Etzel JA, Castelli F, Adolphs R, Keysers C. Primary somatosensory cortex discriminates affective significance in social touch. Proc Natl Acad Sci U S A 109: 10, 2012.

135. Geyer S, Schleicher A, Zilles K. Areas 3a, 3b, and 1 of human primary somatosensory cortex. Neuroimage 10: 63–83, 1999.

136. Geyer S, Schormann T, Mohlberg H, Zilles K. Areas 3a, 3b, and 1 of human primary somatosensory cortex. Part 2. Spatial normalization to standard anatomical space. Neuroimage 11: 684–96, 2000.

137. Gharbawie OA, Stepniewska I, Kaas JH. Cortical connections of functional zones in posterior parietal cortex and frontal cortex motor regions in new world monkeys. Cereb Cortex 21: 1981–2002, 2011.

138. Gharbawie OA, Stepniewska I, Qi H-X, Kaas JH. Multiple Parietal–Frontal Pathways Mediate Grasping in Macaque Monkeys. J Neurosci 31: 11660–11677, 2011.

139. Ghez C, Gordon J, Ghilardi MF, Sainburg R. Contributions of vision and proprioception to accuracy in limb movements. The MIT Press, 1995.

140. Goldring AB, Cooke DF, Baldwin MKL, Recanzone GH, Gordon AG, Pan T, Simon SI, Krubitzer LA. Reversible deactivation of higher-order posterior parietal areas. II. Alterations in response properties of neurons in areas 1 and 2. J Neurophysiol 112: 2545–2560, 2014.

141. Goodman JM, Bensmaia SJ. A Variation Code Accounts for the Perceived Roughness of Coarsely Textured Surfaces. Sci Rep 7: 46699, 2017.

142. Goodwin AW, Wheat HE. How is tactile information affected by parameters of the population such as non-uniform fiber sensitivity, innervation geometry and response variability? Behav Brain Res 135: 5–10, 2002.

143. Grefkes C, Fink GR. The functional organization of the intraparietal sulcus in humans and monkeys. J Anat 207: 3–17, 2005.

144. Gregoriou GG, Borra E, Matelli M, Luppino G. Architectonic organization of the inferior parietal convexity of the macaque monkey. J Comp Neurol 496: 422–451, 2006.

145. Grigg P, Greenspan BJ. Response of primate joint afferent neurons to mechanical stimulation of knee joint. J Neurophysiol 40: 1–8, 1977.

146. Guest S, Catmur C, Lloyd D, Spence C. Audiotactile interactions in roughness perception. Exp Brain Res 146: 161–171, 2002.

147. Hansen EW. The Development of Maternal and Infant Behavior in the Rhesus Monkey. Behaviour 27: 107–148, 1966.

148. Harlow HF, F. H. The nature of love. Am Psychol 13: 673–685, 1958.

149. Harvey MA, Saal HP, Dammann 3rd JF, Bensmaia SJ, Dammann JF. Multiplexing Stimulus Information through Rate and Temporal Codes in Primate Somatosensory Cortex. PLoS Biol 11: e1001558, 2013.

150. Hayward V, Terekhov A V, Wong S, Geborek P, Bengtsson F, Jörntell H. Spatio-temporal skin strain distributions evoke low variability spike responses in cuneate neurons. J R Soc Interface 11: 20131015, 2014.

151. Hernández A, Nácher V, Luna R, Zainos A, Lemus L, Alvarez M, Vázquez Y, Camarillo L, Romo R. Decoding a perceptual decision process across cortex. Neuron 66: 300–314, 2010.

152. Hernández A, Zainos A, Romo R. Neuronal correlates of sensory discrimination in the somatosensory cortex. Proc Natl Acad Sci U S A 97: 6191–6196, 2000.

153. Hertenstein M. The communicative functions of touch in adulthood. In: The handbook of touch: Neuroscience, behavioral, and health perspectives., edited by Hertenstein MJ, Weiss SJ. New York, New York, USA: Springer, 2011, p. 299–327.

154. Hihara S, Taoka M, Tanaka M, Iriki A. Visual Responsiveness of Neurons in the Secondary Somatosensory Area and its Surrounding Parietal Operculum Regions in Awake Macaque Monkeys. Cereb Cortex 25: 4535–4550, 2015.

155. Hollins M, Risner SR. Evidence for the duplex theory of tactile texture perception. Percept Psychophys 62: 695–705, 2000.

156. Hsiao SS. Central mechanisms of tactile shape perception. Curr Opin Neurobiol 18: 418–424, 2008.

157. Hsiao SS, O'Shaughnessy DM, Johnson KO. Effects of selective attention on spatial form processing in monkey primary and secondary somatosensory cortex. J Neurophysiol 70: 444–7, 1993.

158. Huerta MF, Pons TP. Primary motor cortex receives input from area 3a in macaques. Brain Res

537: 367–371, 1990.

159. Huffman KJ, Krubitzer LA. Area 3a: Topographic Organization and Cortical Connections in Marmoset Monkeys. Cereb Cortex 11: 849–867, 2001.

160. Hulliger M. The mammalian muscle spindle and its central control. Rev Physiol Biochem Pharmacol 101: 1–110, 1984.

161. Hummelsheim H, Wiesendanger R, Wiesendanger M, Bianchetti M. The projection of low-threshold muscle afferents of the forelimb to the main and external cuneate nuclei of the monkey. Neuroscience 16: 979–987, 1985.

162. Hwang EJ, Hauschild M, Wilke M, Andersen RA. Inactivation of the Parietal Reach Region Causes Optic Ataxia, Impairing Reaches but Not Saccades. Neuron 76: 1021–1029, 2012.

163. Hyvärinen J. Regional distribution of functions in parietal association area 7 of the monkey. Brain Res 206: 287–303, 1981.

164. Hyvärinen J. Posterior parietal lobe of the primate brain. Physiol Rev 62: 1060–1129, 1982.

165. Hyvärinen J, Poranen A. Receptive field integration and submodality convergence in the hand area of the post-central gyrus of the alert monkey. J Physiol 283: 539–56, 1978.

166. Hyvärinen J, Poranen A. Movement-sensitive and direction and orientation-selective cutaneous receptive fields in the hand area of the post-central gyrus in monkeys. J Physiol 283: 523–37, 1978.

167. Hyvärinen J, Poranen A, Jokinen Y. Influence of attentive behavior on neuronal responses to vibration in primary somatosensory cortex of the monkey. J Neurophysiol 43: 870–882, 1980.

168. Iriki A, Tanaka M, Iwamura Y. Attention-induced neuronal activity in the monkey somatosensory cortex revealed by pupillometrics. Neurosci Res 25: 173–181, 1996.

169. Iwamura Y. Hierarchical somatosensory processing. Curr Opin Neurobiol 8: 522–528, 1998.

170. Iwamura Y, Iriki A, Tanaka M. Bilateral hand representation in the postcentral somatosensory cortex. Nature 369: 554–556, 1994.

171. Iwamura Y, Tanaka M. Postcentral neurons in hand region of area 2: their possible role in the form discrimination of tactile objects. Brain Res 150: 662–666, 1978.

172. Iwamura Y, Tanaka M, Sakamoto M, Hikosaka O. Converging patterns of finger representation and complex response properties of neurons in area 1 of the first somatosensory cortex of the conscious monkey. Exp Brain Res 51: 327–337, 1983.

173. Iwamura Y, Tanaka M, Sakamoto M, Hikosaka O. Functional subdivisions representing different finger regions in area 3 of the first somatosensory cortex of the conscious monkey. Exp Brain Res 51: 569–576, 1983.

174. Iwamura Y, Tanaka M, Sakamoto M, Hikosaka O. Diversity in receptive field properties of vertical neuronal arrays in the crown of the postcentral gyrus of the conscious monkey. Exp Brain Res 58: 400–411, 1985.

175. Iwamura Y, Tanaka M, Sakamoto M, Hikosaka O. Vertical neuronal arrays in the postcentral gyrus signaling active touch: a receptive field study in the conscious monkey. Exp Brain Res 58: 412–420, 1985.

176. Iwamura Y, Tanaka M, Sakamoto M, Hikosaka O. Rostrocaudal gradients in the neuronal receptive field complexity in the finger region of the alert monkey's postcentral gyrus. Exp Brain Res 92: 360–368, 1993.

177. Jain N, Catania KC, Kaas JH. Deactivation and reactivation of somatosensory cortex after dorsal spinal cord injury. Nature 386: 495–498, 1997.

178. Jain N, Catania KC, Kaas JH. A histologically visible representation of the fingers and palm in primate area 3b and its immutability following long-term deafferentations. Cereb Cortex 8: 227–236, 1998.

179. Jain N, Florence SL, Kaas JH. Reorganization of Somatosensory Cortex After Nerve and Spinal Cord Injury. News Physiol Sci 13: 143–149, 1998.

180. Jeannerod M, Arbib MA, Rizzolatti G, Sakata H. Grasping objets: The cortical mechanisms of visuomotor transformation. Trends Neurosci 18: 314–320, 1995.

181. Jiang W, Tremblay F, Chapman CE. Neuronal encoding of texture changes in the primary and the secondary somatosensory cortical areas of monkeys during passive texture discrimination. J Neurophysiol 77: 1656–62, 1997.

182. Johansson RS. Tactile sensibility in the human hand: receptive field characteristics of mechanoreceptive units in the glabrous skin area. J Physiol 281: 101–125, 1978.

183. Johansson RS, Flanagan JR. Somatosensation. In: The senses: A comprehensive reference, edited by Gardner E, Kaas JH. San Diego: Academic press, 2008, p. 67–86.

184. Johansson RS, Flanagan JR. Coding and use of tactile signals from the fingertips in object manipulation tasks. Nat Rev Neurosci 10: 345–359, 2009.

185. Johansson RS, Landström U, Lundström R. Sensitivity to edges of mechanoreceptive afferent units innervating the glabrous skin of the human head. Brain Res 244: 27–35, 1982.

186. Johansson RS, Landström U, Lundström R, Landstrom U, Lundstrom R. Responses of mechanoreceptive afferent units in the glabrous skin of the human hand to sinusoidal skin displacements. Brain Res 244: 17–25, 1982.

187. Johansson RS, Vallbo AB. Tactile sensibility in the human hand: relative and absolute densities of four types of mechanoreceptive units in glabrous skin. J Physiol 286: 283–300, 1979.

188. Johansson RS, Vallbo AB. Spatial properties of the population of mechanoreceptive units in the glabrous skin of the human hand. Brain Res 184: 353–366, 1980.

189. Johnson KO. The roles and functions of cutaneous mechanoreceptors. Curr Opin Neurobiol 11: 455–461, 2001.

190. Johnson KO, Lamb GD. Neural mechanisms of spatial tactile discrimination: neural patterns evoked by braille-like dot patterns in the monkey. J Physiol 310: 117–44, 1981.

191. Johnson LA, Wander JD, Sarma D, Su DK, Fetz EE, Ojemann JG. Direct electrical stimulation of the somatosensory cortex in humans using electrocorticography electrodes: a qualitative and quantitative report. J Neural Eng 10: 36021, 2013.

192. Jones EG. Lamination and differential distribution of thalamic afferents within the sensory-motor cortex of the squirrel monkey. J Comp Neurol 160: 167–203, 1975.

193. Jones EG. Lack of collateral thalamocortical projections to fields of the first somatic sensory cortex in monkeys. Exp Brain Res 52: 375–384, 1983.

194. Jones EG, Coulter JD, Hendry SHC. Intracortical connectivity of architectonic fields in the somatic sensory, motor and parietal cortex of monkeys. J Comp Neurol 181: 291–347, 1978.

195. Jones EG, Friedman DP. Projection pattern of functional components of thalamic ventrobasal complex on monkey somatosensory cortex. J Neurophysiol 48: 521–544, 1982.

196. Jörntell H, Bengtsson F, Geborek P, Spanne A, Terekhov A V, Hayward V. Segregation of Tactile Input Features in Neurons of the Cuneate Nucleus. Neuron 83: 1–15, 2014.

197. Kaas JH. What, if anything, is SI? Organization of first somatosensory area of cortex. Physiol Rev 63: 206–231, 1983.

198. Kaas JH, Gharbawie O a., Stepniewska I. The Organization and Evolution of Dorsal Stream Multisensory Motor Pathways in Primates. Front Neuroanat 5: 34, 2011.

199. Kaas JH, Nelson RJ, Sur M, Lin CS, Merzenich MM. Multiple representations of the body within the primary somatosensory cortex of primates. Science 204: 521–523, 1979.

200. Kalaska JF, Caminiti R, Georgopoulos AP. Cortical mechanisms related to the direction of two-dimensional arm movements: relations in parietal area 5 and comparison with motor cortex. Exp Brain Res 51: 247–260, 1983.

201. Kalaska JF, Cohen DAD, Prud'homme M, Hyde ML. Parietal area 5 neuronal activity encodes movement kinematics, not movement dynamics. Exp Brain Res 80: 351–364, 1990.

202. Kalaska JF, Scott SH, Cisek P, Sergio LE. Cortical control of reaching movements. Curr Opin Neurobiol 7: 849–859, 1997.

203. Keysers C, Kaas JH, Gazzola V. Somatosensation in social perception. Nat Rev Neurosci 11: 417–428, 2010.

204. Kim JH, Greenspan JD, Coghill RC, Ohara S, Lenz FA. Lesions Limited to the Human Thalamic Principal Somatosensory Nucleus (Ventral Caudal) Are Associated with Loss of Cold Sensations and Central Pain. J Neurosci 27: 4995–5004, 2007.

205. Kim S, Callier T, Tabot GA, Gaunt RA, Tenore F V., Bensmaia SJ. Behavioral assessment of sensitivity to intracortical microstimulation of primate somatosensory cortex. Proc Natl Acad Sci 112: 15202–15207, 2015.

206. Kim SS, Gomez-Ramirez M, Thakur PH, Hsiao SS. Multimodal Interactions between Proprioceptive and Cutaneous Signals in Primary Somatosensory Cortex. Neuron (2015). doi: 10.1016/j.neuron.2015.03.020.

207. Klaes C, Shi Y, Kellis S, Minxha J, Revechkis B, Andersen RA. A cognitive neuroprosthetic that uses cortical stimulation for somatosensory feedback. J Neural Eng 11: 56024, 2014.

208. Klocker A, Arnould C, Penta M, Thonnard J-L. Rasch-built measure of pleasant touch through active fingertip explorations. Front Neurorobot 6: 1–9, 2012.

209. Klöcker A, Wiertlewski M, Théate V, Hayward V, Thonnard J-L. Physical Factors Influencing Pleasant Touch during Tactile Exploration. PLoS One 8: e79085, 2013.

210. Knibestöl M. Stimulus-response functions of rapidly adapting mechanoreceptors in human glabrous skin area. J Physiol 232: 427–52, 1973.

211. Knibestöl M. Stimulus-response functions of slowly adapting mechanoreceptors in the human glabrous skin area. J Physiol 245: 63–80, 1975.

212. Krubitzer LA, Baldwin MKL. Revisiting Kaas and Colleagues – The homunculus: The discovery of multiple representations within the "primary" somatosensory cortex. In: Revisiting the Classic Studies in Behavioral Neuroscience, edited by Kolb B, Whishaw I. Los Angeles: Sage, 2017, p. 33–54.

213. Krubitzer LA, Calford MB. Five topographically organized fields in the somatosensory cortex of the flying fox: Microelectrode maps, myeloarchitecture, and cortical modules. J Comp Neurol 317: 1–30, 1992.

214. Krubitzer LA, Clarey J, Tweedale R, Elston G, Calford MB. A redefinition of somatosensory areas in the lateral sulcus of macaque monkeys. J Neurosci 15: 3821–39, 1995.

215. Krubitzer LA, Huffman KJ, Disbrow E, Recanzone G. Organization of Area 3a in Macaque Monkeys: Contributions to the Cortical Phenotype. J Comp Neurol 471: 97–111, 2004.

216. Krubitzer LA, Kaas JH. The organization and connections of somatosensory cortex in marmosets. J Neurosci 10: 952–74, 1990.

217. Krubitzer LA, Kaas JH. The somatosensory thalamus of monkeys: Cortical connections and a redefinition of nuclei in marmosets. J Comp Neurol 319: 123–140, 1992.

218. de Lafuente V, Romo R. Neural correlate of subjective sensory experience gradually builds up across cortical areas. Proc Natl Acad Sci U S A 103: 14266–14271, 2006.

219. Lederman SJ. Tactile roughness of grooved surfaces: The touching process and effects of macro- and microsurface structure. Percept Psychophys 16: 385–395, 1974.

220. Lederman SJ. Tactual roughness perception: spatial and temporal determinants. Can J Psychol 37: 498–511, 1983.

221. Lederman SJ, Klatzky RL. Hand movements: a window into haptic object recognition. Cogn Psychol 19: 342–68, 1987.

222. Lederman SJ, Taylor MM. Fingertip force, surface geometry, and the perception of roughness by active touch. Percept Psychophys 12: 401–408, 1972.

223. Leinonen L, Hyvärinen J, Nyman G, Linnankoski I. I. Functional properties of neurons in lateral part of associative area 7 in awake monkeys. Exp Brain Res 34: 299–320, 1979.

224. Leinonen L, Nyman G. II. Functional properties of cells in anterolateral part of area 7 associative face area of awake monkeys. Exp Brain Res 34: 321–333, 1979.

225. Lenz FA, Seike M, Lin YC, Baker FH, Rowland LH, Gracely RH, Richardson RT. Neurons in the area of human thalamic nucleus ventralis caudalis respond to painful heat stimuli. Brain Res 623: 235–240, 1993.

226. Lewis JW, Van Essen DC. Mapping of architectonic subdivisions in the macaque monkey, with emphasis on parieto-occipital cortex. J Comp Neurol 428: 79–111, 2000.

227. Lewis JW, Van Essen DC. Corticocortical connections of visual, sensorimotor, and multimodal processing areas in the parietal lobe of the macaque monkey. J Comp Neurol 428: 112–137, 2000.

228. Liu XB, Honda CN, Jones EG. Distribution of four types of synapse on physiologically identified relay neurons in the ventral posterior thalamic nucleus of the cat. J Comp Neurol 352: 69–91, 1995.

229. Löken LS, Wessberg J, Morrison I, McGlone F, Olausson H. Coding of pleasant touch by unmyelinated afferents in humans. Nat Neurosci 12: 547–548, 2009.

230. London BM, Jordan LR, Jackson CR, Miller LE. Electrical Stimulation of the Proprioceptive Cortex (Area 3a) Used to Instruct a Behaving Monkey. 16: 32–36, 2008.

231. London BM, Miller LE. Responses of somatosensory area 2 neurons to actively and passively generated limb movements. J Neurophysiol 109: 1505–13, 2013.

232. Luck SJ, Chelazzi L, Hillyard S a, Desimone R. Neural mechanisms of spatial selective attention in areas V1, V2, and V4 of macaque visual cortex. J Neurophysiol 77: 24–42, 1997.

233. Mackevicius EL, Best MD, Saal HP, Bensmaia SJ. Millisecond precision spike timing shapes tactile perception. J Neurosci 32: 15309–17, 2012.

234. Makous JC, Friedman RM, Vierck CJ. Effects of a dorsal column lesion on temporal processing within the somatosensory system of primates. Exp Brain Res 112: 253–267, 1996.

235. Manfredi LR, Saal HP, Brown KJ, Zielinski MC, Dammann JF, Polashock VS, Bensmaia SJ. Natural scenes in tactile texture. J Neurophysiol 111: 1792–802, 2014.

236. Marasco PD, Kim K, Colgate JE, Peshkin MA, Kuiken TA. Robotic touch shifts perception of embodiment to a prosthesis in targeted reinnervation amputees. Brain 134: 747–758, 2011.

237. Marconi B, Genovesio A, Battaglia-Mayer A, Ferraina S, Squatrito S, Molinari M, Lacquaniti F, Caminiti R. Eye-Hand Coordination during Reaching. I. Anatomical Relationships between Parietal and Frontal Cortex. Cereb Cortex 11: 513–527, 2001.

238. Matthews BH. Nerve endings in mammalian muscle. J Physiol 78: 1–53, 1933.

239. Maunsell JHR, Cook EP. The role of attention in visual processing. Philos Trans R Soc B Biol Sci 357: 1063–1072, 2002.

240. Mcglone F, Olausson H, Boyle JA, Jones-Gotman M, Dancer C, Guest S, Essick GK. Touching and feeling: Differences in pleasant touch processing between glabrous and hairy skin in humans. Eur J Neurosci 35: 1782–1788, 2012.

241. McGlone F, Reilly D. The cutaneous sensory system. Neurosci Biobehav Rev 34: 148–59, 2010.

242. Meftah E-M, Belingard L, Chapman CE. Relative effects of the spatial and temporal characteristics of scanned surfaces on human perception of tactile roughness using passive touch. Exp brain Res 132: 351–61, 2000.

243. Meftah E-M, Bourgeon S, Chapman CE. Instructed delay discharge in primary and secondary somatosensory cortex within the context of a selective attention task. J Neurophysiol 101: 2649–2667, 2009.

244. Meftah E-M, Shenasa J, Chapman CE. Effects of a cross-modal manipulation of attention on somatosensory cortical neuronal responses to tactile stimuli in the monkey. J Neurophysiol 88: 3133–49, 2002.

245. Mima T, Nagamine T, Nakamura K, Shibasaki H. Attention modulates both primary and second somatosensory cortical activities in humans: A magnetoencephalographic study. J Neurophysiol 80: 2215–2221, 1998.

246. Mishkin M. Analogous neural models for tactual and visual learning. Neuropsychologia 17: 139–151, 1979.

247. Moran J, Desimone R. Selective attention gates visual processing in the extrastriate cortex. Science 229: 782–784, 1985.

248. Morrison I, Björnsdotter M, Olausson H. Vicarious Responses to Social Touch in Posterior Insular Cortex Are Tuned to Pleasant Caressing Speeds. J Neurosci 31: 9554–9562, 2011.

249. Mountcastle VB. The sensory hand: neural mechanisms of somatic sensation. Harvard University Press, 2005.

250. Mountcastle VB. Central Nervous Mechanisms in Mechanoreceptive Sensibility. In: Comprehensive Physiology. Hoboken, NJ, USA: John Wiley & Sons, Inc., 2011, p. 33–89.

251. Mountcastle VB, Lynch JC, Georgopoulos A, Sakata H, Acuña C. Posterior parietal association cortex of the monkey: command functions for operations within extrapersonal space. J Neurophysiol 38: 871–908, 1975.

252. Mountcastle VB, Talbot WH, Sakata H, Hyvärinen J. Cortical neuronal mechanisms in flutter-vibration studied in unanesthetized monkeys. Neuronal periodicity and frequency discrimination. J Neurophysiol 32: 452–84, 1969.

253. Muniak MA, Ray S, Hsiao SS, Dammann JFJF, Bensmaia SJ. The neural coding of stimulus intensity: linking the population response of mechanoreceptive afferents with psychophysical behavior. J Neurosci 27: 11687–99, 2007.

254. Murata A, Gallese V, Luppino G, Kaseda M, Sakata H. Selectivity for the Shape, Size, and Orientation of Objects for Grasping in Neurons of Monkey Parietal Area AIP. J Neurophysiol 83: 2580–2601, 2000.

255. Murray EA, Mishkin M. Relative contributions of SII and area 5 to tactile discrimination in monkeys. Behav Brain Res 11: 67–83, 1984.

256. Murray JD, Bernacchia A, Freedman DJ, Romo R, Wallis JD, Cai X, Padoa-Schioppa C, Pasternak T, Seo H, Lee D, Wang X-J. A hierarchy of intrinsic timescales across primate cortex. Nat Neurosci 17: 1661–3, 2014.

257. Murthy VN, Fetz EE. Coherent 25- to 35-Hz oscillations in the sensorimotor cortex of awake behaving monkeys. Proc Natl Acad Sci U S A 89: 5670–4, 1992.

258. Nakatani M, Maksimovic S, Baba Y, Lumpkin EA. Mechanotransduction in epidermal Merkel cells. Pflugers Arch. (July 23, 2014). doi: 10.1007/s00424-014-1569-0.

259. Neal JW, Pearson RC a, Powell TPS. The cortico-cortical connections of area-7b, PF, in the parietal lobe of the monkey. Brain Res 419: 341–6, 1987.

260. Neal JW, Pearson RCA, Powell TPS. The ipsilateral cortico-cortical connections of area 7b, PF, in the parietal and temporal lobes of the monkey. Brain Res 524: 119–132, 1990.

261. Nelson RJ. Activity of monkey primary somatosensory cortical neurons changes prior to active movement. Brain Res 406: 402–407, 1987.

262. Nelson RJ, Sur M, Felleman DJ, Kaas JH. Representations of the body surface in postcentral parietal cortex of Macaca fascicularis. J Comp Neurol 192: 611–43, 1980.

263. Newman HF. Vibratory Sensitivity of the Penis. Fertil Steril 21: 791–793, 1970.

264. Niu J, Ding L, Li J, Kim H, Liu J, Li H, Moberly A, Badea T, Duncan I, Son Y-J, Scherer S, Luo W. Modality-Based Organization of Ascending Somatosensory Axons in the Direct Dorsal Column Pathway. J Neurosci 33: 17691–17709, 2013.

265. Nolano M, Provitera V, Crisci C, Stancanelli A, Wendelschafer-Crabb G, Kennedy WR, Santoro L. Quantification of myelinated endings and mechanoreceptors in human digital skin. Ann Neurol 54: 197–205, 2003.

266. Olausson H, Cole J, Rylander K, McGlone F, Lamarre Y, Wallin BG, Krämer H, Wessberg J, Elam M, Bushnell MC, Vallbo AB. Functional role of unmyelinated tactile afferents in human hairy skin: Sympathetic response and perceptual localization. Exp Brain Res 184: 135–140, 2008.

267. Olausson H, Lamarre Y, Backlund H, Morin C, Wallin BGG, Starck G, Ekholm S, Strigo I, Worsley

K, Vallbo AB, Bushnell MCC. Unmyelinated tactile afferents signal touch and project to insular cortex. Nat Neurosci 5: 900–904, 2002.

268. Olshausen BA, Field DJ. Emergence of simple-cell receptive field properties by learning a sparse code for natural images. Nature 381: 607–609, 1996.

269. Pack CC, Bensmaia SJ. Seeing and Feeling Motion: Canonical Computations in Vision and Touch. PLOS Biol 13: e1002271, 2015.

270. Padberg J, Cerkevich C, Engle J, Rajan AT, Recanzone G, Kaas JH, Krubitzer LA. Thalamocortical connections of parietal somatosensory cortical fields in macaque monkeys are highly divergent and convergent. Cereb Cortex 19: 2038–2064, 2009.

271. Padberg J, Recanzone G, Engle J, Cooke D, Goldring A, Krubitzer LA. Lesions in Posterior Parietal Area 5 in Monkeys Result in Rapid Behavioral and Cortical Plasticity. J Neurosci 30: 12918–12935, 2010.

272. Pandya DN, Seltzer B. Intrinsic connections and architectonics of posterior parietal cortex in the rhesus monkey. J Comp Neurol 204: 196–210, 1982.

273. Pearson RCA, Brodal P, Powell TPS. The projection of the thalamus upon the parietal lobe in the monkey. Brain Res 144: 143–148, 1978.

274. Pearson RCA, Powell TPS. The projection of the primary somatic sensory cortex upon area 5 in the monkey. Brain Res Rev 9: 89–107, 1985.

275. Pei Y-C, Denchev P V, Hsiao SS, Craig JC, Bensmaia SJ. Convergence of submodality-specific input onto neurons in primary somatosensory cortex. J Neurophysiol 102: 1843–1853, 2009.

276. Pei Y-C, Hsiao SS, Bensmaia SJ. The tactile integration of local motion cues is analogous to its visual counterpart. Proc Natl Acad Sci U S A 105: 8130–8135, 2008.

277. Pei Y-C, Hsiao SS, Craig JC, Bensmaia SJ. Shape invariant coding of motion direction in somatosensory cortex. PLoS Biol 8: e1000305, 2010.

278. Pei Y-C, Hsiao SS, Craig JC, Bensmaia SJ. Neural mechanisms of tactile motion integration in somatosensory cortex. Neuron 69: 536–47, 2011.

279. Penfield W, Boldrey E. Somatic Motor and Sensory Representation in the Cerebral Cortex of Man as Studied by Electrical Stimulation. Brain 60: 389–443, 1937.

280. Petrides M, Pandya DN. Projections to the Frontal-Cortex from the Posterior Parietal Region in the Rhesus-Monkey. J Comp Neurol 228: 105–116, 1984.

281. Phillips JR, Johansson RS, Johnson KO. Responses of human mechanoreceptive afferents to embossed dot arrays scanned across fingerpad skin. J Neurosci 12: 827–39, 1992.

282. Phillips JR, Johnson KO. Tactile spatial resolution. II. Neural representation of Bars, edges, and gratings in monkey primary afferents. J Neurophysiol 46: 1192–203, 1981.

283. Phillips JR, Johnson KO, Hsiao SS. Spatial pattern representation and transformation in monkey somatosensory cortex. Proc Natl Acad Sci U S A 85: 1317–21, 1988.

284. Pons TP, Garraghty PE, Cusick CG, Kaas JH. The somatotopic organization of area 2 in macaque monkeys. J Comp Neurol 241: 445–466, 1985.

285. Pons TP, Garraghty PE, Friedman DP, Mishkin M. Physiological evidence for serial processing in somatosensory cortex. Science 237: 417–20, 1987.

286. Pons TP, Garraghty PE, Mishkin M. Serial and Parallel Processing of Tactual Information in Somatosensory Cortex of Rhesus-Monkeys. J Neurophysiol 68: 518–527, 1992.

287. Pons TP, Kaas JH. Corticocortical connections of area 2 of somatosensory cortex in macaque monkeys: a correlative anatomical and electrophysiological study. J Comp Neurol 248: 313–335, 1986.

288. Poranen A, Hyvärinen J. Effects of attention on multiunit responses to vibration in the somatosensory regions of the monkey's brain. Electroencephalogr Clin Neurophysiol 53: 525–537, 1982.

289. Prud'homme MJ, Cohen DA, Kalaska JF. Tactile activity in primate primary somatosensory cortex during active arm movements: cytoarchitectonic distribution. J Neurophysiol 71: 173–81, 1994.

290. Prud'homme MJ, Kalaska JF. Proprioceptive activity in primate primary somatosensory cortex during active arm reaching movements. J Neurophysiol 72: 2280–301, 1994.

291. Pruett JR, Sinclair RJ, Burton H. Response Patterns in Second Somatosensory Cortex (SII) of Awake Monkeys to Passively Applied Tactile Gratings. J Neurophysiol 84, 2000.

292. Pruszynski JA, Flanagan JR, Johansson RS. Fast and accurate edge orientation processing during object manipulation. bioRxiv (2017). doi: 10.1101/163790.

293. Pruszynski JA, Johansson RS. Edge-orientation processing in first-order tactile neurons. Nat Neurosci 17: 1404–1409, 2014.

294. Qi H-X, Gharbawie OA, Wong P, Kaas JH. Cell-poor septa separate representations of digits in the ventroposterior nucleus of the thalamus in monkeys and prosimian galagos. J Comp Neurol

519: 738–758, 2011.

295. Qi H-X, Kaas JH. Myelin stains reveal an anatomical framework for the representation of the digits in somatosensory area 3b of macaque monkeys. J Comp Neurol 477: 172–187, 2004.

296. Qi H-X, Lyon DC, Kaas JH. Cortical and thalamic connections of the parietal ventral somatosensory area in marmoset monkeys (Callithrix jacchus). J Comp Neurol 443: 168–182, 2002.

297. Randolph M, Semmes J. Behavioral consequences of selective subtotal ablations in the postcentral gyrus of Macaca mulatta. Brain Res 70: 55–70, 1974.

298. Rasmussen AT, Peyton WT. The course and termination of the medial lemniscus in man. J Comp Neurol 88: 411–424, 1948.

299. Rathelot J-A, Dum RP, Strick PL. Posterior parietal cortex contains a command apparatus for hand movements. Proc. Natl. Acad. Sci. (2017). doi: 10.1073/pnas.1608132114.

300. Rathelot J-A, Strick PL. Muscle representation in the macaque motor cortex: an anatomical perspective. Proc Natl Acad Sci U S A 103: 8257–8262, 2006.

301. Reed JL, Pouget P, Qi H-X, Zhou Z, Bernard MR, Burish MJ, Haitas J, Bonds a B, Kaas JH. Widespread spatial integration in primary somatosensory cortex. Proc Natl Acad Sci U S A 105: 10233–10237, 2008.

302. Reed JL, Qi H-X, Kaas JH. Spatiotemporal properties of neuron response suppression in owl monkey primary somatosensory cortex when stimuli are presented to both hands. J Neurosci 31: 3589–601, 2011.

303. Reed JL, Qi H-X, Pouget P, Burish MJ, Bonds a B, Kaas JH. Modular processing in the hand representation of primate primary somatosensory cortex coexists with widespread activation. J Neurophysiol 104: 3136–3145, 2010.

304. Reed JL, Qi H, Zhou Z, Bernard MR, Burish MJ, Bonds AB, Kaas JH. Response Properties of Neurons in Primary Somatosensory Cortex of Owl Monkeys Reflect Widespread Spatiotemporal Integration. (2010). doi: 10.1152/jn.00709.2009.

305. Richardson AG, Weigand PK, Sritharan SY, Lucas TH. A chronic neural interface to the macaque dorsal column nuclei. J. Neurophysiol. (2016). doi: 10.1152/jn.01083.2015.

306. Rincon-Gonzalez L, Warren JP, Meller DM, Helms Tillery S. Haptic Interaction of Touch and Proprioception: Implications for Neuroprosthetics. IEEE Trans Neural Syst Rehabil Eng 19: 490–500, 2011.

307. Rinvik E, Walberg F. Studies on the cerebellar projections from the main and external cuneate nuclei in the cat by means of retrograde axonal transport of horseradish peroxidase. Brain Res 95: 371–381, 1975.

308. Ro T, Ellmore TM, Beauchamp MS. A neural link between feeling and hearing. Cereb Cortex 23: 1724–30, 2013.

309. Robinson CJ, Burton H. Somatotopographic organization in the second somatosensory area of M. fascicularis. J Comp Neurol 192: 43–67, 1980.

310. Robinson CJ, Burton H. Somatic submodality distribution within the second somatosensory (SII), 7b, retroinsular, postauditory, and granular insular cortical areas of M. fascicularis. J Comp Neurol 192: 93–108, 1980.

311. Robinson CJ, Burton H. Organization of somatosensory receptive fields in cortical areas 7b, retroinsula, postauditory and granular insula of M. fascicularis. J Comp Neurol 192: 69–92, 1980.

312. Romo R, Hernández A, Zainos A, Lemus L, Brody CD. Neuronal correlates of decision-making in secondary somatosensory cortex. Nat Neurosci 5: 1217–1225, 2002.

313. Romo R, Hernández A, Zainos A, Salinas E. Somatosensory discrimination based on cortical microstimulation. Nature 392: 387–90, 1998.

314. Romo R, de Lafuente V. Conversion of sensory signals into perceptual decisions. Prog Neurobiol 103: 41–75, 2013.

315. Romo R, Salinas E. Cognitive neuroscience: Flutter Discrimination: neural codes, perception, memory and decision making. Nat Rev Neurosci 4: 203–218, 2003.

316. Rouiller EM, Welker E. A comparative analysis of the morphology of corticothalamic projections in mammals. Brain Res Bull 53: 727–741, 2000.

317. Rowe MJ, Turman a B, Murray GM, Zhang HQ. Parallel organization of somatosensory cortical areas I and II for tactile processing. Clin Exp Pharmacol Physiol 23: 931–8, 1996.

318. Rowland DL. Penile sensitivity in men: a composite of recent findings. Urology 52: 1101–1105, 1998.

319. Roy A, Steinmetz PN, Hsiao SS, Johnson KO, Niebur E. Synchrony: a neural correlate of somatosensory attention. J Neurophysiol 98: 1645–61, 2007.

320. Rozzi S, Calzavara R, Belmalih A, Borra E, Gregoriou GG, Matelli M, Luppino G. Cortical connections of the inferior parietal cortical convexity of the macaque monkey. Cereb Cortex 16:

1389–1417, 2006.

321. Ruben J, Schwiemann J, Deuchert M, Meyer R, Krause T, Curio G, Villringer K, Kurth R, Villringer A. Somatotopic organization of human secondary somatosensory cortex. Cerbral Cortex 11: 463–473, 2001.

322. Saal HP, Bensmaia SJ. Touch is a team effort: interplay of submodalities in cutaneous sensibility. Trends Neurosci 2: 1–9, 2014.

323. Saal HP, Harvey MA, Bensmaia SJ. Rate and timing of cortical responses driven by separate sensory channels. Elife 4: e10450, 2015.

324. Saal HP, Wang X, Bensmaia SJ. Importance of spike timing in touch: an analogy with hearing? Curr Opin Neurobiol 40: 142–149, 2016.

325. Sainburg RL, Ghilardi MF, Poizner H, Ghez C. Control of limb dynamics in normal subjects and patients without proprioception. J Neurophysiol 73: 820–35, 1995.

326. Sakata H, Takaoka Y, Kawarasaki A, Shibutani H. Somatosensory properties of neurons in the superior parietal cortex (area 5) of the rhesus monkey. Brain Res 64: 85–102, 1973.

327. Salimi I, Brochier T, Smith AM. Neuronal activity in somatosensory cortex of monkeys using a precision grip. III. Responses to altered friction perturbations. J Neurophysiol 81: 845–857, 1999.

328. Salimi I, Brochier T, Smith AM. Neuronal activity in somatosensory cortex of monkeys using a precision grip. I. Receptive fields and discharge patterns. J Neurophysiol 81: 825–34, 1999.

329. Salimi I, Brochier T, Smith AM. Neuronal activity in somatosensory cortex of monkeys using a precision grip. II. Responses To object texture and weights. J Neurophysiol 81: 835–44, 1999.

330. Salinas E, Hernandez A, Zainos A, Romo R, Hernández A. Periodicity and firing rate as candidate neural codes for the frequency of vibrotactile stimuli. J Neurosci 20: 5503–15, 2000.

331. Sánchez-Panchuelo RM, Besle J, Mougin O, Gowland P, Bowtell R, Schluppeck D, Francis S. Regional structural differences across functionally parcellated Brodmann areas of human primary somatosensory cortex. Neuroimage 93: 221–230, 2014.

332. Seal J, Commenges D. A quantitative analysis of stimulus- and movement-related responses in the posterior parietal cortex of the monkey. Exp Brain Res 58: 144–153, 1985.

333. Seelke AMH, Padberg J, Disbrow E, Purnell SM, Recanzone G, Krubitzer LA. Topographic maps within brodmann's area 5 of macaque monkeys. Cereb Cortex 22: 1834–1850, 2012.

334. Semmes J, Porter L, Randolph M. Further studies of anterior postcentral lesions in monkeys. Cortex 10: 55–68, 1974.

335. Semmes J, Turner B. Effects of cortical lesions on somatosensory tasks. J Invest Dermatol 69: 181–9, 1977.

336. Sinclair RJ, Burton H. Neuronal activity in the primary somatosensory cortex in monkeys (Macaca mulatta) during active touch of textured surface gratings: responses to groove width, applied force, and velocity of motion. J Neurophysiol 66: 153–169, 1991.

337. Sinclair RJ, Burton H. Neuronal activity in the second somatosensory cortex of monkeys (Macaca mulatta) during active touch of gratings. J Neurophysiol 70: 331–50, 1993.

338. Skedung L, Arvidsson M, Chung JY, Stafford CM, Berglund B, Rutland MW. Feeling small: exploring the tactile perception limits. Sci Rep 3: 2617, 2013.

339. Smith MC, Deacon P. Topographical anatomy of the posterior columns of the spinal cord in man. The long ascending fibres. Brain 107 (Pt 3: 671–98, 1984.

340. Snyder LH, Batista AP, Andersen RA. Coding of intention in the posterior parietal cortex. Nature 386: 167–170, 1997.

341. Snyder LH, Grieve KL, Brotchie P, Andersen RA. Separate body- and world-referenced representations of visual space in parietal cortex. Nature 394: 887–891, 1998.

342. Soso MJ, Fetz EE. Responses of identified cells in postcentral cortex of awake monkeys during comparable active and passive joint movements. J Neurophysiol 43: 1090–1110, 1980.

343. Squatrito S, Raffi M, Maioli MG, Battaglia-Mayer A. Visual motion responses of neurons in the caudal area pe of macaque monkeys. J Neurosci 21: RC130, 2001.

344. Sripati AP, Denchev P, Szczepanski S, Yoshioka T, Johnson KO. Spatiotemporal receptive fields from white noise and complex orthogonal pattern stimulation in SI cortex of the alert monkey. 37: 38034, 2000.

345. Steinmetz PN, Roy a, Fitzgerald PJ, Hsiao SS, Johnson KO, Niebur E. Attention modulates synchronized neuronal firing in primate somatosensory cortex. Nature 404: 187–190, 2000.

346. Stepniewska I, Preuss TM, Kaas JH. Architectonics, somatotopic organization, and ipsilateral cortical connections of the primary motor area (M1) of owl monkeys. J Comp Neurol 330: 238–271, 1993.

347. Sur M, Garraghty PE, Bruce CJ. Somatosensory cortex in macaque monkeys: laminar differences in receptive field size in areas 3b and 1. Brain Res 342: 391–5, 1985.

348. Sur M, Merzenich MM, Kaas JH. Magnification, receptive-field area, and "hypercolumn" size in areas 3b and 1 of somatosensory cortex in owl monkeys. J Neurophysiol 44: 295–311, 1980.

349. Sur M, Wall JT, Kaas JH. Modular segregation of functional cell classes within the postcentral somatosensory cortex of monkeys. Science 212: 1059–61, 1981.

350. Sur M, Wall JT, Kaas JH. Modular distribution of neurons with slowly adapting and rapidly adapting responses in area 3b of somatosensory cortex in monkeys. J Neurophysiol 51: 724–744, 1984.

351. Suresh AK, Winberry J, Versteeg C, Chowdhury RH, Tomlinson T, Rosenow JM, Miller LE, Bensmaia SJ. Methodological Considerations for a Chronic Neural Interface With the Cuneate Nucleus of Macaques. J Neurophysiol 95162: jn.00436.2017, 2017.

352. Suzuki Y, Gyoba J, Sakamoto S. Selective effects of auditory stimuli on tactile roughness perception. Brain Res 1242: 87–94, 2008.

353. Tabot GA, Dammann JF, Berg J a., Tenore F V., Boback JL, Vogelstein RJ, Bensmaia SJ. Restoring the sense of touch with a prosthetic hand through a brain interface. Proc Natl Acad Sci U S A 110: 18279–84, 2013.

354. Tabot GA, Kim SS, Winberry JE, Bensmaia SJ. Restoring tactile and proprioceptive sensation through a brain interface. Neurobiol Dis 83: 191–198, 2014.

355. Talbot WH, Darian-Smith I, Kornhuber HH, Mountcastle VB. The sense of flutter-vibration: comparison of the human capacity with response patterns of mechanoreceptive afferents from the monkey hand. J Neurophysiol 31: 301–34, 1968.

356. Taoka M, Toda T, Hihara S, Tanaka M, Iriki A, Iwamura Y. A systematic analysis of neurons with large somatosensory receptive fields covering multiple body regions in the secondary somatosensory area of macaque monkeys. J Neurophysiol 116, 2016.

357. Taoka M, Toda T, Iriki A, Tanaka M, Iwamura Y. Bilateral receptive field neurons in the hindlimb region of the postcentral somatosensory cortex in awake macaque monkeys. Exp Brain Res 134: 139–146, 2000.

358. Taoka M, Toda T, Iwamura Y. Representation of the midline trunk, bilateral arms, and shoulders in the monkey postcentral somatosensory cortex. Exp Brain Res 123: 315–322, 1998.

359. Taylor MM, Lederman SJ. Tactile roughness of grooved surfaces: A model and the effect of friction. Percept Psychophys 17: 23–36, 1975.

360. Thakur PH, Fitzgerald PJ, Hsiao SS. Second-order receptive fields reveal multidigit interactions in area 3b of the macaque monkey. J Neurophysiol 108: 243–262, 2012.

361. Tomlinson T, Miller LE. Toward a Proprioceptive Neural Interface that Mimics Natural Cortical Activity. Adv Exp Med Biol 957: 367–388, 2016.

362. Tommerdahl M. Ipsilateral Input Modifies the Primary Somatosensory Cortex Response to Contralateral Skin Flutter. J Neurosci 26: 5970–5977, 2006.

363. Tommerdahl M, Delemos K a, Favorov O V, Metz CB, Vierck CJ, Whitsel BL. Response of anterior parietal cortex to different modes of same-site skin stimulation. J Neurophysiol 80: 3272–3283, 1998.

364. Tommerdahl M, Delemos K a, Vierck CJ, Favorov O V, Whitsel BL. Anterior parietal cortical response to tactile and skin-heating stimuli applied to the same skin site. J Neurophysiol 75: 2662–2670, 1996.

365. Tommerdahl M, Favorov O V, Whitsel BL. Effects of high-frequency skin stimulation on SI cortex: mechanisms and functional implications. Somatosens Mot Res 22: 151–169, 2005.

366. Tommerdahl M, Favorov O, Whitsel BL, Nakhle B, Gonchar YA. Minicolumnar activation patterns in cat and monkey si cortex. Cereb Cortex 3: 399–411, 1993.

367. Tommerdahl M, Whitsel BL, Favorov O V, Metz CB, O'Quinn BL. Responses of contralateral SI and SII in cat to same-site cutaneous flutter versus vibration. J Neurophysiol 82: 1982–1992, 1999.

368. Tremblay N, Bushnell MC, Duncan GH. Thalamic VPM nucleus in the behaving monkey. II. Response to air-puff stimulation during discrimination and attention tasks. J Neurophysiol 69: 753–763, 1993.

369. Treue S, Maunsell JHR. Attentional modulation of visual motion processing in cortical areas MT and MST. Nature 382: 539–541, 1996.

370. Vallbo AB, Johansson RS. Skin Mechanoreceptors in the Human Hand : Neural and Psychophysical. Sens. Funct. Ski. (1966). doi: 10.1016/B978-0-08-021208-1.50021-7.

371. Vallbo AB, Olausson H, Wessberg J. Unmyelinated afferents constitute a second system coding tactile stimuli of the human hairy skin. J Neurophysiol 81: 2753–63, 1999.

372. Vallbo AB, Olausson H, Wessberg J, Kakuda N. Receptive field characteristics of tactile units with myelinated afferents in hairy skin of human subjects. J Physiol 483: 783–95, 1995.

373. Vazquez Y, Zainos a., Alvarez M, Salinas E, Romo R. Neural coding and perceptual detection in the primate somatosensory thalamus. Proc Natl Acad Sci 109: 15006–15011, 2012.

374. Vega-Bermudez F, Johnson KO. SA1 and RA receptive fields, response variability, and

population responses mapped with a probe array. J Neurophysiol 81: 2701–2710, 1999.

375. de Vito JL. Corticothalamic connections of suprasylvian cortex in monkey. Exp Neurol 32: 489–501, 1971.

376. Wang X, Zhang M, Cohen IS, Goldberg ME. The proprioceptive representation of eye position in monkey primary somatosensory cortex. Nat Neurosci 10: 640–646, 2007.

377. Warren S, Hamalainen HA, Gardner EP. Objective Classification of Motion-and Direction-Sensitive Neurons in Primary Somatosensory Cortex of Awake Monkeys. Journalof Neurophysiol 56, 1986.

378. Warren S, Hamalainen HA, Gardner EP. Coding of the spatial period of gratings rolled across the receptive fields of somatosensory cortical neurons in awake monkeys. J Neurophysiol 56: 623–39, 1986.

379. Weaver ICG, Cervoni N, Champagne FA, D'Alessio AC, Sharma S, Seckl JR, Dymov S, Szyf M, Meaney MJ. Epigenetic programming by maternal behavior. Nat Neurosci 7: 847–854, 2004.

380. Weber AI, Saal HP, Lieber JD, Cheng J-WWJW, Manfredi LR, Dammann 3rd JF, Bensmaia SJ, Dammann JF. Spatial and temporal codes mediate the tactile perception of natural textures. Proc Natl Acad Sci 110: 17107–17112, 2013.

381. Weber JT, Yin TC. Subcortical projections of the inferior parietal cortex (area 7) in the stump-tailed monkey. J Comp Neurol 224: 206–30, 1984.

382. Wheat HE, Salo LM, Goodwin AW. Cutaneous afferents from the monkeys fingers: responses to tangential and normal forces. J Neurophysiol 103: 950–961, 2010.

383. Whitsel BL, Franzen O, Dreyer DA, Hollins M, Young M, Essick GK, Wong C. Dependence of subjective traverse length on velocity of moving tactile stimuli. Somatosens Res 3: 185–96, 1986.

384. Whitsel BL, Petrucelli LM, Werner G. Symmetry and connectivity in the map of the body surface in somatosensory area II of primates. J Neurophysiol 32: 170–83, 1969.

385. Witham CL, Baker SN. Modulation and transmission of peripheral inputs in monkey cuneate and external cuneate nuclei. J Neurophysiol 106: 2764–75, 2011.

386. Witney AG, Wing AM, Thonnard J-L, Smith AM. The cutaneous contribution to adaptive precision grip. Trends Neurosci 27: 637–643, 2004.

387. Woolsey CN, Fairman D. Contralateral, ipsilateral, and bilateral representation of cutaneous receptors in somatic areas I and II of the cerebral cortex of pig, sheep, and other mammals.

Surgery 19: 684–702, 1946.

388. Xu J, Wall JT. Cutaneous representations of the hand and other body parts in the cuneate nucleus of a primate, and some relationships to previously described cortical representations. Somatosens Mot Res 13: 187–97, 1996.

389. Xu J, Wall JT. Functional organization of tactile inputs: From the hand in the cuneate nucleus and its relationship to organization in the somatosensory cortex. J Comp Neurol 411: 369–389, 1999.

390. Yau JM, Connor CE, Hsiao SS. Representation of tactile curvature in macaque somatosensory area 2. J Neurophysiol 109: 2999–3012, 2013.

391. Yau JM, Kim SS, Thakur PH, Bensmaia SJ. Feeling form: the neural basis of haptic shape perception. J Neurophysiol 115: 631–642, 2016.

392. Yau JM, Pasupathy A, Fitzgerald PJ, Hsiao SS, Connor CE. Analogous intermediate shape coding in vision and touch. Proc Natl Acad Sci U S A 106: 16457–62, 2009.

393. Yeterian EH, Pandya DN. Corticothalamic connections of the posterior parietal cortex in the rhesus monkey. J Comp Neurol 237: 408–26, 1985.

394. Yumiya H, Kubota K, Asanuma H. Activities of neurons in area 3a of the cerebral cortex during voluntary movements in the monkey. Brain Res 78: 169–177, 1974.

395. Zhang HQ, Zachariah MK, Coleman GT, Rowe MJ. Hierarchical equivalence of somatosensory areas I and II for tactile processing in the cerebral cortex of the marmoset monkey. J Neurophysiol 85: 1823–35, 2001.

396. Zimny ML. Mechanoreceptors in articular tissues. Am J Anat 182: 16–32, 1988.

CHAPTER 2 | TEXTURE IS ENCODED IN PRECISE TEMPORAL SPIKING PATTERNS IN SOMATOSENSORY CORTEX[2]

We are exquisitely sensitive to the microstructure and material properties of surfaces. In the peripheral nerves, two separate mechanisms convey texture information: coarse textural features are encoded in spatial patterns of activation that reflect their spatial layout and fine features are encoded in highly repeatable, texture specific temporal spiking patterns evoked as the skin moves across the surface. In the present study, we examined whether this temporal code is preserved in the responses of neurons in somatosensory cortex. To this end, we scanned a diverse set of everyday textures across the fingertip of awake macaques while recording the responses evoked in individual cortical neurons. We found that temporal spiking patterns are highly repeatable across multiple presentations of the same texture, with millisecond precision. As a result, texture identity can be reliably decoded from the temporal patterns themselves, even after information carried in the spike rates is eliminated. However, a neural code that combines rate and timing is more informative than either code in isolation. The temporal precision of the texture response is heterogenous across cortical neurons and depends on the submodality composition of their input and on their location along the somatosensory neuraxis. Furthermore, temporal spiking patterns in cortex dilate and contract with decreases and increases in scanning speed and this systematic relationship between speed and patterning may contribute to the observed perceptual invariance to speed. Finally, we find that the quality of a texture percept

[2] This chapter is under review at Nature Communications and published on biorXiv at https://doi.org/10.1101/2021.04.11.439354

can be better predicted when these temporal patterns are taken into consideration. We conclude that high-precision spike timing complements rate-based signals to encode texture in somatosensory cortex.

2. 1 | INTRODUCTION

Spike timing at the level of single milliseconds has been shown to carry stimulus information in the somatosensory nerves (Saal et al., 2016). For example, the frequency composition of skin vibrations is encoded in the phase locked responses of individual nerve fibers (birznieks, I. and Vickery, R.M., 2017; Mackevicius et al., 2012; Talbot et al., 1968) and is observed for frequencies up to 1000 Hz in a subpopulation of nerve fibers, namely Pacinian corpuscle-associated (PC) fibers. Temporal coding of vibratory frequency is also observed in somatosensory cortex and is particularly prominent in neurons that receive a preponderance of their input from PC fibers (Harvey et al., 2013; Saal et al., 2015). The preservation of spike timing in cortex at this level of precision is surprising given that these signals have already passed through several synapses, including the cuneate nucleus, and the thalamus (Dykes et al., 1982; Krubitzer and Kaas, 1992; Padberg et al., 2009; Rinvik and Walberg, 1975). Note, however, that similar precision is observed in rodent barrel cortex (Celikel et al., 2004; Jadhav et al., 2009; Panzeri et al., 2001; Zuo et al., 2015) and along the auditory neuraxis with equivalent synaptic passes (Kayser et al., 2010; Phillips et al., 2002; Saal et al., 2016; Wehr and Zador, 2003).

By extension, the perception of texture – particularly of fine texture – is supported by a temporal code. Indeed, scanning a textured surface across the fingertip leads to the elicitation of vibrations in the skin that reflect the spatial structure of the surface (Bensmaia and Hollins, 2003; Manfredi

et al., 2014) and depend on the speed at which it is scanned (Greenspon et al., 2020). The frequency-composition of these texture-elicited vibrations is encoded in temporally patterned responses in vibration-sensitive nerve fibers, including PC fibers (Weber et al., 2013). As a result, afferent responses are much more informative about texture identity when spike timing is taken into consideration than when it is not (Weber et al., 2013). The responses of neurons in somatosensory cortex, particularly those that receive strong PC input, have also been shown to exhibit temporal patterning (Lieber and Bensmaia, 2019). However, the reliability of this patterning, its informativeness about texture, or its relation to perception have never been investigated. To fill these gaps, we first gauge the precision and reliability of the temporal patterning in cortical responses to texture. Second, we assess the degree to which and the temporal resolution at which texture information is encoded in temporal spiking patterns in cortex. Third, we examine how texture-specific temporal spiking patterns change with changes in scanning speed. Finally, we examine the degree to which temporal spiking patterns are predictive of the resulting texture percepts.

2.2 | RESULTS

We recorded the responses of 141 neurons in somatosensory cortex (SC) of 2 monkeys – 35 in Brodmann's area 3b, 81 in area 1, and 25 in area 2 – as we scanned each of 59 diverse, everyday textures across the fingertips with precisely controlled speed and contact force (Lieber and Bensmaia, 2019, 2020) (Supplemental Table 1).

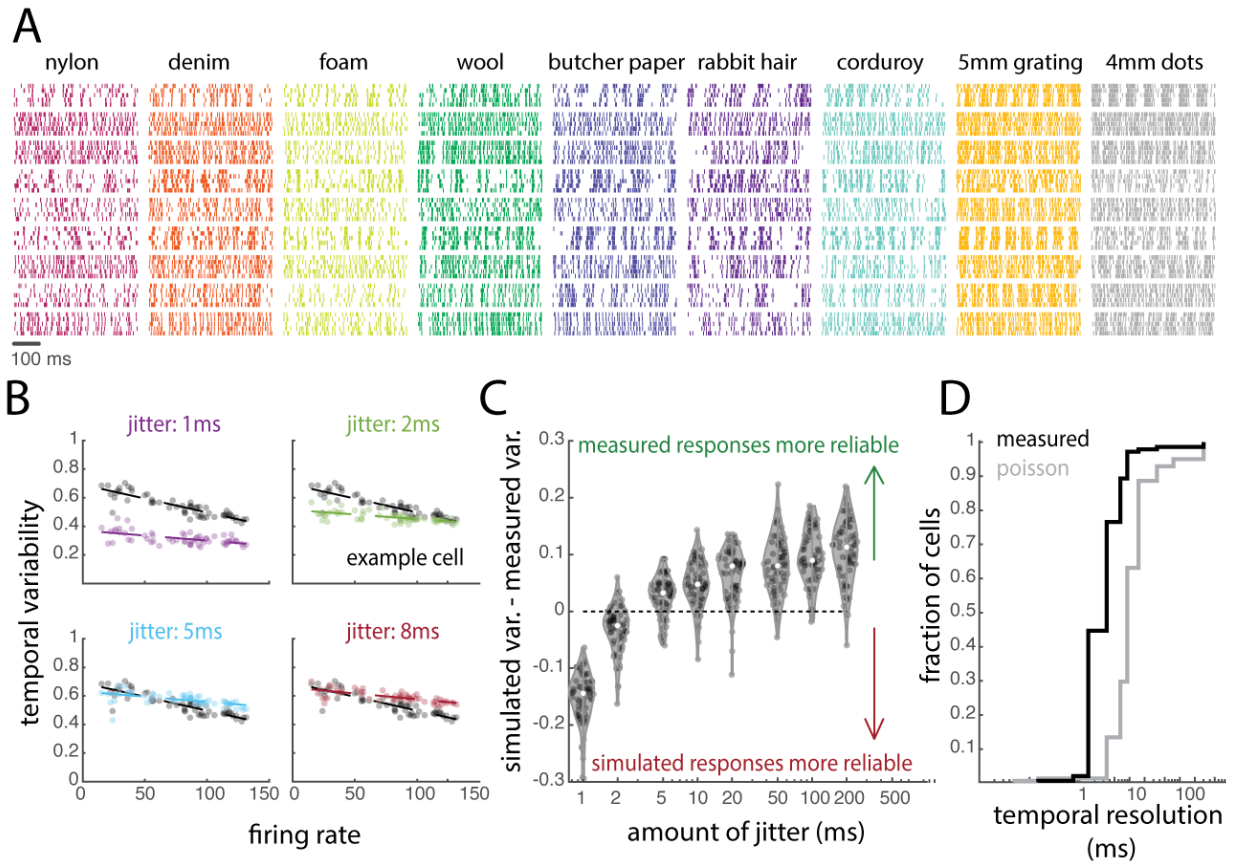

Figure 2.1: Responses in somatosensory cortex are temporally precise. A| Responses of nine example neurons to five repeated presentations of nine (of 59) textures. Each color is a different texture, each row is the response of an individual neuron across five repeated presentations of that texture. **B|** Temporal variability across repeats of each texture in one example neuron. Each point represents the mean temporal variability (spike distance, evaluated at q=500, divided by rate) for one texture. **C|** Variability in the simulated response minus the variability in the measured responses for each amount of jitter for the example neuron shown in panel B. For most textures, measured responses are more reliable than simulated responses with jitter set to 5 ms. **D|** Cumulative distribution of the temporal resolutions of all neurons.

2.2.1 | Reliability of temporal patterns in somatosensory cortex

A temporal spiking pattern signals the presence of a stimulus to the extent that the pattern is reliably evoked when the stimulus is presented. In the peripheral nerves, the temporal patterning of texture-evoked responses is nearly identical across multiple repeats, yielding a robust

temporal code of texture identity (Weber et al., 2013). Having observed temporal patterning in the cortical responses to textures (Figure 2.1A), we quantified the reliability of this patterning across repeated presentations of the same texture and assessed its temporal fidelity. To these ends, we computed the dissimilarity between the responses of individual cortical neurons to repeated presentations of the same texture using a spike distance metric, which computes the cost of transforming one spike train into another (de Lafuente and Romo, 2006; Victor and Purpura, 1997). Varying the cost of shifting spikes in time allows us to manipulate the temporal resolution of this metric: At one extreme, small jitter in the spike timing drives large dissimilarity values; at the other extreme, spike trains differ only to the extent that they contain different numbers of spikes. If responses are temporally precise across repeated presentations of the same stimulus, the pairwise dissimilarity of the responses should be low, even when evaluated at a high temporal resolution. Even for large shifting costs, however, spike distance is driven in part by spike count. To isolate the contribution of spike timing to dissimilarity, then, we computed the spike distance metric for rate-matched simulated responses whose temporal precision could be systematically manipulated. In one case, responses were simulated using a Poisson model, thereby eliminating any information in spike timing. In the other case, a measured response was repeatedly jittered by a specific amount (Supplemental Figure S.2.1A).

We first assessed the temporal precision by comparing real data to spike trains with imposed jitter. We compared each individual cell to its rate-matched jitter models, and we assessed the temporal variability for each presented texture (Figure 2.1B). For each neuron and texture, we then identified the amount of imposed jitter at which the temporal variability across simulated

responses exceeded that of the measured responses (Figure 1C, Supplemental Figure S.2.1B). For each neuron, the median of the distribution of temporal resolutions across textures was then taken to be the temporal resolution. We repeated this same analysis using the Poisson neurons to assess the resolution this approach would yield in the absence of temporal patterning. We found that most cortical neurons are more temporally precise than rate-matched Poisson neurons. Furthermore, the temporal precision resolution varied widely across neurons, though most neurons (75%) yielded temporal resolutions less than 5 ms (Figure 1D).

2.2.2 | RATE VS TIMING CODES

For a temporal pattern to signal the presence of a stimulus, it must not only be reliable, but it must also be stimulus specific. With this in mind, we assessed the degree to which we could classify textures based on temporal spiking patterns. To isolate the contribution of timing to texture identification, we implemented a classifier based on pairwise correlations of single-trial time-varying firing rates. In brief, a texture was correctly classified to the extent that the time-varying response it evokes – the smoothed time-varying firing rate – is consistent across repeated presentations and different from responses evoked by other textures. For this analysis, we used cross-correlation as a metric of similarity between spike trains to exclude information carried by firing rate. By smoothing the spike trains with filters of varying width, we could vary the temporal resolution at which spiking similarity was compared across trials. In agreement with our temporal precision findings using jittered spike trains, we found that classification performance peaked at a high temporal resolution (<5 ms) in individual cortical cells (Figure 2.2A). As expected, simulated responses of Poisson neurons, which by design do not contain any temporal

patterning, yielded chance classification performance (Figure 2.2A, dashed lines). To further validate this approach, we verified that our classifiers' performance peaked at the resolution matching the amount of jitter introduced in the simulated responses (Supplemental Figure S. 2.3).

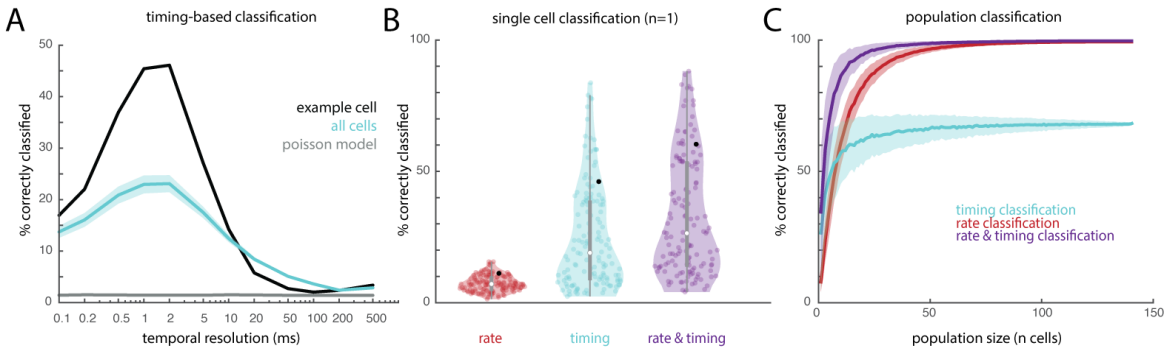

Figure 2.2: Temporal spiking patterns in somatosensory cortex carry texture information. Al Classification performance is best at high temporal resolutions (1-5 ms). The temporal resolution denotes the standard deviation of the Gaussian filter used to smooth the neuronal response. Performance derived from an example neuron is shown in black, mean performance across all cortical neurons is shown in blue, mean performance from rate-matched Poisson simulated neurons is shown in grey. Simulated Poisson responses, which do not carry texture information in their timing, yield chance classification performance (1/59 textures ~ 2%). Shaded area denotes standard error of the mean. **Bl** Single cell classification performance for all 141 neurons for rate (red), timing (blue), and their optimal combination (purple). Black points denote the example neuron shown in panel A. **Cl** Classification performance with neuronal populations of different sizes; shaded area denotes standard deviation across 1000 iterations at each sample size. Timing-based classification yields better performance than does its rate-based counterpart for small neuronal populations, but timing-based performance levels off at a much lower level than does rate-based performance. Rate is nearly perfect with even a small population of 50-100 cells, but a combination of rate and timing is better at any size population of cells and reaches 90% performance with only 13 cells (as compared to rate, which requires 29 cells).

Next, we compared rate coding, timing coding, and their combination. Because neurons vary in the precision of their temporal patterning, we evaluated the combination of rate and timing at

each neuron's optimal resolution and weighted rate and timing to optimize classification performance. We found that, at the single-cell level, classification performance based on rates alone was poorer than classification based on timing alone, but in every cell, performance with both rate and timing exceeded that with either code (Figure 2.2B).

Finally, we assessed how these coding schemes scaled at the population level by assessing classification performance based on temporal and rate codes across neuronal samples of increasing size. To this end, we averaged the (inverted then standardized) correlation and rate difference for each pair of textures across the neuronal sample and then computed a weighted sum of the two distance matrices to obtain a distance metric that integrates timing and rate. We found that classifiers with both rate and timing reached asymptotic performance with fewer neurons than did classifiers with rate or timing in isolation and that timing-based classifiers leveled off at a lower performance level (Figure 2.2C). That is, to achieve 90% classification accuracy required 29 neurons with rate alone, 13 neurons with both rate and timing, and timing alone never yielded that level of accuracy. We also evaluated the performance of a population classifier in which timing and rate were equally rated and we found performance to be nearly indistinguishable from the weighted combination (Supplemental Figure S.2.4).

2.2.3 | TEMPORAL CODING DEPENDS ON SUBMODALITY INPUT

The glabrous skin of the hand is innervated by three main classes of nerve fibers, each of which terminates in a different type of mechanoreceptor, responds to a different aspect of skin deformation (Goodman and Bensmaia, 2020), and makes a distinct contribution to texture coding (Lieber et al., 2017; Weber et al., 2013). PC fibers transduce texture-elicited vibrations

into highly precise temporal spiking patterns; slowly-adapting afferents type-1 (SA1) fibers tend to respond to slower, larger skin deflections and, accordingly, reflect coarse textural features in their spatial pattern of activation; RA fibers exhibit response and texture-coding properties that are intermediate between those of PC and SA1 fibers (Weber et al., 2013).

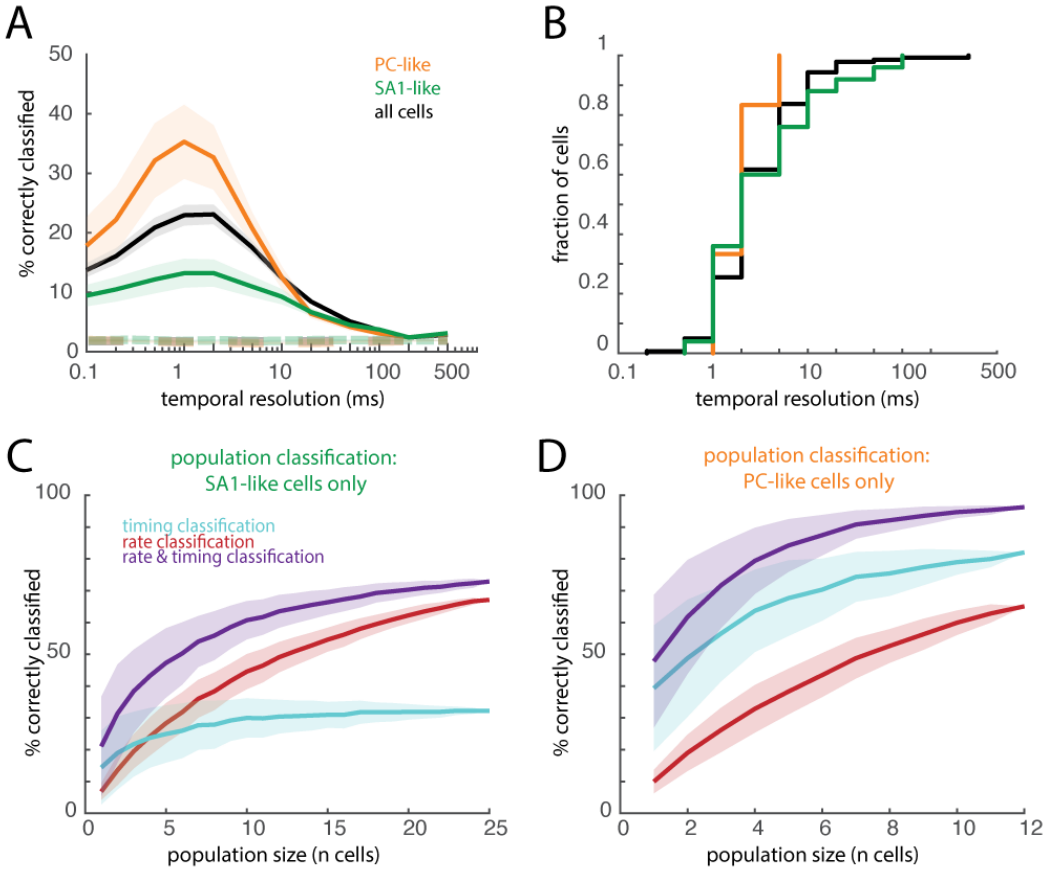

Figure 2.3: Heterogeneity of cortical timing is related to the submodality composition of a neuron's input. A| Mean classification performance for individual PC-like neurons (n=12), SA1-like neurons (n=25), and for all cortical neurons (n=141). PC-like responses allow for better classification than do SA1-like responses, and both are better than the simulated Poisson responses (dashed lines). Shaded regions denote standard error of the mean across neurons. **B|** Cumulative distribution of the peak temporal resolution for individual neurons. **C-D|** Population classification using rate, timing, and both for SA1-like neurons **(C)** or PC-like neurons **(D).** Shaded regions denote the standard deviation across 500 iterations.

Individual cortical neurons receive convergent input from multiple tactile submodalities (SA1, RA, PC) (Pei et al., 2009; Saal et al., 2015; Saal, H.P. and Bensmaia, S.J., 2020) and exhibit highly idiosyncratic responses to texture that can be explained in part by the nature of their afferent input (Lieber and Bensmaia, 2019, 2020). For example, cortical cells that receive dominant input from PC fibers are more likely to exhibit temporally patterned responses to textures than are cells that receive dominant input from SA1 fibers (Lieber and Bensmaia, 2019).

With this in mind, we investigated the relationship between the submodality composition of a neuron's afferent input and its tendency to convey texture information via precise spike timing. To this end, we first grouped cortical cells as PC-like or SA1-like based only on their pattern of texture-evoked firing rates. In brief, we regressed the response of each cortical neuron on the mean response of each class of nerve fiber and identified populations of neurons whose PC or SA1 regression coefficient was high (>0.8). Note that RA fibers exhibit response properties that are intermediate between those of PC and SA1 fibers so RA coefficients do not differentiate textural response properties in cortex. Importantly, the strategy adopted to group cortical neurons by dominant submodality did not take temporal patterning into consideration.

First, we found that spiking patterns of PC-like cortical cells were far more informative than were those of SA1-like cortical cells, as expected given the relative propensities of PC and SA1 nerve fibers to exhibit temporal patterning (Mackevicius et al., 2012; Weber et al., 2013) (Figure 2.3A). Second, the informativeness of the responses of PC-like neurons always peaked at high temporal resolutions while that of SA1-like responses often did not (Figure 2.3B). Note that the high temporal resolutions of many SA1-like neurons could either reflect the contribution of (non-

dominant) PC input or the maintained temporal reliability of some SA1 afferents across multiple repeats (Supplemental Figure S.2.7).

Next, we compared the temporal coding in cortex to its counterpart in the nerves using a shared set of 24 textures (Supplemental Figure S.2.7). We found striking similarities between PC-like cortical cells and PC afferents: they yield similar classification performance with similar optimal temporal resolutions. Similarly, temporal coding is weak in both SA1 fibers and SA1-like cortical neurons, though spike timing in the former is more informative than in the latter. The contrast between the two populations of nerve fibers and their downstream targets is also observed at the population level. In small populations of both PC fibers and PC-like cortical cells, timing classification exceeds rate classification for any size population of cells (Figure 2.3D, Supplemental Figure S.2.6B,D). In contrast, populations of SA1 fibers and SA1-like cortical cells yield better classification performance with rate than with timing (Figure 2.3C, Supplemental Figure S.2.6A,C). These results bolster the hypothesis that the temporal coding properties of cortical neurons are inherited from their inputs.

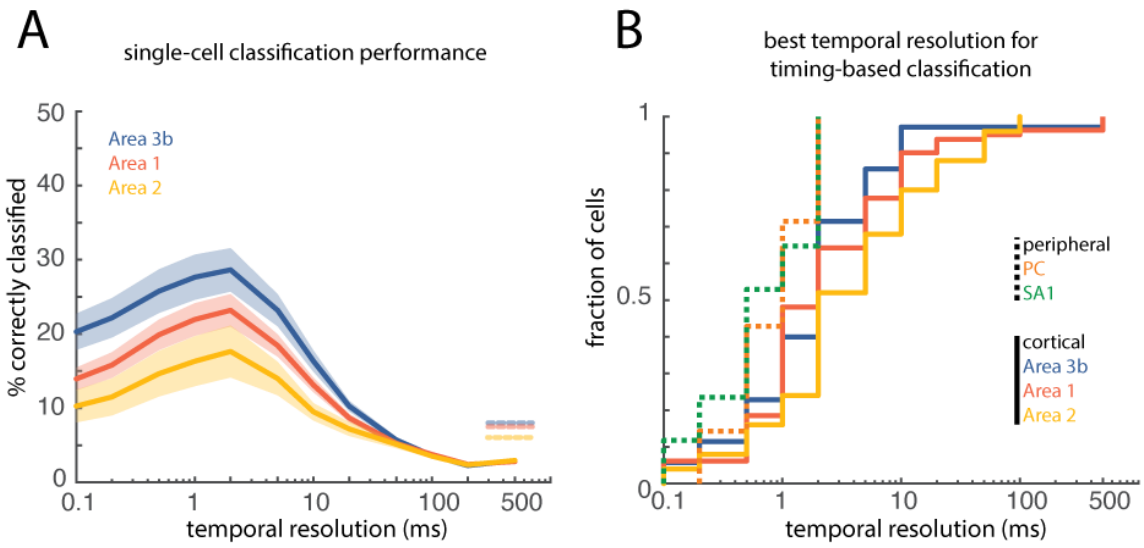

Figure 2.4. Differences in informativeness of temporal patterns across cortical fields. Al Mean timing-based classification for individual neurons in areas 3b (n = 35, blue), 1 (n = 81, red), and 2 (n = 25, yellow). Shaded area represents standard error of the mean across neurons. Dashed lines on the right denote the mean classification performance based on firing rates for each area. **Bl** Cumulative distribution of the best decoding resolutions separated for nerve fibers and cortical neurons.

Nerve fibers exhibit responses to vibrations that are far more precisely phase-locked than do neurons in somatosensory cortex. This loss in spike timing precision is also observed at successive stages of processing in cortex (Harvey et al., 2013). Indeed, a subpopulation of neurons in Brodmann's area 3b – the first stage of cortical processing – exhibits entrained responses to sinusoidal stimulation at frequencies up to 800 Hz; neurons in area 1, a downstream target of area 3b, are less susceptible to high-precision temporal patterning, and neurons in area 2 even less so. Accordingly, we examined whether this progressive loss of temporal precision was also observed in cortical responses to texture. As expected, the preponderance of neurons that carry information about texture in spike timing decreased at successive stages of processing

as evidenced by better spike-timing based texture classification in area 3b, followed by area 1 then area 2 (Figure 2.4A, Supplemental Figure S.2.8). The weaker temporal patterning in higher cortical areas was not accompanied by a dramatic decrease in temporal resolution, however (Figure 2.4B), suggesting that, to the extent that temporal patterns propagate, their timescale is preserved. Notably, differences in the prevalence of temporally precise neurons across cortical fields is not driven by differences in submodality input. That is, area 3b contained the most temporally precise neurons despite the fact that none were classified as receiving dominant input from PC fibers (Supplemental Figure S.2.8).

2.2.5 | Robustness of temporal codes across changes in scanning speed

In the nerve, temporal spiking patterns reflect vibrations elicited in the skin as the surface is scanned (Weber et al., 2013), which themselves depend on both the texture (Manfredi et al., 2014) and the scanning speed (Greenspon et al., 2020). Indeed, texture-elicited skin vibrations systematically dilate and contract with decreases and increases in scanning speed, as do the evoked temporal spiking patterns in the nerve. In contrast, the perception of texture remains remarkably invariant to changes in scanning speed despite these speed-dependent changes in afferent responses (Boundy-Singer et al., 2017; Lederman, 1974; Meftah el-M et al., 2000). The systematic effects of speed on temporal patterning can be reversed by multiplying the inter-spike intervals by the speed, thereby expressing spike trains in space rather than time. To test the impact of changing scanning speed on texture-elicited temporal spiking patterns, we recorded the responses of a subset of cortical neurons as 10 textures were scanned across the fingertip at a range of behaviorally relevant speeds (60 to 120 mm/s) (Callier et al., 2015). We

then examined the degree to which the temporal patterning in the cortical response was speed dependent and assessed whether texture information could be extracted from these temporal patterns across speeds.

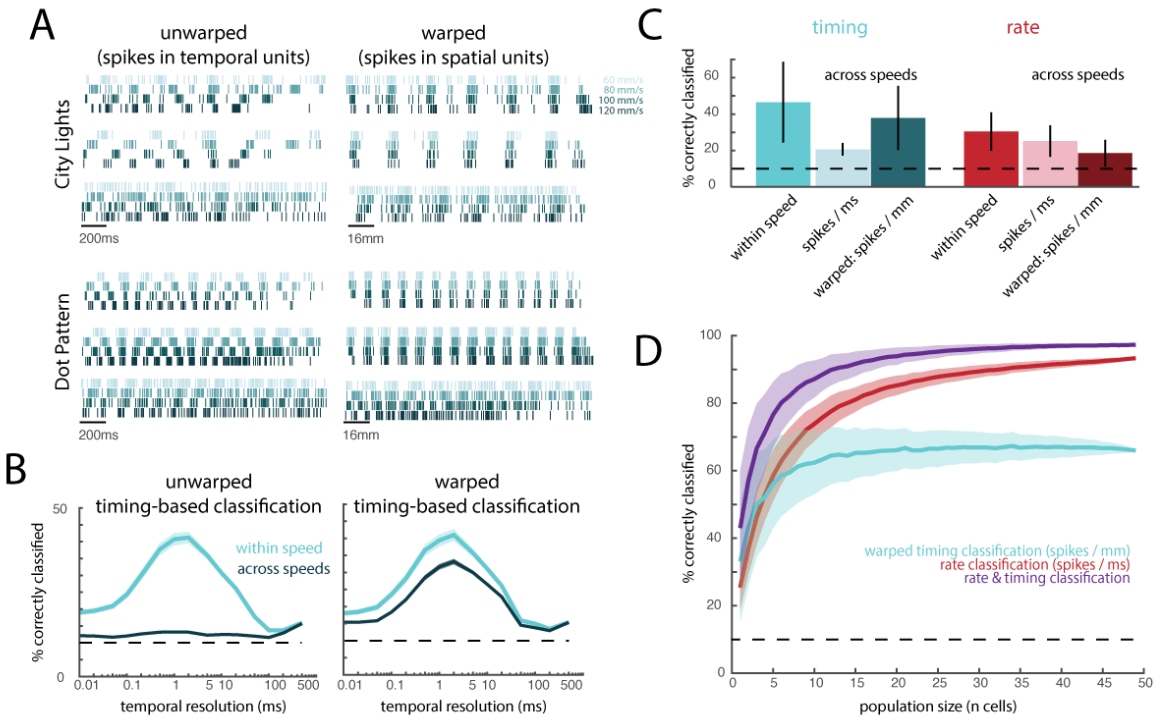

Figure 2.5: Temporal spiking patterns depend on scanning speed. A| Responses of three example neurons to two different textures (City Lights, a fabric with fine textural features and coarse ridges, as well as a dot pattern). Colors denote scanning speed, with darker colors corresponding to faster speeds. On the left, spikes are plotted across time. On the right, spikes times are "warped" such that each spike is plotted per mm of the texture rather than ms in time (by multiplying inter-spike intervals with scanning speed). **B|** Timing-based classification of texture when trained on responses to textures presented at one speed (60, 80, 100, or 120 mm/s) and tested either within speed cyan) or across speeds (dark blue). On the right, spike times are warped as in (A), and classifiers are trained and tested on these warped spike trains. Chance performance is 10% (dashed line). **C|** Mean classification based on timing (blue) or rate (red), within and across speeds. Two cross-speed classifiers were assessed; light bars represent unwarped (spikes / ms), dark bars represent warped (spikes / mm) spike trains. Error bars denote the standard deviation across neurons and speed combinations. **D|** Mean cross-speed population classification based on rate (unwarped), timing (warped), and an averaged combination of both. Shaded regions denote standard deviation across 1000 iterations of randomly sampled populations of neurons.

First, we replicated the finding, documented for tactile nerve fibers, that texture-elicited temporal spiking patterns scale systematically with scanning speed (Figure 2.5A). Indeed, spikes evoked by a given texture at different speeds could be aligned by expressing the neuronal response in space rather than time. To quantitatively assess the impact of scanning speed on the temporal code for texture, we trained timing-based classifiers on responses at one speed (training speed) and tested them at other speeds. Without warping the spike trains by speed, classification was approximately at chance level (Figure 2.5B, left; Figure 2.5C). When spike trains were warped by speed, the peak performance of cross-speed classifiers was almost equivalent to that of within-speed classifiers (Figure 2.5B, right, Figure 2.5C). In contrast, warping spike trains into spatial units decreased the performance of rate classifiers by overcompensating for the speed-dependent modulation of speed (Figure 2.5C).

At the population level, combining rate and (warped) timing codes yields higher classification performance than does either code in isolation (Figure 2.5D) and this improvement cannot be accounted for by the increase in the number of predictors (Supplemental Figure S.2.9). Furthermore, population classification performance levels off at a higher level using both codes than it does with rate or timing alone, indicating that the timing code provides information not easily accessible in the rates, even in larger populations of neurons (Figure 2.5D).

2.2.6 | TEMPORAL PATTERNING SHAPES TEXTURE PERCEPTION

To establish a neural code requires not only to demonstrate that the neuronal signals carry information about stimuli but also that these neuronal signals covary with the perception of these stimuli. Having demonstrated that temporal patterning in cortical responses carries texture

information, we thus set out to gauge whether differences in these temporal patterns also relate to differences in the perception of texture. In other words, do textures feel different to the extent that they evoke different temporal patterns? To test this, we asked human subjects to rate the dissimilarity of pairs of 13 textures (Lieber and Bensmaia, 2019) (Supplemental Table 1). The advantage of this approach is that the ratings take into account every way in which each pair of textures might differ.

First, we assessed the degree to which the perceived dissimilarity of a pair of textures could be predicted from differences in the firing rates evoked in the cortical population by the two textures. We found that rate differences were poor predictors of dissimilarity ratings (Supplemental Figure S.2.11B), as might be expected as population firing rate encodes roughness (Lieber and Bensmaia, 2019), one of many perceptual attributes of texture (Hollins et al., 2000). We might then expect that the contribution of roughness to dissimilarity would be subsumed by the population firing rate. Consistent with this hypothesis, we found that differences in population firing rate accounted for around 20% of the variance in the dissimilarity rating, as did differences in roughness ratings (Supplemental Figure S.2.11B,C).

Second, we examined whether differences in temporal patterning might covary with perceptual dissimilarity. According to this hypothesis, two textures should feel dissimilar to the extent that the correlation between their PSTHs is low. Contrary to this prediction, we found this gauge of temporal dissimilarity to be a poor predictor of dissimilarity ratings (Supplemental Figure S.2.11D). However, this analysis averaged timing differences across the entire population, disregarding the fact that neurons vary widely in their susceptibility to carry texture information

in their timing. We reasoned that informative temporal patterning might be more susceptible to drive perception. To test this hypothesis, we limited the correlation-based analysis to the responses of PC-like neurons, which carry the most texture information in their temporal patterning. We found that timing differences in this neuronal population yielded far better predictions of perceived dissimilarity, far exceeding predictions based on the firing rates of this same neuronal population (Figure 2.6A, Supplemental Figure S.2.11E). However, because timing differences are most predictive of perception does not entail that they solely determine it. With this in mind, we investigated whether the combination of rate and timing might drive perception. To this end, we performed a multiple regression of rate and timing differences onto dissimilarity ratings, separating the regressors by cortical subpopulations (PC-like and SA1-like). We found that the combination of rate and timing distributed over PC-like and SA1 like neurons yielded the best prediction of dissimilarity (Figure 2.6B,C). In other words, perceived texture is shaped by both the rate and the timing of neurons across the entire cortical population. However, the timing of PC-like responses and the rate of SA1-like responses yielded predictions that were nearly equivalent to those of the full model, suggesting that these two texture signals – which happen to be the most informative about texture identity – also play a dominant role in giving rise to texture percepts.

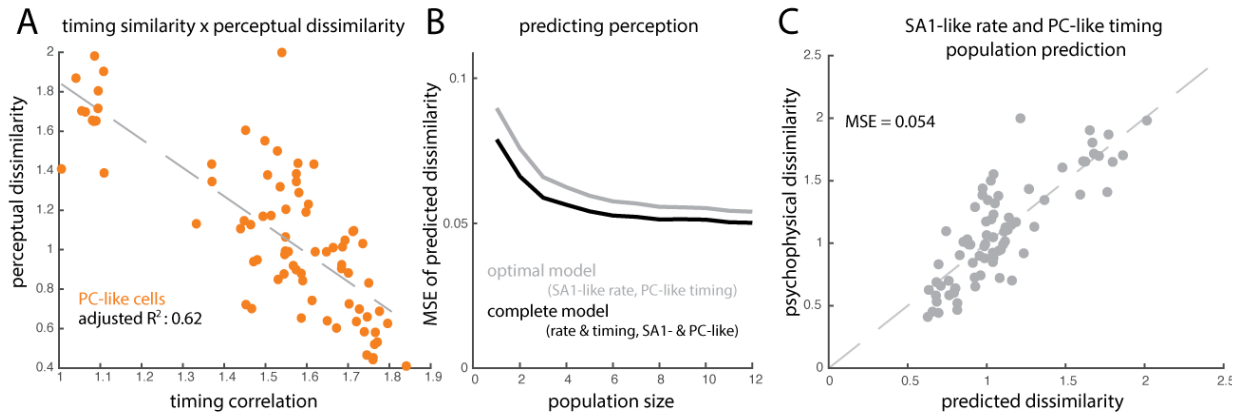

Figure 2.6: Temporal patterns predict texture perception. Al The correlation between the temporal spiking patterns evoked by texture pairs in PC-like neurons is negatively correlated with perceived dissimilarity of those same texture pairs. **Bl** Mean squared error (MSE) of the prediction of perceived dissimilarity derived from a linear combination of rate and timing differences of increasing-size populations of SA1 and PC-like neurons. Grey line indicates a two-factor model that includes PC-like timing and SA1-like rate (grey), and this model performs almost as well as a model that includes all four factors (black trace, SA1- and PC-like, both rate and timing). **Cl** Accuracy of the optimal model (average n=12 population response of SA1 rate and PC timing) in predicting perceived dissimilarity. Each circle represents one texture pair.

2.3 | Discussion

2.3.1 | Temporal coding along the somatosensory neuraxis

A central question in neuroscience is whether the precise timing of spikes carries behaviorally relevant information. The somatosensory system is well suited to address this question because high-frequency deformations of the skin evoke responses in the nerve and in the brain that are repeatably patterned with millisecond precision (Saal et al., 2016). We can thus examine how informative this temporal patterning is at each stage of processing and the timescale at which stimulus information is carried. We have previously shown that temporal patterning in afferent responses conveys information about the frequency composition of skin vibrations (Mackevicius et al., 2012) and, by extension, about textures, particularly fine textures (Weber et al., 2013). The

temporal precision varies across afferent classes: PC responses are most acute, on the order of 2-5 ms, RA responses exhibit intermediate precision, around 5 ms, and SA1 responses carry little information in their timing. In the nerve, information about vibratory frequency and fine texture is not carried in the firing rates and the perception of vibration and texture cannot be accounted for based solely on rates (Mackevicius et al., 2012; Weber et al., 2013).

The role of timing in cortex has been more controversial because cortical neurons exhibit much greater heterogeneity in their firing rate properties than do nerve fibers (Lieber and Bensmaia, 2019). As a result, rate codes are far harder to disambiguate from temporal ones in cortex than in the nerve. Indeed, the responses of individual cortical neurons can be described as temporal filters – each implementing an idiosyncratic temporal differentiation operation on the afferent input –, which effectively signal the presence of specific temporal patterns in the input (Saal et al., 2015). As a result, some of the information carried in the timing is converted into a rate-based code by these neurons. The question is whether the remaining temporal patterning is still informative and behaviorally relevant. A case in point of this ambiguity is in the coding of vibratory frequency in somatosensory cortex. Cortical neurons have long been known to exhibit robust phase locking to vibrations (Harvey et al., 2013; Mountcastle et al., 1969; Salinas et al., 2000) and this phase locking was hypothesized to encode vibratory frequency, particularly at the low frequencies (< 50 Hz)(Mountcastle et al., 1969). However, firing rate was shown to also systematically covary with frequency over this range, which argued for a rate code (Salinas et al., 2000). On the other hand, the relationship between frequency and rate breaks down at the high

frequencies because individual neurons can no longer fire on each stimulus cycle (Harvey et al., 2013). At those frequencies, then, frequency information seems to be carried solely in the timing. Vibratory frequency per se is not an ecologically relevant stimulus quantity. One might therefore argue that the temporal code for frequency in somatosensory cortex is an artifact of the highly contrived laboratory stimulus (vibrations delivered by a motor) and associated sensory task (frequency discrimination). The ethological relevance of this result might then be called into question. In the present study, we show that millisecond level temporal patterning in the cortical response carries information about more naturalistic stimuli, namely textures, as has been shown in the barrel cortex of rodents (Arabzadeh et al., 2006; Zuo et al., 2015).

2.3.2 | TEMPORAL RESOLUTION DEPENDS ON AFFERENT INPUT

As a rule, individual neurons in somatosensory cortex receive convergent input from multiple tactile submodalities (Pei et al., 2009; Saal et al., 2015; Saal, H.P. and Bensmaia, S.J., 2020). Ascribing the response properties of individual cortical neurons to specific classes of input is thus not always straightforward. However, differences between SA1 and PC fibers are very pronounced, with SA1 fibers responding primarily to slow skin deflections and PC fibers responding to rapid ones (Goodman and Bensmaia, 2020). Accordingly, neurons that receive dominant input from SA1 fibers can be distinguished from those that receive dominant input from PC fibers. Examination of neurons at the two extremes of this dominant axis of variance in cortical responses (Lieber and Bensmaia, 2019) can shed light onto the relationship between the submodality composition of a neuron's input and that neuron's temporal coding properties. Here, we show that PC-like cortical neurons exhibit more reliable temporal patterning and carry

more information about texture in their spike timing than do their SA1-like counterparts. As mentioned above, however, these neural populations are at extremes of a continuum: Neurons that receive balanced PC and SA1 input will exhibit intermediate response properties. However, to the extent that they receive PC input, they are liable to carry texture information in the temporal patterning of their response. Consistent with this hypothesis, the optimal decoding resolution is on the order of a few milliseconds, even in many cells that receive dominant SA1 input, despite the low temporal resolution of this dominant input.

2.3.3 | TEMPORAL PATTERNS SCALE SYSTEMATICALLY WITH SPEED

A central question in neuroscience is how we achieve robust object representations despite changing sensory input. Texture perception constitutes an example of this phenomenon. Indeed, afferent responses scale systematically – both in their patterning and in their strength – with changes in scanning speed (Weber et al., 2013). Despite the speed dependence of the texture signal emanating from the periphery, our perception of texture is almost completely independent of scanning speed, even if the texture is scanned passively across the skin (Boundy-Singer et al., 2017; Lederman, 1974; Meftah el-M et al., 2000). Scanning speed-related signals in the nerve must thus somehow be discounted in the computation of texture. This process is not trivial, as evidenced by the fact that the converse is not true: Tactile speed perception is highly dependent on texture, with rougher textures being systematically perceived as moving faster across the skin (Delhaye et al., 2019).

We have previously shown that rate-based signals in cortex are more robust to changes in scanning speed than are their counterparts in the nerve (Lieber and Bensmaia, 2020). This

increased robustness to speed could in part be attributed to computations applied to the afferent input and reflected in the output of cortical neurons. Specifically, populations of simulated cortical neurons that reflected temporal and spatial differentiations of their afferent input exhibited responses that were less speed-dependent than was the afferent input itself. Here, we show that this increase in robustness of a rate-based code is complemented by the propagation of the temporal code, which itself scales systematically with speed. One possibility is that this temporal patterning is further converted into a rate-based signal through successive differentiation operations. According to this hypothesis, downstream neurons – in secondary somatosensory cortex, e.g. – would carry more texture information in their rates and this rate-based representation would be more invariant to changes in speed.

2.3.4 | TEMPORAL PATTERNING OF THE CORTICAL RESPONSE SHAPES TEXTURE PERCEPTION

First, the role of temporal spiking patterns in cortex in shaping perception has been elusive. Probably the most compelling evidence is that information about the frequency of high-frequency vibrations is carried in the temporal patterning and not the rates; yet their frequency is still discriminable (Harvey et al., 2013). The link between perception and neural response is thus circumstantial. Here, we provide a more explicit link between temporal patterning and perception: perceptual ratings are better predicted by temporal patterning than by rates.

Second, rate and temporal codes are often put in opposition, where one purportedly drives behavior and the other does not. Our results imply a synergistic integration of the two types of codes: perceived texture is best predicted from the combination of spike rate and timing. This integrative neural code reflects the two codes that carry texture signals in the peripheral nerves:

Spatial and temporal. In cortex, texture information carried in spatial patterns of activation of SA1 and RA fibers has been converted into a rate code by the spatial filtering properties of subpopulations of cortical neurons (Bensmaia et al., 2008; DiCarlo et al., 1998; Lieber and Bensmaia, 2019), which individually act as detectors of spatial features in the input. Texture information carried in temporal patterns of activation RA and PC fibers is converted into a rate code by temporal filters (Saal et al., 2015), which act as detectors of temporal features in the input. As one ascends the somatosensory neuraxis, successive temporal differentiations convert temporal patterns into rate, but this process is not complete in SC as evidenced by the residual informativeness of temporal patterning and its ability to predict perception above and beyond rate. As a result, spatial and temporal codes coexist in SC to encode texture, as seems to be the case in barrel cortex (Zuo et al., 2015).

2.4 | Conclusions

Temporal spiking patterns in somatosensory cortex are precise and informative about texture identity. Cells vary in the degree to which texture information is carried in their temporal patterning and this heterogeneity is in part driven by the afferent input: Neurons that receive dominant input from PC fibers, which carry textural information in their spike timing, themselves carry information in their spike timing. Information carried in the temporal spiking patterns in cortex complements that carried in firing rates. The combination of rate and timing is more predictive of texture perception than are rate or timing in isolation.

2. 6 | METHODS

The cortical responses have been described in two previous studies (Lieber and Bensmaia, 2019, 2020) and the peripheral nerve responses have been described in another two studies (Lieber et al., 2017; Weber et al., 2013).

2.6.1 | ANIMALS

All experimental procedures involving animals were approved by the University of Chicago Institutional Animal Care and Use Committee. Cortical data were obtained from two rhesus macaques (males, 6-8 years old and 8-11kg), instrumented with a custom head-post to allow for head immobilization (for eye-tracking and stable neurophysiological recordings) and a 22-mm wide recording chamber centered on the hand representation in anterior parietal cortex. During training and data collection, animals performed a visual contrast discrimination task so that they would remain awake and calm. In brief, animals fixated on a go-target to initiate the trial, and two circles appeared on the computer monitor. The animal made a saccade to the brighter target to obtain a juice reward. Peripheral responses were collected from 6 anesthetized rhesus macaques as previously described (Weber et al., 2013).

2.6.2 | NEUROPHYSIOLOGY

Cortical responses: Procedures have been previously described in detail (Lieber and Bensmaia, 2019, 2020). In brief, extracellular recordings were obtained using tungsten electrodes (Epoxylite insulated probes, FHC Inc.) driven into somatosensory cortex – Brodmann's areas 3b, 1, and 2 – using a computer-controlled microdrive (NAN Instruments, Nazaret Illit, Israel). We collected the responses from neurons whose receptive fields were centered on the distal fingerpads of digits

2-5. A full recording session (59 textures, presented 5 times at 80mm/s) lasted at least 30 minutes and we only report the responses of neurons whose action potential waveforms remained stable over the entire session. For a subset of 49 highly stable neurons, we also collected responses to 10 textures at three additional speeds (60mm/s, 100mm/s, and 120mm/s, (Lieber and Bensmaia, 2020)).

Peripheral responses: Procedures have been previously described in detail (Talbot et al., 1968; Weber et al., 2013). In brief, we obtained extracellular recordings of 17 SA1, 15 RA, and 7 PC fibers in the median and ulnar nerves of six macaques under isoflurane anesthesia.

2.6.3 | TACTILE STIMULI

We presented a diverse set of textures at a controlled speed (80 ± 0.1 mm/s) and force (25 ± 10 g) using a custom-built and designed texture-drum stimulator (Weber et al., 2013) for both the peripheral and cortical experiments though the texture set was different albeit overlapping. The cortical texture set included 59 textures, including furs, fabrics, papers, and 3-D printed gratings and dot patterns. These textures were selected to include features that span spatial scales. The peripheral texture set included 55 textures, 24 of which overlap with the cortical set (Supplemental Table 1). Each texture was presented for 2 seconds, though in these analyses, we only evaluated 500 ms of the steady-state response (excluding the onset and offset transients).

2.6.4 | HUMAN PSYCHOPHYSICS

Ten human subjects rated the dissimilarity between pairs of textures. The stimulus set included 13 textures (Supplemental Table 1), yielding 78 unique pairs, and each texture pair was presented 5 times to each subject. If a pair was perceived as identical, the subjects ascribed it

a rating of zero. If one pair of textures was perceived as being twice as different as another, the former was to be ascribed a number that was twice as was the latter. Subjects were free to use the range and were encouraged to use fractions and decimals. Ratings obtained from each subject were normalized by the mean rating across textures in each session and then averaged across sessions.

2.6.5 | DATA ANALYSIS

Neurophysiological recordings yielded spike times spanning a period beginning 1s before and for 3s after skin make contact with a given texture. For all analyses, we used a 500-ms epoch that began 100 ms after the texture contact to exclude transient responses.

Firing rate classification: We calculated each neuron's firing rate to each texture presentation (141 cells x 59 textures x 5 repeats) by counting the number of spikes during the aforementioned 500-ms window. To assess how informative about texture these firing rates were, we performed a nearest-neighbor classification. For single cell classification, we calculated the Euclidian distance between one test trial (one repeat of a given texture) and the mean response across all remaining repeats of every texture in the dataset. The classification was correct if the training texture with the lowest distance was the texture presented in the test trial.

PSTH and cross-correlation classification: We calculated peri-stimulus time histograms (PSTHs) by convolving spike trains with Gaussian kernels of varying widths (ranging from 1 to 500 ms) to assess decoding performance at various temporal precisions. Importantly, all PSTHs were demeaned to remove rate-based information from the signal. All that remained was the waxing and waning of the response in time – a purely time-varying signal that was not confounded by

rate. By convolving neural spike trains with Gaussian kernels of increasing width, we obscured increasing amounts of the fine timing information. To the extent that this fine timing information is just noise, wider Gaussian kernels should de-noise the signal and improve classification performance. Alternatively, if fine timing is informative, obscuring it should degrade classification. To test this, we performed an analogous classification to the firing rate classification described above. We computed the cross-correlation (using Matlab xcov function, as xcov is a zero-mean cross correlation) of one test response (500 ms PSTH, computed at a given resolution for one repeat of a given texture) and all other repeats of every texture. To accommodate the fact that responses may be shifted slightly in phase from one repeat to the next, we selected the max cross-correlation across time. We then averaged the max cross-correlation values across all repeats for a given texture, and the classifier selected the training texture that yielded the highest cross-correlation. The classification was correct if the training texture with the highest correlation was the texture presented in the test trial.

Metric-Space Analysis: We used metric-space analysis to quantify the dissimilarity between responses of a given neuron to repeated presentations of a stimulus. Here, we employed a commonly used method that assigns a minimum cost to transforming one spike train into another. The cost adding or removing a spike is 1, and the cost of moving a spike in time is qldtl, where q is a parameter. When q = 0, there is no penalty to moving spikes in time, such that the minimum cost is simply the difference in spike count. For high values of q, spikes that displaced in time incur a cost. Using this distance metric, we compute a measure of dissimilarity that is influenced by both the firing rate and temporal patterning of two spike trains.

Combined rate and timing classification: To combine rate difference and timing correlation to decode texture identity, we z-scored the distance matrices for each neuron and coding scheme, and multiplied all PSTH cross-correlation values by -1 (to invert similarity into a dissimilarity metric). We then computed the optimal weighted averages of these z-scored distance matrices (rate & timing) for each neuron. To find the optimal weighting, we performed the classification using weights that ranged from 0% rate (100% timing) to 100% rate (0% timing) and identified the weighting that yielded the best performance. To the extent that timing does not improve rate classification, this weighted average would include 100% rate and 0% timing. To the extent that a combination of both coding schemes improves classification performance, the weights would be intermediate. We report the classification performance of the optimal combination, which, in all cases, was an intermediate combination of rate and timing.

Population analyses: For the population analyses, we averaged the z-scored distance matrices of n randomly sampled neurons (without replacement). We then performed the classification using this mean distance matrix. For PSTH classification, we used each neuron's optimal decoding resolution. For rate classification, this population analysis did not require the selection of a temporal resolution, as we assessed rate across the entire 500-ms window. For combined rate and timing classification, we weighted each neuron's timing- and rate- based distance matrices (as described in the previous section) and averaged these combined distance matrices across the neuronal population to perform nearest neighbor classification.

Homogenous Poisson neurons: To validate the timing-based classification approach, we simulated Poisson spike trains generated from the measured firing rates. Simulated responses

contained the same rate information as their measured counterparts but lacked temporal fidelity. To generate these model spike trains, we generated a vector of spike times from a stationary Poisson process where the probability of a spike in each bin (dt = 0.1 ms) was P = r*dt, where r is the measured spike rate.

Jittered spike trains: At the other extreme of a purely Poisson model is a deterministic response that does not vary across repeats. To simulate responses at pre-determined levels of jitter, we took the response to one presentation of each texture and jittered each spike time by a specific amount. Specifically, we introduced jitter probabilistically using a gaussian with mean 0 and a standard deviation defined by the jitter level (between 1 and 200 ms). We then added and removed spikes as necessary to ensure that repetitions in the simulated responses were rate matched with their measured counterparts, given the trial to trial variations in the latter.

Comparing real data to jittered spike trains: To quantify how measured cortical responses compared to their simulated jittered counterparts, we used metric-space analysis (described above) to calculate the distance between multiple repetitions of the same stimulus at a very high temporal resolution (2ms, q = 500). For each neuron, we first calculated the mean pairwise distance between repeats (across all textures) and the mean pairwise distance between rate-matched jittered responses. We then identified the jitter level that yielded a smaller distance and a larger distance to the neuron's cross-repetition distance and averaged these two jitter values to obtain an estimate of that neuron's precision. For example, if a neuron's mean cross-repetition distance was 15, and its jittered model had a distance of 13 with 1-ms jitter and a distance of 21 at 2-ms jitter, the neuron's resolution as 1.5 ms.

Submodality composition of cortical cells: As reported previously (Lieber and Bensmaia, 2019), we estimated the submodality composition of a neuron's peripheral inputs by regressing that neuron's z-scored responses onto the z-scored responses of SA1, RA, and PC afferents to a shared set of 24 textures. We then selected the extremes of this continuum from SA-like to PC-like by selecting cortical cells with a normalized regression weight of > 0.8 to either SA1 or PC fibers. This criterion yielded 12 PC-like cortical cells (n = 10 in area 1, n = 2 in area 2) and 25 SA-like cortical cells (n = 9 in area 3b, n = 14 in area 1, n = 2 in area 2).

Cross-speed classification: To convert neural responses to spikes / mm from spikes / ms, we multiplied spike times by the scanning speed (60, 80, 100, or 120 mm/s). This resulted in warped spike trains that could be compared across speeds. Within-speed classification was performed using a leave-one out procedure. Cross-speed classification was performed in the same way, except that classifiers were trained on four warped repetitions at one speed (ie 80 mm/s), and tested on one left-out warped repetition at a different speed (ie 120 mm/s). All other methods were as described above.

Predicting dissimilarity ratings: We predicted perceived dissimilarity using cross-validated multiple regression. We trained the regression using all but one texture pair and tested it on the left-out texture pair. We then calculated the mean squared error of this prediction across each of the 78 texture pairs.

2.7 | REFERENCES

Arabzadeh, E., Panzeri, S., and Diamond, M.E. (2006). Deciphering the Spike Train of a Sensory Neuron: Counts and Temporal Patterns in the Rat Whisker Pathway. J. Neurosci. 26, 9216–9226.

Bensmaia, S.J., and Hollins, M. (2003). The vibrations of texture. Somatosensory & Motor Research 20, 33–43.

Bensmaia, S.J., Denchev, P.V., Dammann, J.F., Craig, J.C., and Hsiao, S.S. (2008). The Representation of Stimulus Orientation in the Early Stages of Somatosensory Processing. J. Neurosci. 28, 776–786.

birznieks, I. and Vickery, R.M. (2017). Spike Timing Matters in Novel Neuronal Code Involved in Vibrotactile Frequency Perception: Current Biology. Current Biology 27, 1485–1490.

Boundy-Singer, Z.M., Hannes, X., Saal, P., and Bensmaia, S.J. (2017). Speed invariance of tactile texture perception. J Neurophysiol 118, 2371–2377.

Callier, T., Saal, H.P., Davis-Berg, E.C., and Bensmaia, S.J. (2015). Kinematics of unconstrained tactile texture exploration. J. Neurophysiol. 113, 3013–3020.

Celikel, T., Szostak, V.A., and Feldman, D.E. (2004). Modulation of spike timing by sensory deprivation during induction of cortical map plasticity. Nature Neuroscience 7, 534–541.

Delhaye, B.P., O'Donnell, M.K., Lieber, J.D., McLellan, K.R., and Bensmaia, S.J. (2019). Feeling fooled: Texture contaminates the neural code for tactile speed. PLoS Biol 17.

DiCarlo, J.J., Johnson, K.O., and Hsiao, S.S. (1998). Structure of Receptive Fields in Area 3b of Primary Somatosensory Cortex in the Alert Monkey. J. Neurosci. 18, 2626–2645.

Dykes, R.W., Rasmusson, D.D., Sretavan, D., and Rehman, N.B. (1982). Submodality segregation and receptive-field sequences in cuneate, gracile, and external cuneate nuclei of the cat. Journal of Neurophysiology 47, 389–416.

Goodman, J.M., and Bensmaia, S.J. (2020). The Neural Mechanisms of Touch and Proprioception at the Somatosensory Periphery. In The Senses, (Elsevier), p.

Greenspon, C.M., McLellan, K.R., Lieber, J.D., and Bensmaia, S.J. (2020). Effect of scanning speed on texture-elicited vibrations. Journal of The Royal Society Interface 17, 20190892.

Harvey, M.A., Saal, H.P., Dammann, J.F., and Bensmaia, S.J. (2013). Multiplexing Stimulus Information through Rate and Temporal Codes in Primate Somatosensory Cortex. PLoS Biology 11, e1001558.

Hollins, M., Bensmaïa, S., Karlof, K., and Young, F. (2000). Individual differences in perceptual space for tactile textures: Evidence from multidimensional scaling. Perception & Psychophysics 62, 1534–1544.

Jadhav, S.P., Wolfe, J., and Feldman, D.E. (2009). Sparse temporal coding of elementary tactile features during active whisker sensation. NATURE NEUROSCIENCE 12, 11.

Kayser, C., Logothetis, N.K., and Panzeri, S. (2010). Millisecond encoding precision of auditory cortex neurons. PNAS 107, 16976–16981.

Krubitzer, L.A., and Kaas, J.H. (1992). The somatosensory thalamus of monkeys: Cortical connections and a redefinition of nuclei in marmosets. Journal of Comparative Neurology 319, 123–140.

de Lafuente, V., and Romo, R. (2006). Neural correlate of subjective sensory experience gradually builds up across cortical areas. Proceedings of the National Academy of Sciences of the United States of America 103, 14266–14271.

Lederman, S.J. (1974). Tactile roughness of grooved surfaces: The touching process and effects of macro- and microsurface structure. Perception & Psychophysics 16, 385–395.

Lieber, J.D., and Bensmaia, S.J. (2019). High-dimensional representation of texture in somatosensory cortex of primates. Proceedings of the National Academy of Sciences 116, 3268–3277.

Lieber, J.D., and Bensmaia, S.J. (2020). Emergence of an Invariant Representation of Texture in Primate Somatosensory Cortex. Cerebral Cortex 30, 3228–3239.

Lieber, J.D., Xia, X., Weber, A.I., and Bensmaia, S.J. (2017). The neural code for tactile roughness in the somatosensory nerves. J Neurophysiol 118, 3107–3117.

Mackevicius, E.L., Best, M.D., Saal, H.P., and Bensmaia, S.J. (2012). Millisecond Precision Spike Timing Shapes Tactile Perception. J. Neurosci. 32, 15309–15317.

Manfredi, L.R., Saal, H.P., Brown, K.J., Zielinski, M.C., Dammann, J.F., Polashock, V.S., and Bensmaia, S.J. (2014). Natural scenes in tactile texture. Journal of Neurophysiology 111, 1792–1802.

Meftah el-M, E.M., Belingard, L., and Chapman, C.E. (2000). Relative effects of the spatial and temporal characteristics of scanned surfaces on human perception of tactile roughness using passive touch. Experimental Brain Research 132, 351–361.

Mountcastle, V.B., Talbot, W.H., Sakata, H., and Hyvärinen, J. (1969). Cortical neuronal mechanisms in flutter-vibration studied in unanesthetized monkeys. Neuronal periodicity and frequency discrimination. Journal of Neurophysiology 32, 452–484.

Oladazimi, M., Brendel, W., and Schwarz, C. (2018). Biomechanical Texture Coding in Rat Whiskers. Scientific Reports 8, 11139.

Padberg, J.J., Cerkevich, C., Engle, J., Rajan, A.T., Recanzone, G., Kaas, J.H., and Krubitzer, L.A. (2009). Thalamocortical connections of parietal somatosensory cortical fields in macaque monkeys are highly divergent and convergent. Cerebral Cortex 19, 2038–2064.

Panzeri, S., Petersen, R.S., Schultz, S.R., Lebedev, M., and Diamond, M.E. (2001). The Role of Spike Timing in the Coding of Stimulus Location in Rat Somatosensory Cortex. Neuron 29, 769–777.

Pei, Y.C., Denchev, P. V, Hsiao, S.S., Craig, J.C., and Bensmaia, S.J. (2009). Convergence of submodality-specific input onto neurons in primary somatosensory cortex. Journal of Neurophysiology 102, 1843–1853.

Phillips, D.P., Hall, S.E., and Boehnke, S.E. (2002). Central auditory onset responses, and temporal asymmetries in auditory perception. Hearing Research 167, 192–205.

Rinvik, E., and Walberg, F. (1975). Studies on the cerebellar projections from the main and external cuneate nuclei in the cat by means of retrograde axonal transport of horseradish peroxidase. Brain Research 95, 371–381.

Saal, H.P., Harvey, M.A., and Bensmaia, S.J. (2015). Rate and timing of cortical responses driven by separate sensory channels. Elife 4.

Saal, H.P., Wang, X., and Bensmaia, S.J. (2016). Importance of spike timing in touch: an analogy with hearing? Current Opinion in Neurobiology 40, 142–149.

Saal, H.P. and Bensmaia, S.J. (2020). Touch is a team effort: interplay of submodalities in cutaneous sensibility: Trends in Neurosciences. Trends in Neuroscience 37, 689–697.

Salinas, E., Hernández, A., Zainos, A., and Romo, R. (2000). Periodicity and Firing Rate As Candidate Neural Codes for the Frequency of Vibrotactile Stimuli. J. Neurosci. 20, 5503–5515.

Schwarz, C. (2016). The Slip Hypothesis: Tactile Perception and its Neuronal Bases. Trends in Neurosciences 39, 449–462.

Talbot, W.H., Darian-Smith, I., Kornhuber, H.H., and Mountcastle, V.B. (1968). The sense of flutter-vibration: comparison of the human capacity with response patterns of mechanoreceptive afferents from the monkey hand. Journal of Neurophysiology 31, 301–334.

Victor, J.D., and Purpura, K.P. (1997). Metric-space analysis of spike trains: theory, algorithms and application. Network: Computation in Neural Systems 8, 127–164.

Weber, A.I., Saal, H.P., Lieber, J.D., Cheng, J.W., Manfredi, L.R., Dammann 3rd, J.F., and Bensmaia, S.J. (2013). Spatial and temporal codes mediate the tactile perception of natural textures. Proceedings of the National Academy of Sciences of the United States of America 110, 17107–17112.

Wehr, M., and Zador, A.M. (2003). Balanced inhibition underlies tuning and sharpens spike timing in auditory cortex. Nature 426, 442–446.

Yang, Y., and Zador, A.M. (2012). Differences in Sensitivity to Neural Timing among Cortical Areas. J. Neurosci. 32, 15142–15147.

Zuo, Y., Safaai, H., Notaro, G., Mazzoni, A., Panzeri, S., and Diamond, M.E. (2015). Complementary Contributions of Spike Timing and Spike Rate to Perceptual Decisions in Rat S1 and S2 Cortex. Current Biology 25, 357–363.

2.8 | APPENDIX: CHAPTER TWO SUPPLEMENTAL FIGURES

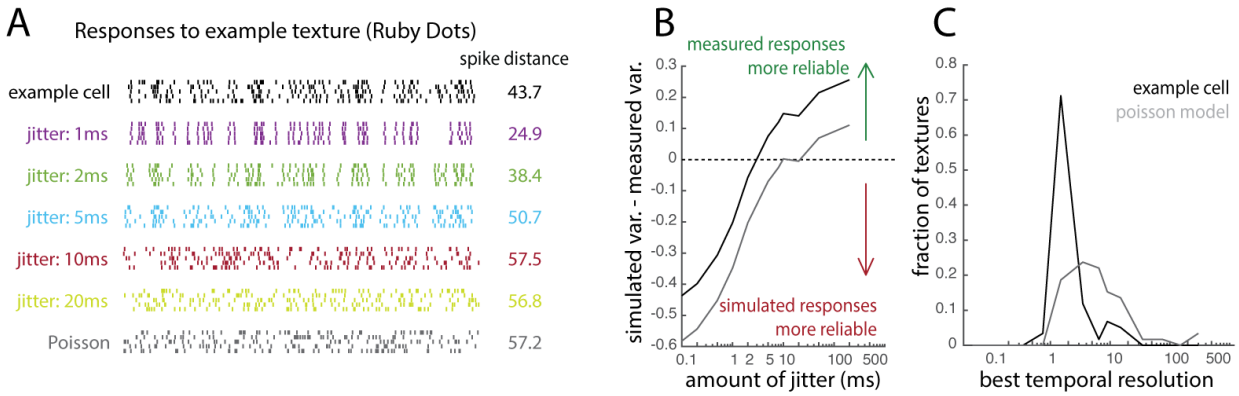

Supplemental Figure S.2.1: Characterizing the temporal resolution for each individual cortical cell. Al Response of one example neuron to 5 repeated presentations of one example texture. Colored rasters represent rate-matched simulated responses with different amounts of jitter. Grey raster is a rate-matched Poisson model. Spike distance values (q=500) represent mean pairwise spike distance across the 5 repetitions shown. Bl Simulated variability – measured variability is calculated by (1) dividing the neuron's spike distance by the mean firing rate across repetitions and (2) subtracting this value from the analogous value calculated from the simulated response. The point at which this line crosses the x-intercept represents the point at which the measured responses become more temporally reliable than their simulated counterparts. Cl Histogram of resolutions across all 59 textures for this example neuron.

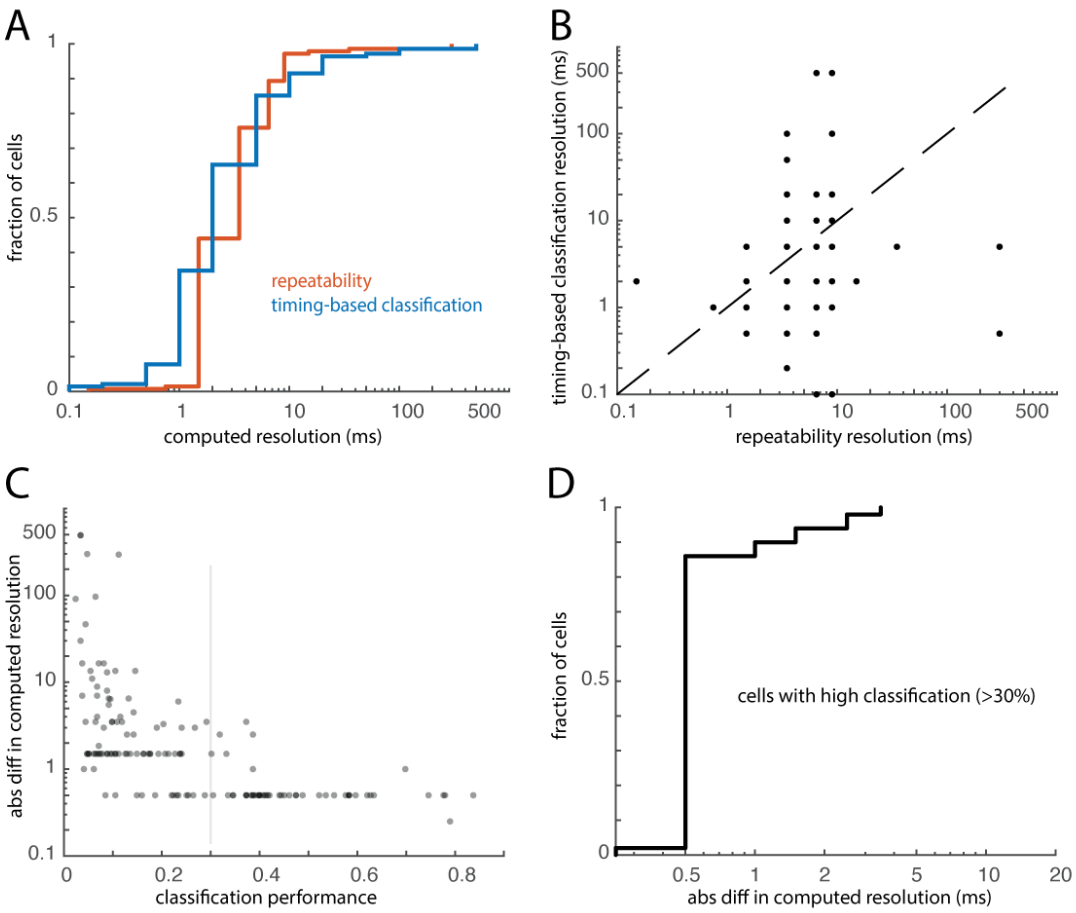

Supplemental Figure S.2.2: Temporal resolutions derived from the repeatability and classification analyses. Al Cumulative distribution of optimal resolutions for the repeatability and timing-based classification analyses. Bl Comparison of the resolution determined from repeatability analysis and timing-based classification. Each point represents one neuron; dashed line denotes unity. Cl Absolute difference in resolution between repeatability analysis and timing-based classification as a function of each neuron's classification performance. Dl In neurons with a classification performance better than 30% (those to the right of the grey line in C), the resolution estimated from the timing-based classification is within 5 ms of the resolutions estimated from the repeatability analysis.

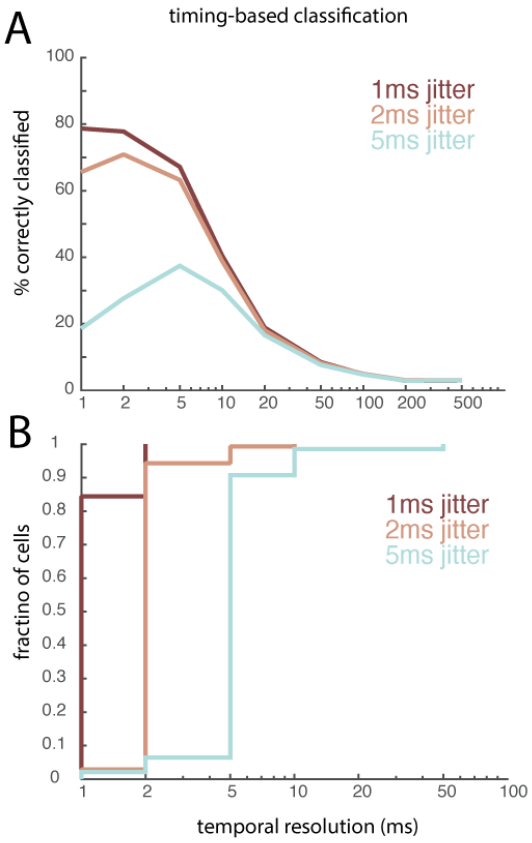

Supplemental Figure S.2.3: Timing-based classification using simulated jittered responses. Al Less jitter in simulated spike trains results in better timing-based classification performance. Bl The best classification resolution coincides with the amount of imposed jitter in these simulated responses.

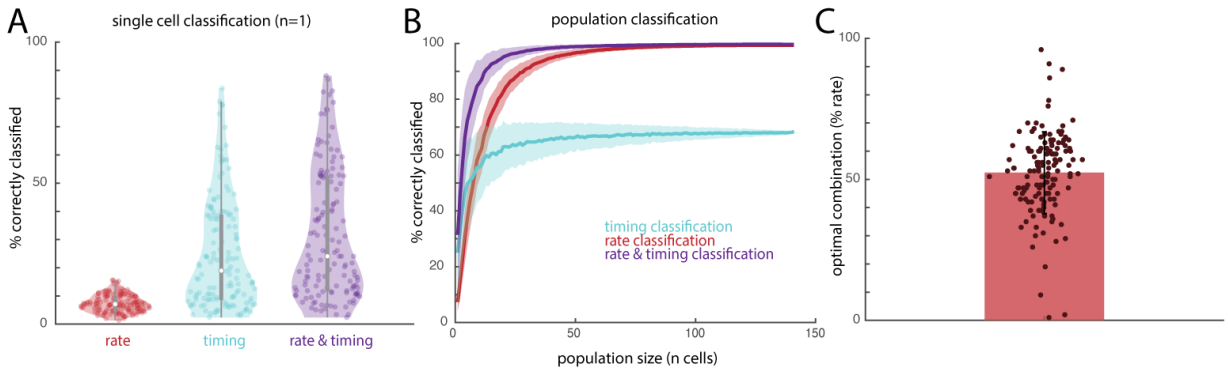

Supplemental Figure S.2.4: Single-cell and population classification using rate, timing, and a simple averaged combination of both. Al Single cell classification performance using rate dissimilarity, timing correlation, and an average of both (rather than an optimal combination). Same conventions as in Figure 2.2B. Bl Population classification using rate dissimilarity, timing correlation, and an average of both (rather than an optimal combination), averaged across the full neuronal population. Same conventions as in Figure 2.2C. Cl The weighting of rate and timing that yields the highest classification performance for each individual cell. Each point denotes a single cell's optimal % rate. Error bars represent standard deviation across 141 cells. The average optimal weighting is 52.4%, which is a likely explanation for why both A and B (in which all cells' weightings are set to 50%) are nearly indistinguishable from Figure 2.2B and C (in which each cell has its optimal weighting).

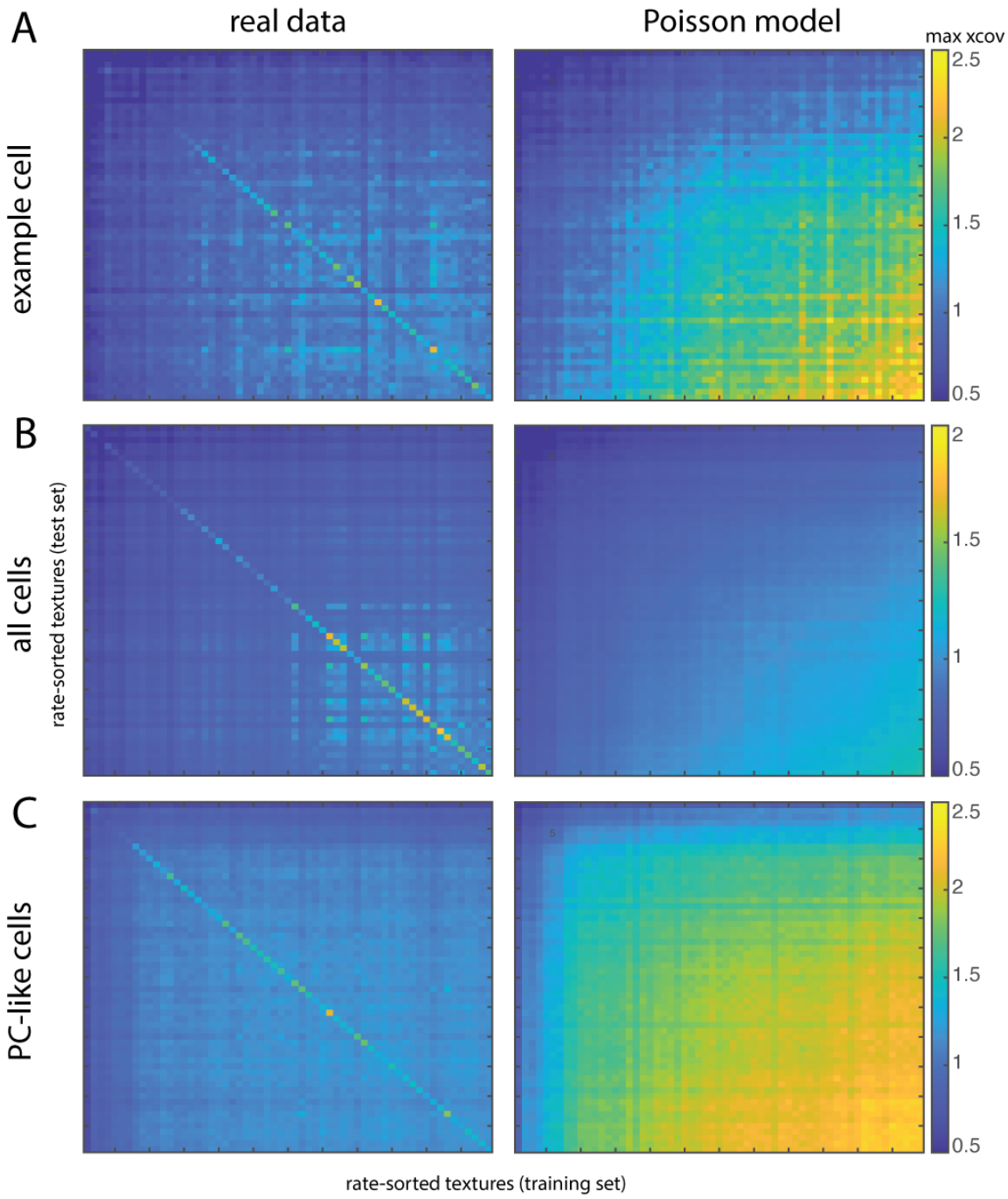

Supplemental Figure S.2.5: Confusion matrices of max cross-correlation in real and Poisson data.

Al Confusion matrices for an example cell, the same example cell used throughout this paper.

Each pixel represents the average of pairwise max cross-correlation values between responses

to a training texture (abscissa) and test texture (ordinate). Correlation values scale with firing rate in Poisson neurons and, to a much lesser extent, in measured responses to texture. For the measured resposnes, correlation values for responses to the same training and test texture are higher than mismatched pairs, whereas in the Poisson model, no such structure exists. Bl Same convention as A with average values across all cells. Cl Same convention as A and B with average values across a subpopulation of PC-like cells.

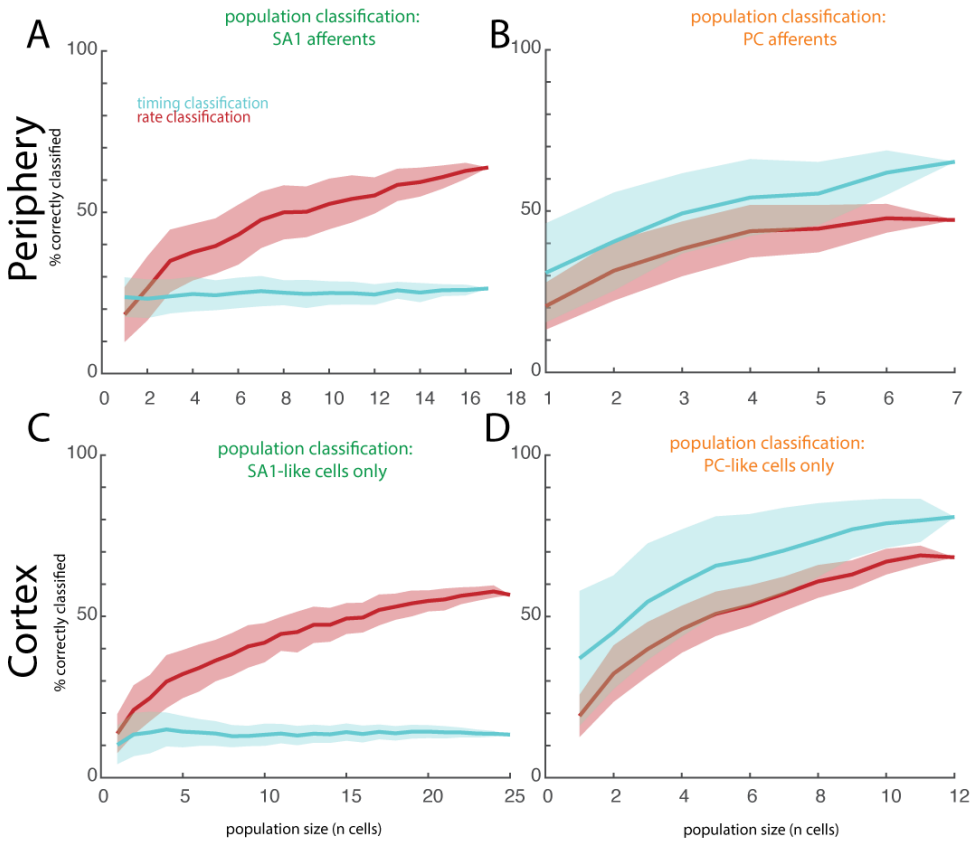

Supplemental Figure S.2.6: Classification of textures based on peripheral vs cortical population responses. Al Classification of 24 textures (chance = 1/24, 4.2%) based on the rate and timing of

the response of populations of SA1 fibers. Shaded area denotes the standard deviation across 100 randomly sampled populations of 1-17 neurons. Bl Same, with 1-7 PC fibers. Cl SA1-like cortical cell population classification of the same 24 textures, with 1-25 SA1-like cortical cells. Dl Same, with 1-12 PC-like cortical neurons.

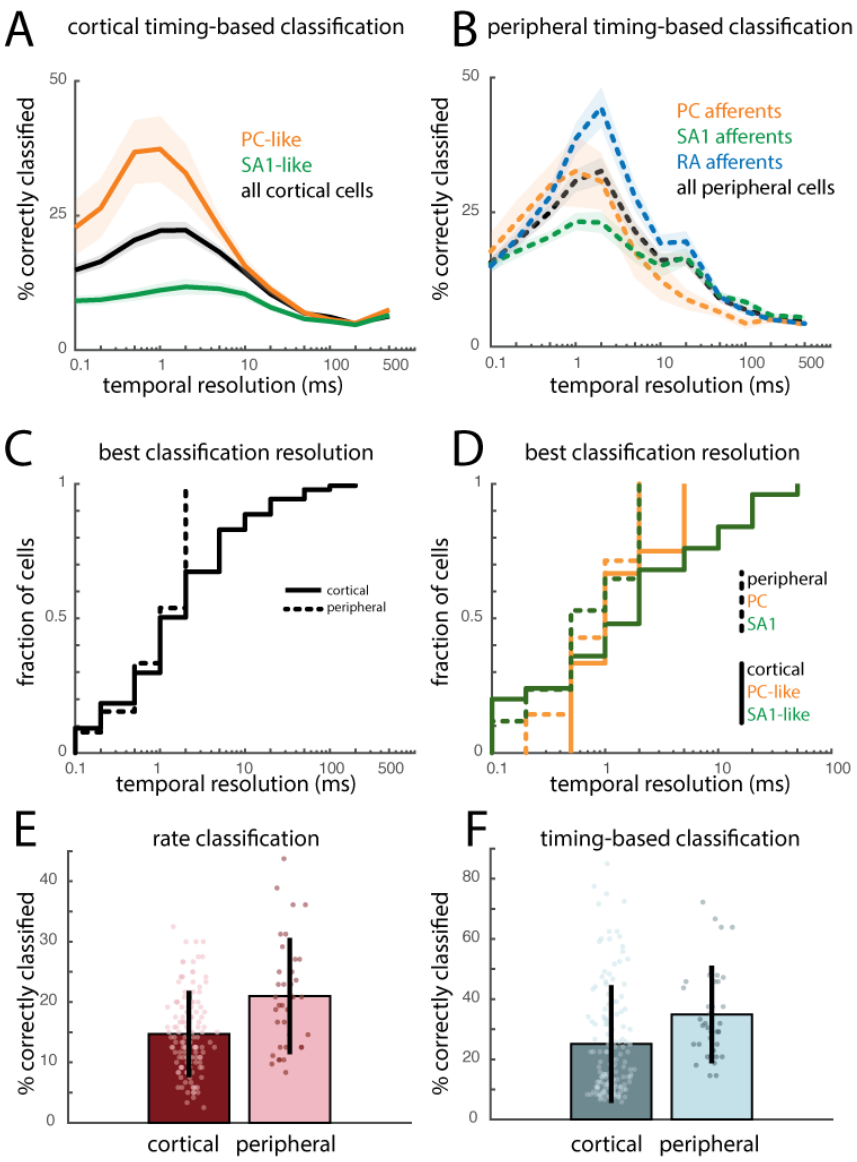

Supplemental Figure S.2.7: Timing-based classification based on peripheral and cortical responses for a matched texture set. Al Similar to Figure 2.3, timing-based classification performance across temporal resolutions for PC-like, SA1-like, and all cortical cells for a subset of 24 textures that were used in both the cortical and peripheral experiments. Bl Timing-based classification performance for the same 24 textures based on PC, SA1, and RA afferent

responses. Cl The best classification resolutions are similar for cortical and peripheral neurons, but some cortical neurons are temporally imprecise whereas no afferents are. Dl The temporal resolutions of PC fibers and PC-like cortical neurons overlap, whereas some SA1-like cortical neurons are more imprecise than any SA1 fibers. El Single-cell classification based on firing rates evoked in cortical and peripheral neurons. Each point represents one neuron's classification performance. Error bars denote standard deviation across 141 cortical and 39 peripheral neurons. Fl Same as in E, but for timing-based classification.

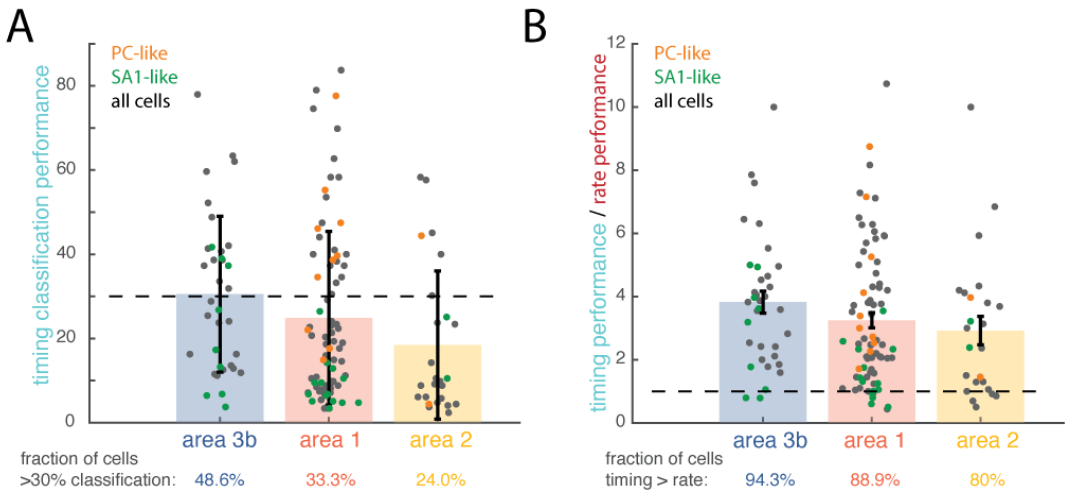

Supplemental Figure S.2.8: Differences in temporal resolution across cortical fields. Al Single-cell timing-based classification performance across different cortical fields. Each circle represents one neuron's performance; orange and green circles are color-coded based on the neuron's dominant submodality input. Error bars denote the standard deviation across cells. Bl Ratio of timing performance / rate performance. Same conventions as in panel A. Dashed line represents

equal performance for rate- and timing-based classifiers. Points above the line denote neurons for which timing outperforms rate.

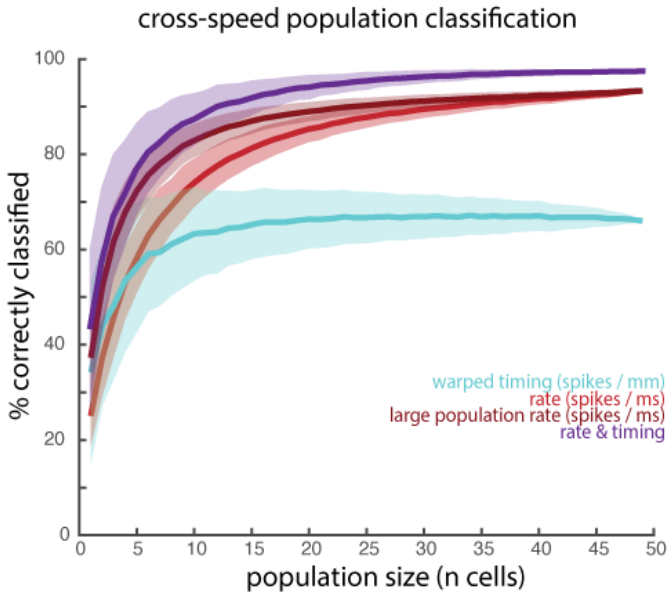

Supplemental Figure S.2.9: Classification based on both rate and timing outperforms classification based on rate. Mean cross-speed population classification based on rate (unwarped), timing (warped), the combination of both. As a control, we averaged rate over a population twice the size (large population rate classification) to test the extent to which the improved performance with rate and timing was simply driven by more predictors. Performance from the large population never exceeds that of rate & timing. Shaded regions denote standard deviation across 1000 iterations of randomly sampled populations of 49 neurons.

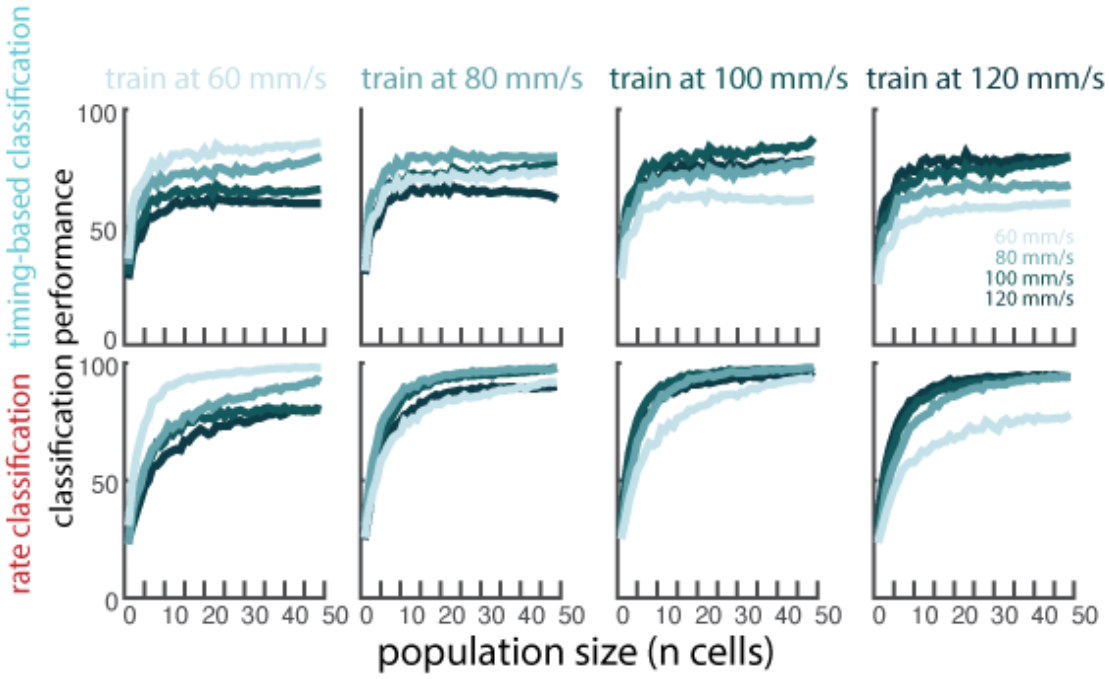

Supplemental Figure S.2.10: Population classifiers trained on responses to textures presented at one speed and tested on responses to textures at all speeds. Timing-based classification with warped spike trains (top row) and rate-based classifiers with unwarped spike trains (bottom row), trained and tested at all combinations of speeds.

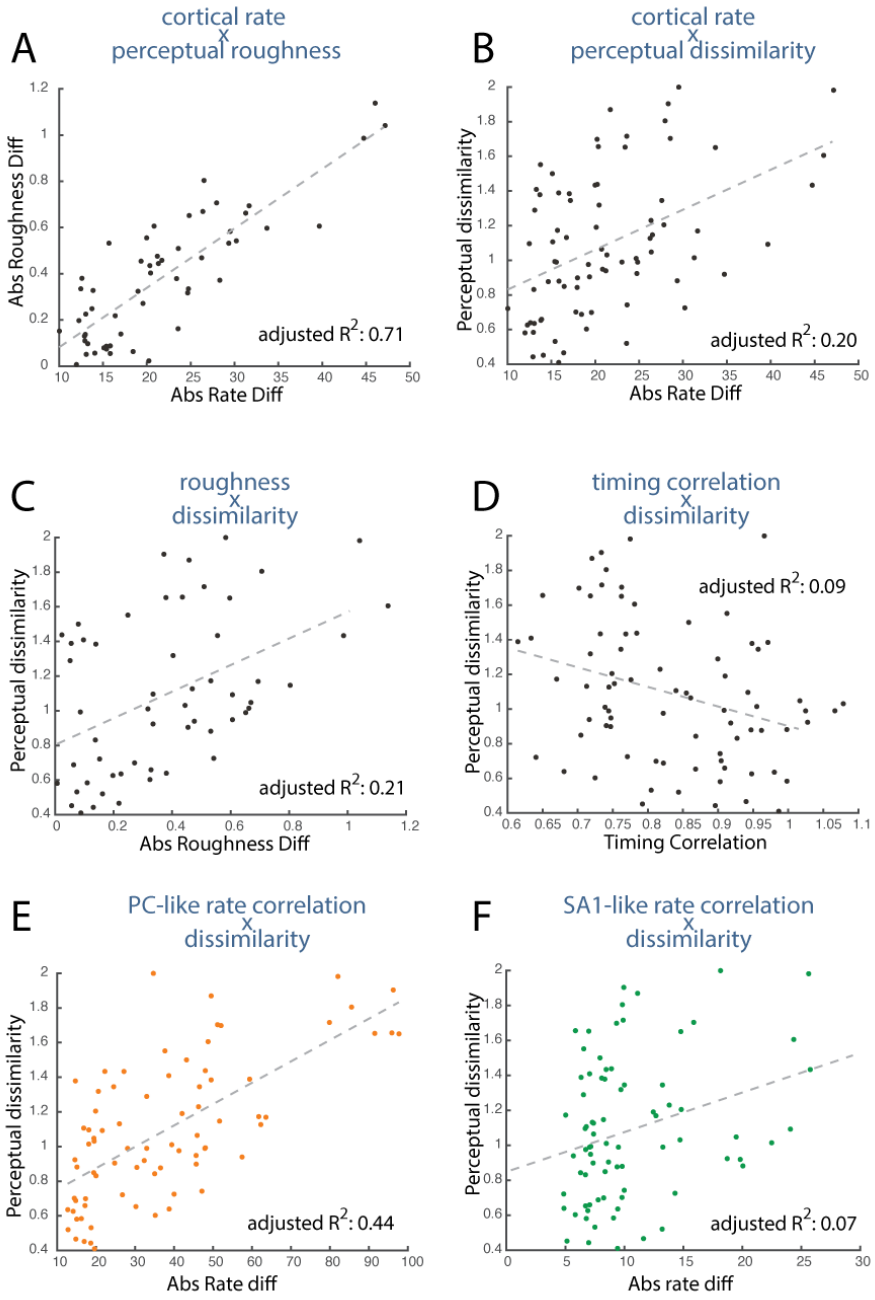

Supplemental Figure S.2.11: Roughness, but not dissimilarity, is predicted by firing rate. Al The absolute difference in mean firing rate across the full population of 141 cortical cells vs. the absolute difference in roughness ratings for the same texture pairs. Differences in firing rate predict differences in perceived roughness. Bl Differences in firing rate only account for 20% of

the variance in the dissimilarity ratings. Cl Similarly, differences in roughness account for 20% of the variance in dissimilarity ratings. Thus, many textures are similarly rough but feel very different nonetheless. Dl Mean timing correlation across the full population of 141 cortical neurons is a poor predictor of dissimilarity. El Although firing rate differences across all neurons do not correlate with perceived dissimilarity (as in C), firing rate differences in a population of 12 PC-like cortical cells do. Fl Mean firing rate differences in a population of 25 SA1 fibers are poor predictors of dissimilarity ratings.

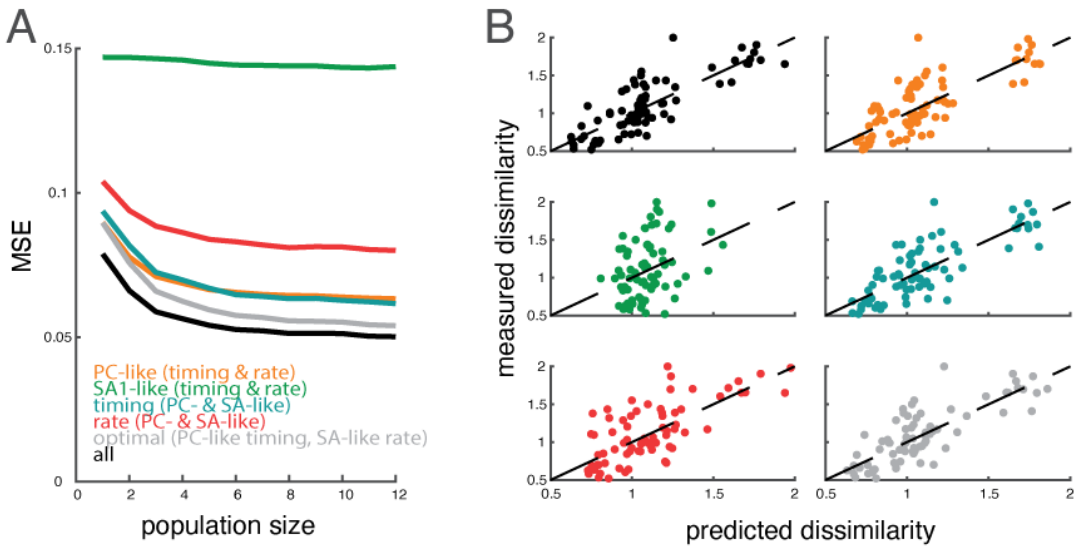

Supplemental Figure S.2.12: Two-factor multiple regression onto perceived dissimilarity of texture pairs. Al Cross-validated mean squared error of predicted dissimilarity vs. population size. Bl Population (n = 12) predicted vs. measured dissimilarity for all 78 texture pairs using the regression models shown in (A). Dashed lines denote unity.

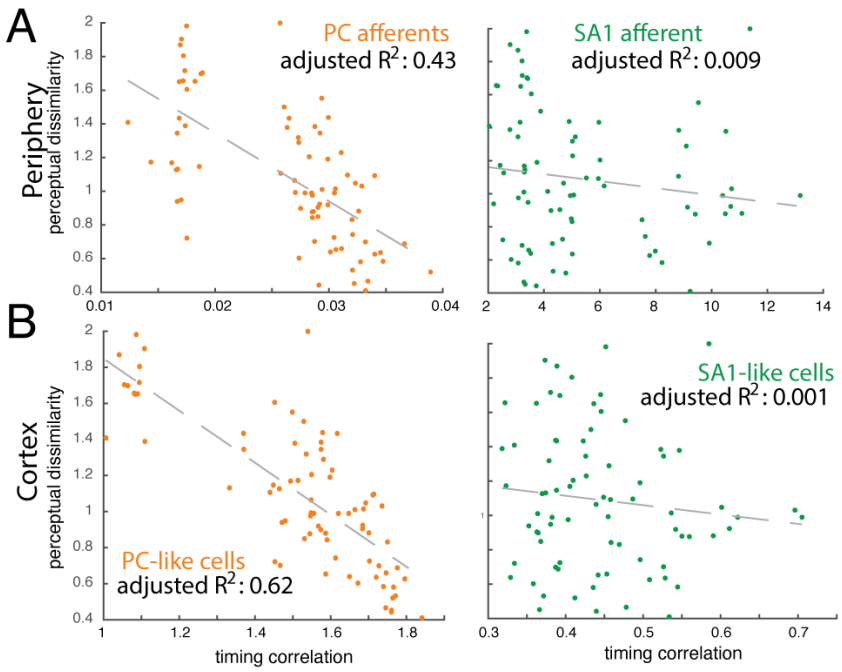

Supplemental Figure S.2.13: Temporal patterns of PC fibers and PC-like cortical neurons more closely reflect perceptual ratings than do their SA counterparts. Regression of timing correlation on perceived dissimilarity. Each point represents one texture pair. Dashed lines represent the best linear fit. Al Peripheral afferents. BlPC-like and SA1-like cortical cells.

All textures	Shared with peripheral data	Dissimilarity texture set	Speed set
Chiffon	X	X	X
Nylon	X	X	X
Stretch Denim	X		X
Hucktowel	X	X	X
City Lights			X
Deck Chair (Sunbrella)			X
Dots / 1 Grating			X
Fuzzy Upholstery (Blue)			X
Dots / Blank			X
Faux Croc Skin			X
Onyx Pavillion (Upholstery)			
Grid Upholstery			
Red Grating Upholstery			
Green Upholstery			
Unknown Pleasures			
Wrapping Paper (Bumpy)			
Crinkled Silk	X	X	
Parchment Paper			
20 Gauge Vinyl	X		
Microsuede	X	X	
Sueded Cuddle (Suede Side)	X	X	
Foam (Drapery Tape)	X		
5/500 Grating			
5/1 Grating			
Wool Blend	X	X	
Denim	X	X	
Satin	X	X	
Wool Gabardine	X		
Metallic Silk	X	X	
Velvet	X		
Computer Paper			
Careerwear Flannel	X		
Butcher Paper			
Organza	X		
Ruby Dots (Front)			
Yellow Upholstery		X	
Beach Mat (Tan)			
Corduroy - Thick Ridges	X	X	
Leathery Dots			
Long Hair Rabbit			
Short Hair Rabbit			
Snowflake Fleece (Fuzzy Side)	X		
20 Percent Wool Felt	X		
Possum Fur			
Sting Ray Skin			
Blank - Acrylic			
5 mm Grating	X		
1 mm Grating	X		
500 micron Grating			
RF 1			
Black Fabric Grating		X	
Embossed Dots - 4mm	X		
Embossed Dots - 5mm	X		
Dots / 500 Grating			
RF 2			
Tan Upholstery			
Lizard Skin			
Bumpy Polyester			
Ruby Dots (Backing)			

Supplemental Table 1: Texture set for each experiment. Column 1 includes all 59 textures used in the cortical experiments. Column 2 shows the 24 textures that overlapped with those used in the peripheral experiments. Column 3 shows the 13 textures used in the psychophysical

experiments. Column 4 shows the 10 textures that were presented at 4 speeds (60, 80, 100, 120 mm/s).

CHAPTER 3 | TEXTURE CODING IN HIGHER ORDER SOMATOSENSORY CORTICES

Our sense of touch confers to us a sensitivity to texture that spans six orders in magnitude in spatial scale, from tens of nanometers to tens of millimeters. In early stages of processing, from the nerve through somatosensory cortex (SC) – including Brodmann's areas 3b, 1, and 2 – individual neurons respond promiscuously to most textures and, as a population, carry a large shared signal that drives the perceived roughness, the dominant perceptual dimension of texture. Nothing is known about how natural textures are encoded in higher order cortices, including secondary somatosensory cortex (S2) and parietal ventral cortex (PV). To fill this gap, we monitored single-unit activity in S2/PV as non-human primates performed a texture discrimination task, in which they indicated whether pairs of naturalistic textures were the same or different. We then characterized the neuronal responses at the single-cell and population levels and compared these to their counterparts in SC. First, we found that a small fraction of S2/PV neurons carry texture signals, in contrast to their counterparts in SC, which usually do. Second, texture-modulated neurons in S2/PV exhibited sparse responses to texture, only responding to a small subset of textures, in contrast to SC neurons, which often respond to most textures. As a result, the representation in S2/PV is higher dimensional than is that in SC. Finally, S2/PV neurons carry cognitive signals about task variables such as trial type (same, different) and the animals' eventual decision, unlike their SC counterparts. The present study constitutes the first attempt to characterize the sensory representations in S2/PV using a complex, naturalistic stimulus set.

3.1 | INTRODUCTION

Our sense of touch imparts us with a sensitivity to texture that spans six orders in magnitude in spatial scale, from tens of nanometers to tens of millimeters. The most salient sensory dimensions of texture are roughness, hardness, stickiness, and warmth – associated with the coarseness, compliance, friction, and thermal conductivity of a surface, respectively (Hollins et al., 2000) – but surfaces give rise to myriad sensory qualities that are not captured by these four sensory continua – velvetiness, furriness, silkiness, etc. At the somatosensory periphery, texture information is relayed via different types of neural signals carried by different classes of nerve fibers (Weber et al., 2013): Coarse texture features – measured in millimeters – are reflected in the spatial pattern of activation in one population of nerve fibers, whereas smaller features are encoded in temporal spiking patterns evoked as the skin moves across the surface in two other afferent populations (Weber et al., 2013). These spatial and temporal signals in the nerve are integrated to give rise to a high-dimensional neural representation of texture in somatosensory cortex (SC) – including Brodmann's areas 3b, 1 and 2 (Lieber & Bensmaia, 2019). These insights into the neural basis of texture perception have relied critically on probing neural representations of texture stimuli that span the range of everyday tactile experience. Indeed, classic studies using parametrized stimuli – such as gratings and embossed dot patterns – failed to engage all the neural mechanisms that mediate the complex space of texture.

Higher order somatosensory cortex – including secondary somatosensory cortex (S2) and parietal ventral cortex (PV) – have never been probed using naturalistic stimuli so little is known about texture representations in these areas. On the other hand, previous studies have shown that

neurons in S2/PV not only carry sensory information – as do their counterparts in earlier stages of neuronal processing – but also task-related information, for example about stimulus category (i.e. increase vs decrease in vibratory frequency) or about the animal's decision (i.e. change vs no change) (Chapman & Meftah, 2005; Jiang et al., 1997; Romo et al., 2002; Rossi-Pool et al., 2021).

The goal of the present study is to investigate the representation of texture in S2/PV using naturalistic stimuli and to assess the degree to which neurons in these areas carry task-related information. To this end, we trained two monkeys to perform a texture discrimination task while we measured the responses evoked in S2/PV. We then compared the texture representation in S2/PV to that in SC. First, we found that individual S2/PV neurons respond more sparsely to texture than do SC neurons. Second, the population response to texture is higher dimensional in S2/PV and less driven by a shared response to low-level textural features. Third, S2/PV responses carry a wide variety of signals not related to the sensory stimuli themselves but rather to the task the animals are performing.

3.2 | RESULTS

Two rhesus macaques were trained to perform a texture discrimination task. On each trial, two textured surfaces were scanned across the animal's fingertip at a precisely controlled speed and contact force (80 mm/s, 25 g) using a rotating drum stimulator. The animals' task was to indicate whether the two stimuli were the same or different (e.g. Nylon-Nylon or Nylon-Silk, Figure 3.1A). A total of 44 diverse textures (including fabrics, furs, papers, and an additional catch trial in which no texture contacted the fingertip) were presented in 90 unique combinations (45 'same' and 45

'different' pairs). Both animals were slow to learn this task, requiring at least two full years of daily training sessions to establish stable behavior for neural recordings. Although this performance was stable across days, performance levelled off between 54-70% correct (chance = 50%, Supplemental Figure S.3.1), indicating that this task remained challenging even after extensive training. While animals performed this task, we recorded the responses of 95 neurons (three hemispheres in two monkeys) in S2/PV whose receptive fields included the distal digits, where the stimuli were delivered.

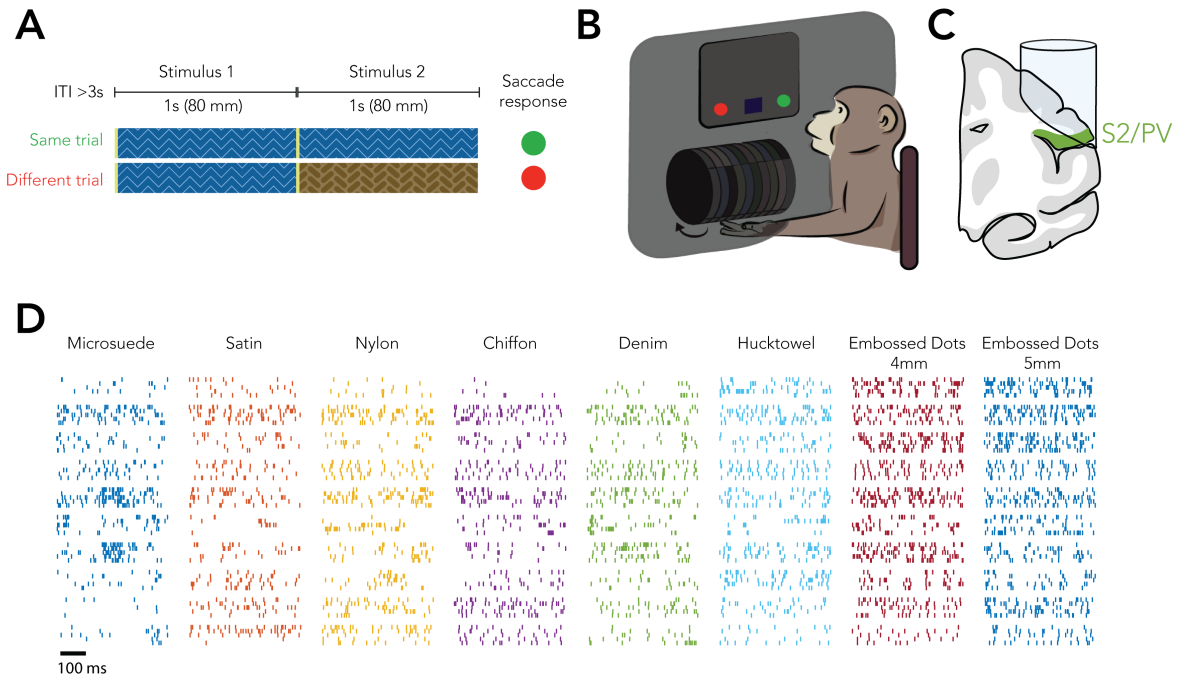

Figure 3.1: Experimental overview. (A) Behavioral paradigm: Upon trial initiation (fixation on a central target), two textures were presented sequentially with no inter-stimulus interval. After the drum lifts off the fingertip, the animal was presented with two targets, one of which indicated a 'same' response and the other a 'different' response. (B) Apparatus: The animal sat with both arms restrained behind a thick curtain to prevent any visual cues. The hand contralateral to the hemisphere of interest was positioned such that only one finger made contact with the stimulator. Initiation and maintenance of a trial required that animals fixate on a central target. At the end of each trial, two colored targets appeared and the animal saccaded to indicate its choice. (C) Recording chambers were centered over the hand representation in lateral parietal cortex (over the upper bank of the lateral sulcus). (D) Responses of 10 example S2/PV neurons (rows) to 5 repeated presentations of 8 example textures (columns). Different colors denote different textures.

3.2.1 / THE TEXTURE REPRESENTATION IN S2/PV IS SPARSE

First, we assessed the extent to which S2/PV neurons respond to texture (Figure 3.1D). Out of 95 cells, 74 cells (78%) responded to at least one texture (Figure 3.2A; permutation test with correction for multiple comparisons, $p < .05$) and, conversely, each of the 44 textures (excluding the catch trial) in the set evoked a response in at least 5% of cells (Figure 3.2A-B). However, 80%

of cells responded to fewer than 30% of the textures (Figure 3.2A) and 80% of the textures evoked a response from fewer than 25% of neurons (Figure 3.2B). In contrast, SC responses to a subset of common textures (40 textures, n = 141 SC cells) exhibited striking differences: SC neurons were far more promiscuous than were their S2/PV counterparts – responding to most textures – and, conversely, most textures evoked a response from most SC cells (Supplemental Figure S.3.2). For this set, most cells in S2/PV responded to fewer than 10% of the textured and most textures evoke a response in <20% of cells (Supplemental Figure S.3.2).

To further quantify the texture responses in S2/PV and compare them to their SC counterparts, we computed a measure of selectivity and another of sparseness (Figure 3.2C-D) (Arcizet et al., 2008; Rolls & Tovee, 1995). The selectivity index gauges the degree to which a neuron is modulated by the stimuli by computing the difference between the neurons response to its preferred and least preferred stimulus. The sparseness index gauges the degree to which a neuron responds to a small subset of stimuli. A neuron with a high selectivity and low sparseness might respond strongly to half the textures and weakly to the other half; a neuron with high selectivity and high sparseness will respond strongly to only a few textures, and weakly to the remainder. We found that S2/PV neurons are more selective and sparser than are SC neurons (two-sample t-test, sparseness: $t(234) = 4.56$, $p=8.1e-6$; selectivity: $t(234) = 5.00$,$p=1.13e-6$;

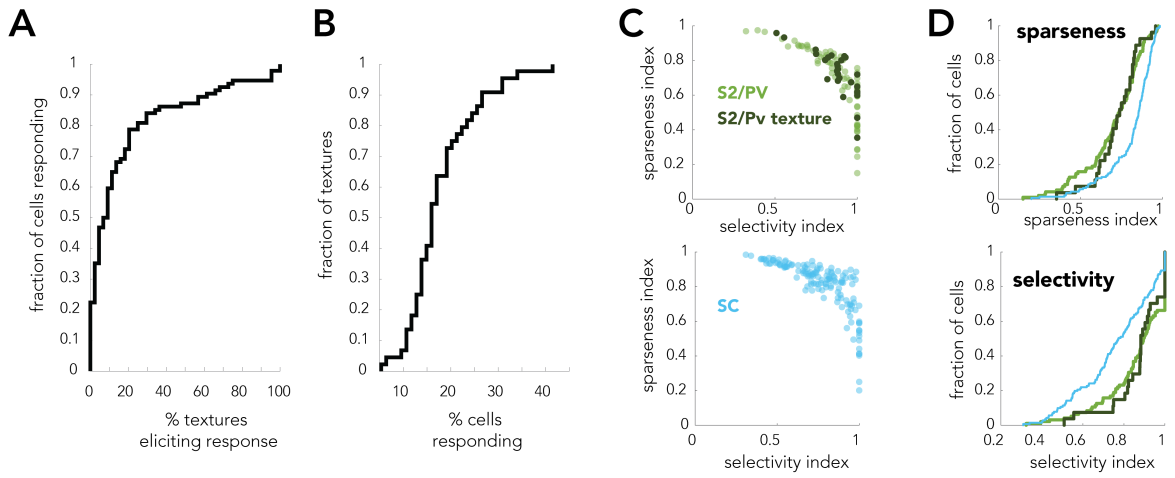

Figure 3.2: S2/PV cells respond sparsely to diverse textures. (A) Cumulative distribution of neurons that respond to increasing proportions of textures in the full stimulus set of 44 textures. >20% of cells do not respond to any textures, and 80% of cells respond to fewer than 30% of textures. (B) Cumulative distribution of textures that evoke a response from increasing proportions of S2/PV cells. Every texture evokes a response in at least 5 cells. (C) Sparseness and selectivity indices for SC, S2/PV, and S2/PV soignificantly texture-modulated neurons. High sparseness values indicate uniform responses across stimuli. High selectivity indices indicate large differences between a neuron's responses to preferred and non-preferred stimuli. Each point denotes one cell. (D) Cumulative distribution of sparseness and selectivity indices for SC, S2/PV, and S2/PV texture-modulated cells. S2/PV cells espond to textures more sparsely and more selectively than do SC cells.

Figure 3.2C-D), even when the indices were only applied to S2/PC neurons whose responses were significantly modulated by texture as revealed by an 1-way ANOVA (correcting for multiple comparisons).

3.2.2 | The texture representation in S2/PV is high-dimensional

Principal components analysis (PCA) of the population responses to texture in SC revealed a high-dimensional representation, in which texture information is distributed over a large number of principle components, though much of the variance (64%) is carried by the first principal component (Lieber & Bensmaia, 2019). Furthermore, the first principal component is highly

predictive of the perceived roughness, the dominant perceptual dimension of texture, reported for the same set of textures by human observers. In contrast, the first principal component of the S2/PV response accounts for far less of the variance (28%), even when the analysis is restricted to texture-modulated cells (38%) (Figure 3.3A). Furthermore, the major axis of variance in the S2/PV responses was a poor predictor of perceived roughness, in contrast its counterpart in the nerve or in SC (Lieber et al., 2017; Lieber & Bensmaia, 2019; Weber et al., 2013) (Figure 3.3B). We verified that no other axis of variance in the S2/PV responses could account for roughness (Supplemental Figure S.3.4). One interpretation of this finding is that low-level perceptual features of a stimulus – roughness is the intensive dimension of texture – are not encoded at early stages of cortical processing but not late ones, where texture representations are sparser and isolate high-level perceptual features.

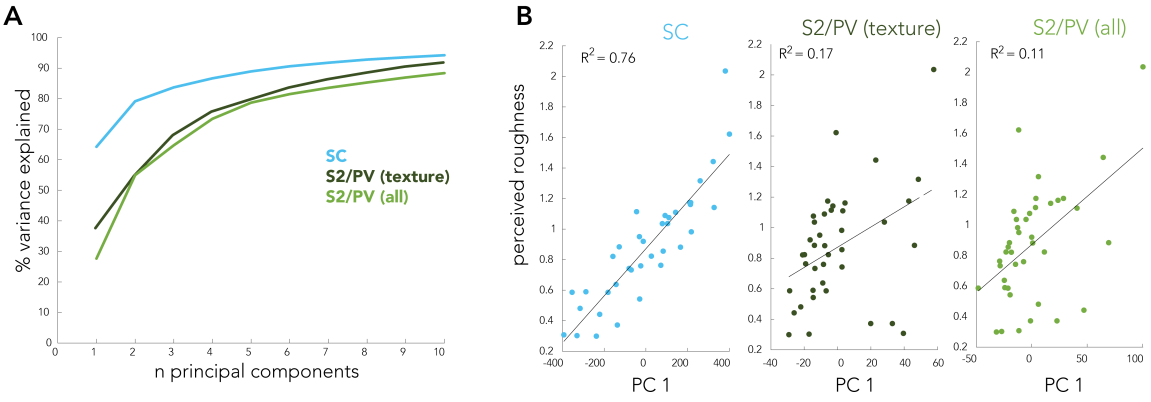

Figure 3.3: Dimensionality of the texture response in SC and S2/PV. (A) Variance explained by the first 10 principal components determined by principal components analysis of texture responses in SC (141 neurons) and S2/PV (95 cells, 27 texture-modulated cells). (B) Regression of perceived roughness of texture onto first principal component (PC) scores obtained from PCA. Each point denotes one texture. In SC, there is a strong correlation (R^2 = 0.87) between the first PC scores and perceived roughness, whereas in S2/PV, no such relationship exits, R^2 = 0.52 full population, R^2 = 0.41 texture-modulated cells).

3.2.3 | S2/PV RESPONSES ARE INFORMATIVE

Next, we tested the extent to which S2/PV responses are informative about texture by classifying texture based on single-cell and population-level firing rates during a 400-ms window of steady-state response during the first stimulus period. Classification performance is high to the extent that neuronal responses differ across textures and remaining consistent across repeated presentations of the same texture. For single-cell classification, we implemented a nearest-neighbor classifier. In brief, we trained the classifier on the vector of mean responses to each of 45 textures across 4 repeats. We then measured the Euclidian distance between these mean training responses and the response to each texture from a fifth, left-out response. A texture was correctly classified if its response in the test repeat was more similar to its mean response in the training set than to the mean response to any other texture in the training set. We repeated this process such that each texture and each repetition was left-out and used as the test response. We found that we could classify texture above chance for most, but not all, cells in S2/PV (Figure 3.4A). On average, single-cell classification performance was low (4.0% or fewer than 1.6 out of 40 stimuli), as implied by the sparseness metric described above. In contrast, classification based on SC responses was much higher (9.3%, or 3.8 out of 40 stimuli), with the best-performing cells in S2/PV performing no better than average cells in SC (Figure 3.4A). Next, we used discriminant analysis (LDA) to classify texture based on the response of populations of S2/PV neurons of increasing size. As expected, classification performance improved as more neurons were samples but remained far lower than that of SC (Figure 3.4B). Performance

improved when only neurons identified as texture-modulated were sampled at the single cell and population level (Figure 3.4A,B) but remained lower than its SC counterpart.

3.2.4 | S2/PV RESPONSES ARE VARIABLE

The lower classification performance achieved with S2/PV responses than with SC responses may be attributed to the sparseness of the texture representation in S2/PV compared to SC: each S2/PV neuron only responds to a small number of textures so the small sample of S2/PV neurons may not sufficiently tile the texture space to achieve good classification performance. Another factor that may contribute to the poor classification for S2/PV is the variability in its response. Indeed, S2/PV responses have been shown to be much more dependent on the animal's engagement in a behavioral task than is SC (Chapman & Meftah, 2005; Rossi-Pool et al., 2021). One might thus expect greater response variability caused by waxing and waning in the animal's attention. To test this possibility, we assessed the degree of variability across repeats by calculating the Fano factor of the responses to individual textures over repeated presentations. We found that Fano factors were much higher for S2/PV responses than for their SC counterparts (2.3 times greater, Figure 3.4C-D) and significantly so (two-sample t-test, $t(232) = 9.71$, $p = 6.5e\text{-}19$), even when the analysis was restricted to texture-modulated neurons in S2/PV (Figure 3.4D). Thus, both sparseness and variability conspire to reduce the ability to classify texture based on S2/PV responses.

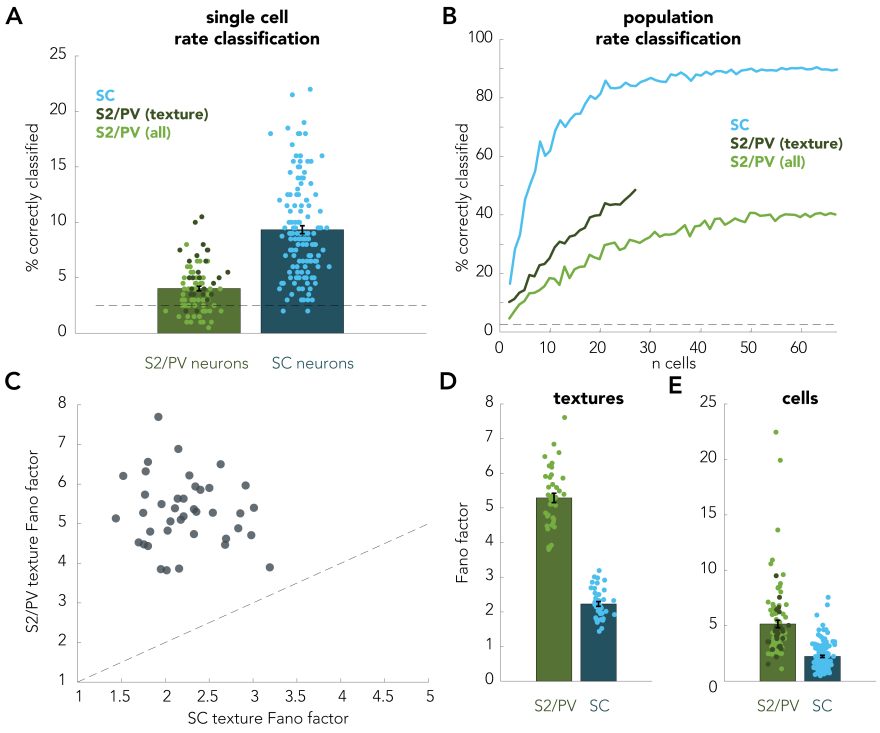

Figure 3.4: Texture classification and response variability. (A) Texture classification performance using nearest-neighbor rate classifiers trained on single cell responses to 40 different textures (chance = 2.5%). Each point denotes a single cell in S2/PV (green) or SC (blue). Error bars denote the standard error of the mean. (B) Population classification using cross-validated linear discriminant analysis with increasing populations of 2-65 neurons. S2/PV (texture), n = 27; S2/PV (all), n = 95; SC, n = 141. (C) Mean Fano factor (variance across repeated presentations of a texture / mean response to texture) across cells in SC vs S2/PV for each texture. Dashed line denotes unity. (D) Fano factors of texture responses in S2/PV are more than double those in SC. Each point denotes one texture. Error bars denote the standard error of the mean. (E) Fano factors vary across cells, but within the S2/PV population, variance does not differ between texture-modulated cells and non texture-modulated cells. Each point denotes each cell's mean Fano factor across all 40 textures.

3.2.5 | S2/PV RESPONSES CARRY TASK VARIABLES

S2/PV responses have been shown to carry information not only about tactile stimuli but also about task-relevant variables (Chapman & Meftah, 2005; Jiang et al., 1997; Romo et al., 2002). With this in mind, in the above analyses we analyzed neuronal responses in the first stimulus interval to isolate the sensory responses (and minimize the cognitive ones). In the following analyses, we examined the responses evoked during the second stimulus period and compared them to their counterparts in the first interval, matched for texture, to identify task-relevant cognitive signals.

Task-modulation was observed in the time-varying texture response of individual cells. One category of cells produced responses that related more closely to the animal's decision than they did to the stimulus or trial type (Figure 3.5A): The neurons' firing rates were higher throughout the second stimulus interval when the animal reported "different," even on 'same' trials. Another category of neurons responded selectively to changes in texture (Figure 3.5B), exhibiting a transient increase in firing rate at the onset of the second stimulus on 'different' trials, regardless of the animal's decision. These "change-detection" cells sometimes carried signals that also covaried with the animal's decision.

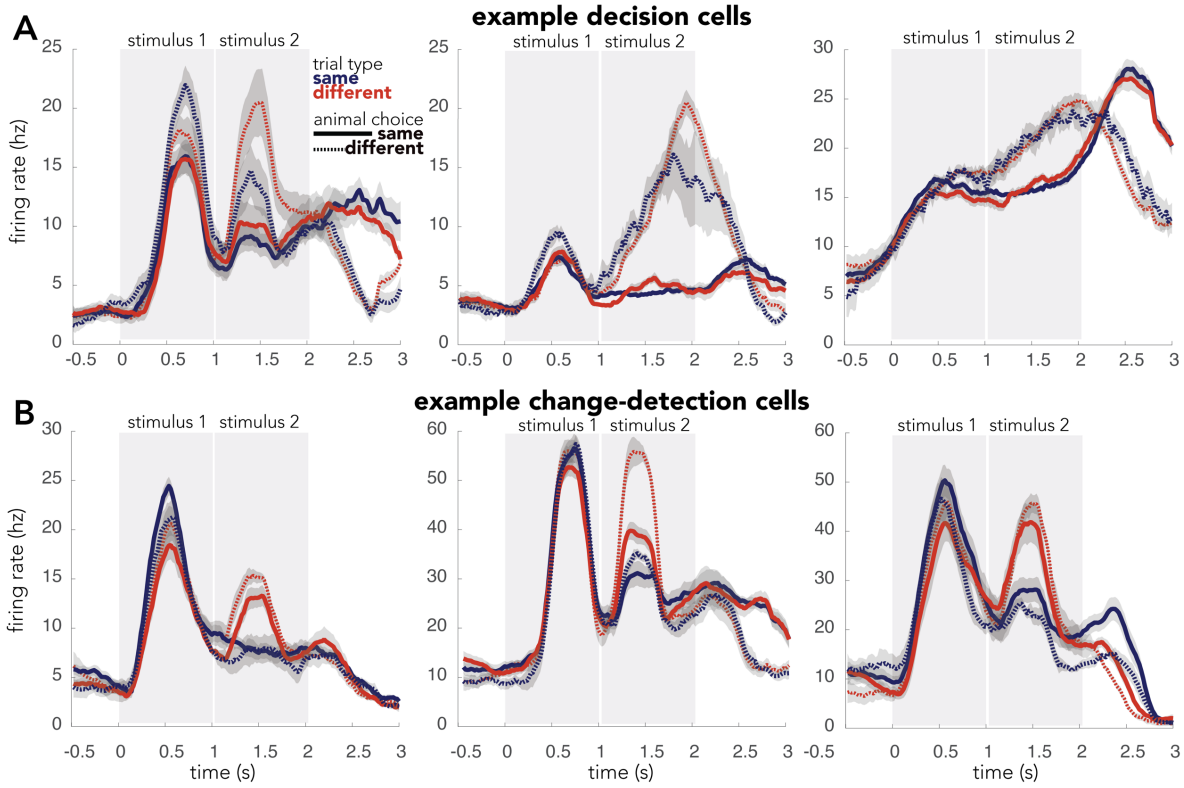

Figure 3.5: Examples of task-modulation in neural responses. Mean Peristimulus time histograms of the responses of six example S2/PV neurons, broken down by trial type. Time-varying firing rates are averaged across all repeats and stimuli within each trial type. Shaded regions denote the standard error of the mean across repeats and stimuli. Stimulus intervals are indicated as shaded regions. (A) Three example cells that are modulated by the animal's decision. For both same and different trial types, firing rates are higher during the second stimulus period of trials during which the animal chooses "different" (dashed lines). (B) Three example cells that respond transiently to a change in texture. This rise in firing rate occurs early in the second stimulus interval on "different" trials (red lines). In the middle panel, the cell's response rises on "different" trials, but the peak of this response is higher on trials for which the animal chooses "different".

Across the population, we found that 7.4% of cells (7/95) were significantly modulated by theanimal's decision and 45% of cells were modulated by the trial type shortly after a change occurred (early in the second stimulus period, Figure 3.6A). It is worth noting that trial-type cells were found in both animals, whereas all of the decision cells were found in Monkey M, who

performed reliably better on the task than did Monkey S. Overall, neurons exhibited heterogenous category-dependent modulation, with some cells responding mores strongly to different textures, and other more strongly to same ones.

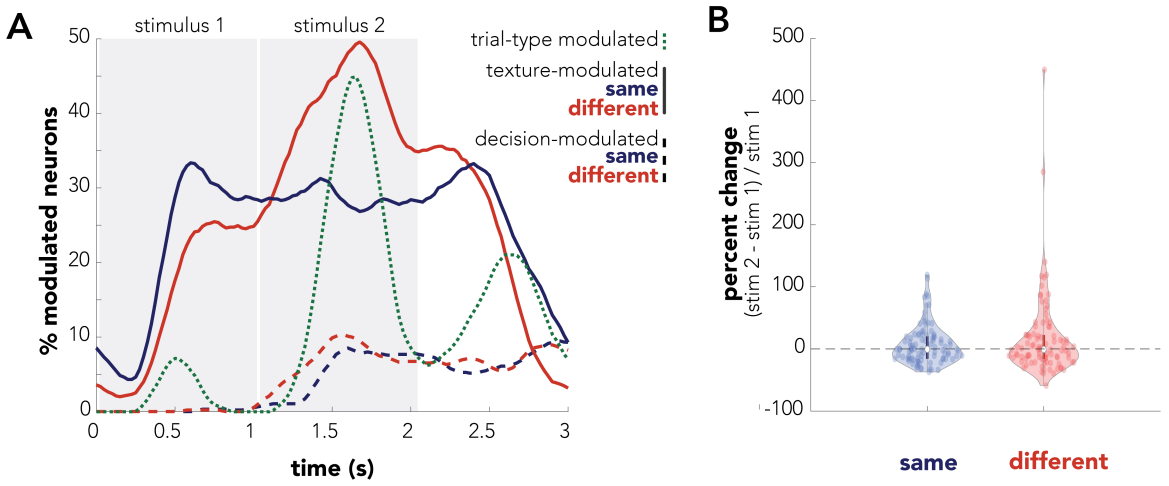

Figure 3.6: Neurons in S2/PV are modulated both by texture and the animal's choice. (A) Percent of neurons modulated by texture, trial type, or decision across time throughout same (blue) and different (red) trials. For any given timepoint (calculated every 10 ms), the fraction of modulated neurons is determined based on mean firing rate across the previous 400 ms. Texture modulated neurons respond differently to the 45 textures in our stimulus set. Decision modulated neurons respond differently between trials on which the animal reports same vs different. Trial-type modulated neurons (green dashed line) respond differently on same vs different trials. (B) Violin plots showing percent change in texture response from the first stimulus interval to the second on same (blue) and different (red) trials. Each point denotes an individual cell's average change across all textures.

3.2.6 | DECISION- AND TASK-RELATED SIGNALS IN S2/PV

Having observed that S2/PV responses seem to be modulated by trial type and the animal's decision, we attempted to decode task variables – texture, trial type, and decision – we could decode from neural responses across time. To this end, we applied LDA to the population response within a 400-ms time window slid across an epoch that spanned 800 ms before the first

texture until after the animal reported his decision in 10-ms intervals. We found that we were able to reliably classify texture across both stimulus intervals (Figure 3.7A). We were also able to classify trial type (same vs different), in particular during the second stimulus period (Figure 3.7B). Trial type-classification unexpectedly rose above chance levels during the first stimulus period, possibly because the specific swath of each texture differed depending on whether it occurred in the first or second interval. Finally, we were able to classify the animal's decisions with high accuracy (77%) from responses across all stimulus pairs and trial types. Decision-related signals

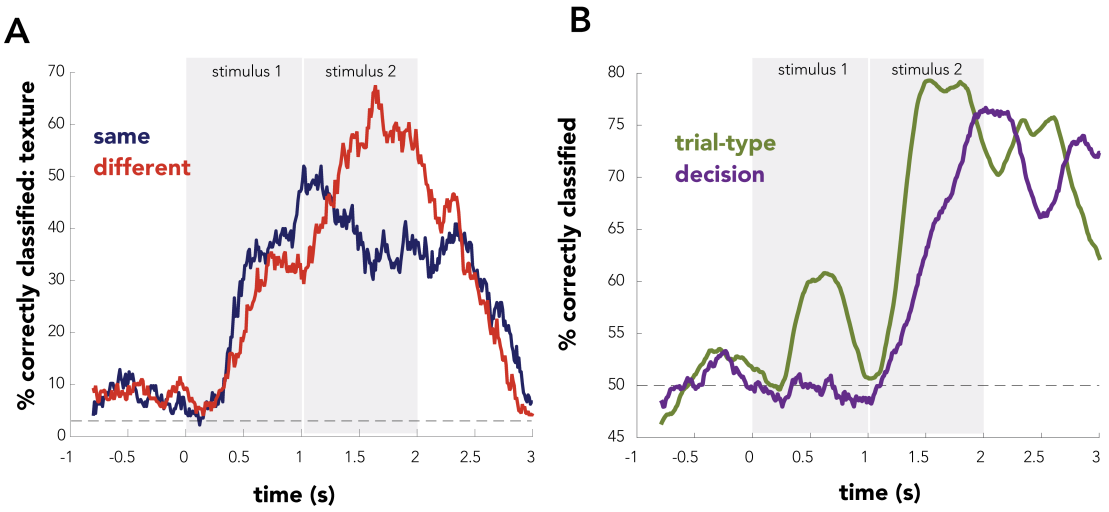

Figure 3.7: Classification of texture, trial type, and animal's decision. (A) LDA population classification of 45 textures (chance = 2.2%). At each timepoint, the LDA classifier is trained on the mean firing rate responses of all 95 cells in S2/PV over the previous 400 ms. (B) LDA population classification of trial-type (same vs different trial, green line, chance = 50%) and decision (animal choice of same or different, purple line, chance = 50%). For the trial-type classifier, all 95 cells were included as features in the model. For the decision classifier, only decision-modulated cells were included (n=7 cells).

emerged after trial-type-related signals In S2/PV, as might be expected if the latter drive the former (Figure 3.7B).

Having identified populations of neurons that carried information about various task variables, we then assessed the degree to which these signals about different variables were carried by different neuronal populations. To this end, we assessed the ability of different subpopulation of neurons, split based on their preference for one task variable, to carry information about other task variables. We found that texture-modulated neurons still carried decision-related signals, though weaker than those carried by neurons identified as being decision-related (Supplemental Figure S.3.6). Similarly, neurons identified as decision-related carried information about texture, though far weaker than their texture-modulated counterparts. between different textures.

3.3 | Discussion

3.3.1 | Sparse and heterogeneous representations of texture

By presenting a wide range of stimuli, we observe, for the first time, sparse activation of S2/PV cells in response to texture. In SC, cells are easily driven by texture, with most cells responding to most textures. In contrast, S2/PV cells are highly selective, with most cells responding to fewer than 20% of textures. This latter observation is consistent with anecdotal finding that a subset of S2 neurons responded only to metal bars on the stimulator but not to the textured stimuli, in this case square-wave gratings (Sinclair & Burton, 1993). The present study is the first to examine S2/PV responses to a wide range of naturalistic stimuli and thus to be able to observe sparse coding in higher order somatosensory cortex. This progression is consistent with observations in other sensory pathways, where dense coding of low-level features in early stages of processing gives way to sparse activation and increased selectivity in higher order cortical fields (Chalk et al., 2018; Okazawa et al., 2017).

3.3.2 | HIGH VARIABILITY IN RESPONSES

Individual cells in S2/PV are less informative about the full texture set than are cells in SC, as evidenced by lower texture classification performance from S2/PV responses than SC responses. This difference is driven by at least two factors. The first is that S2/PV representations of texture are sparser than are their SC counterparts: To the extent that individual neurons only respond to a small fraction of textures, a small sample of such neurons will fail to tile the space and lead to a failure to classify textures that are poorly encoded by any one neuron. Second, the variability of S2/PV responses to repeated presentations of a given texture is double that of its counterpart in SC, which will result in reduced classification performance. This increased variability can be attributed, at least in part, to the fact that S2/PV neurons are also modulated by attention. Indeed, responses to tactile stimuli are significantly attenuated in S2/PV when the stimuli are behaviorally irrelevant, much more so than in SC (Burton et al., 1997; Chapman & Meftah, 2005; Meftah et al., 2002; Rossi-Pool et al., 2021).

Given that the animals struggled to perform the same-different task, we do not have a reliable read-out of the animal's engagement in the task.

3.3.3 | POPULATION REPRESENTATION OF TEXTURE

Cells in SC carry a large shared signal – which accounts for two thirds of the variance in the population response and is highly predictive of perceived texture. However, the responses of individual SC cells comprise an idiosyncratic component such that their population response is also high-dimensional (Lieber & Bensmaia, 2019). That is, attempts to project the population response onto a reduced space reduces its informativeness about texture. S2/PV cells also

respond idiosyncratically to texture but also much more sparsely. As a result, the representation of S2/PV does not comprise a large shared signal, and the overall dimensionality of the signal is even higher than that in SC. Furthermore, in both peripheral nerve and SC, the shared signal is highly predictive of perceived roughness, (Lieber & Bensmaia, 2019; Weber et al., 2013) whereas no such relationship exists in S2/PV. This transition from sensitivity to low-level stimulus features to higher-order ones is observed across sensory modalities (Groen et al., 2017; Rauschecker, 1998; Yamins & DiCarlo, 2016) .

3.3.4 | TASK MODULATION

Across behavioral conditions, a subpopulation of S2/PV neurons has been shown to be modulated by task-relevant variables. In a texture change-detection task, the responses of most neurons indicated the presence, but not magnitude, of a change in texture (Jiang et al., 1997). In an active texture exploration task, many neurons were responsive to a small metal bar that demarcated the beginning, middle, and end of the texture (Sinclair & Burton, 1993). In a vibratory frequency discrimination task, a subset of neurons encoded the difference in frequency of two, sequentially-presented vibratory stimuli, a precursor to the eventual decision (Romo et al., 2002). In a vibratory same-different task, a subset of neurons encoded the trial-type (same, different), as we found here (Rossi-Pool et al., 2021).

In the present study, we found that information about the key task variables – trial type and the monkey's decision – were encoded in S2/PV. However, decision- and task-related signals were multiplexed with texture-related ones, such that information about all these task variables could be decoded from the population response. These different signals were not segregated across

different populations of neurons, as evidenced by the fact that texture could be classified above chance based on the responses of neurons identified as being decision-modulated and decision could be classified from the responses of neurons identified as texture-modulated.

3.4 | Conclusions

S2/PV carries a sparse representation of texture in which signals about low-level stimulus features such as roughness have been strongly attenuated. Sensory signals are multiplexed with signals about task variables, including trial type and the animals' decision. While the cognitive signals found in S2/PV are consistent with those found in previous studies, the selectivity and sparseness of the neuronal response has not been previously characterized as doing so requires monitoring neuronal response to a complex stimulus set, as was done here for the first time.

3.5 | Methods

3.5.1 | Animals

All experimental procedures involving animals were approved by the University of Chicago Institutional Animal Care and Use Committee. Behavioral and neurophysiological data were obtained from two rhesus macaques (males, 10-14 years old, 8-10 kg). Both animals were instrumented with a custom head-post to allow for head immobilization for eye-tracking and stable neurophysiological recordings. After two years of head-fixed training on a behavioral task (described below), animals were instrumented with a 22-mm diameter recording chamber (Crist Instrument Co., Hagerstown, MD) positioned over the upper bank of the lateral sulcus (Figure 3.1C). In both animals, chambers were centered 8-10 mm anterior to ear bar zero, as far lateral as possible, and positioned straight up and down using a steep chamber angle (30-45°) to keep

the edge of the chamber flush with the skull. Coordinates were determined using a stereotaxic instrument (David Kopf Instruments, Tujunga, CA). In one hemisphere of one monkey, a flat 0° chamber was placed flush with the skull, such that it was positioned at a ~40° angle centered over the lateral sulcus. The chamber was placed at this modified angle to accommodate the placement of a 96-channel Utah array (Blackrock Microsystems, Salt Lake City, UT) over the hand representation in Area 1.

3.5.2 | NEUROPHYSIOLOGY

Each day, extracellular responses were obtained using one or two 16-channel linear arrays (V-probes, Plexon Inc, Dallas, TX). Electrodes were moved using a computer-controlled microdrive (NAN Instruments, Nazaret Illit, Isreal) and responses were recorded through a Cereplex Direct and Central software (Blackrock Microsystems, Salt Lake City, UT). Spike sorting was performed manually using Offline Sorter (Plexon Inc, Dallas, TX) in order to identify well-isolated single units that were stable across the recording session.

3.5.3 | BEHAVIORAL TASK

Animals were trained to perform a 2-alternative forced-choice task in which they reported whether two sequentially presented textures were the same of different. Two texture stimuli were presented sequentially, each for 1s, with no interstimulus interval separating them. This design was chosen because a delay period between the stimuli increased the task demands beyond our animals' capabilities. 45 unique textures were presented in 90 pairs for 5 repeats across four experimental blocks. During the first block, 40/90 texture pairs were presented three times each in pseudo-random order. During the second block, the remaining 50/90 texture pairs were

presented three times each in pseudo-random order. The third and fourth blocks followed the same design but contained only two repeats of each stimulus pair.

3.5.4 | SC NEURAL RESPONSES

All SC data were collected from awake macaques that were performing a visual contrast-discrimination task. All stimuli were presented as described below. However, unlike in the present study, only one stimulus was presented in each trial, with at least 3 seconds between trials. Further details on these methods can be found in previous reports on these data (Lieber & Bensmaia, 2019, 2020; Long et al., 2021) .

3.5.5 | TEXTURE STIMULI

Texture were scanned across the fingertip at 80 mm/s and 25 g of force. Textures were presented using a custom stimulator that included a rotation motor (SmartMotor SM23165D; Animatics) connected to a 1:100 gearbox (Animatics), which provided precise control of rotational position (±200 μm) and velocity (±1.1 mm/s). A vertical stage (IMS100V; Newport) controlled the depth of indentation into the skin with a precision of 2 μm. This rotating drum was also connected to a horizontal stage (IMS400CCHA; Newport), allowing for horizontal displacements over a range of 40 cm (±4 μm). With this rig, we maintained precise horizontal, vertical, and rotational positioning of textures. We presented 44 unique textures, including fabrics, furs, papers, and 3 3D-printed stimuli. We also included a 45th stimulus as a catch trial in which the drum moved like in any other trial, but no texture contacted the fingertip. 40 of these 44 textures were also used in our previous examination of texture coding in anterior parietal cortex, and only responses to these 40 textures were used for all comparisons of SC and S2/PV.

3.5.6 | TRIAL STRUCTURE

Same and different trials both followed the same general structure: 1s presentation of an 8 cm strip of texture followed immediately by a second 1 s presentation of a second 8 cm strip of texture (either the same texture or a different one). Same trials began at the start of a given texture strip, such that the full 16cm were scanned across the finger over a 2s period. A thin strip of tape (3 mm wide) placed at the beginning and halfway through each texture (8 cm) demarcated the start of each stimulus period. On different trials, the stimulus pair began at this halfway point on the first texture and moved halfway through the subsequent texture on the drum. The drum never lifted off the fingertip during the trials, and there was no gap between textures. This allowed for easier task demands, as there was no working-memory component to the task. However, it also constrained our stimulus set such that any given texture was, by necessity, always followed by one specific texture rather than a variety of possible comparisons. Following the 2 s trial, the animal saccaded toward a right or left target to indicate whether the two textures were the same or different, respectively.

3.5.7 | HUMAN PSYCHOPHYSICAL DATA

We leveraged a dataset on the perceived roughness of the 40 textures in our shared SC-S2/PV stimulus set. We have already published reports using these data (Lieber & Bensmaia, 2019, 2020). Briefly, we asked six human subjects (5 males, 1 female, ages 18-24) to freely rate the perceived roughness of textures presented in the same manner as described here (80 mm/s, 25 g). All textures were presented six times to each subject and ratings were normalized across experimental blocks and across subjects.

3.5.8 | DATA ANALYSIS

Firing rates: Baseline firing rates were calculated as the mean firing rate rate (spikes / s) over a 400 ms window prior to the texture contacting the skin. Texture-evoked firing rates were calculated over a 400 ms window following the texture-evoked transient during each stimulus interval.

Peri-stimulus time histograms (PSTH): PSTHs were computed by binning spikes in 20 ms bins and calculating a moving average firing rate across 20 sequential bins (400 ms total window slid in 20ms increments).

Permutation test: For a given cell, we first created a distribution of baseline firing rates from the baseline response on each trial (45 textures x 5 repeats). Then, for a given texture, we calculated whether the mean texture response was greater than the mean firing rate in a random draw of 5 baseline responses. We repeated this for 300 iterations and calculated how frequently the texture response was greater than the sampled baseline response. We set a significance threshold at $p<.05$, and we corrected for multiple comparisons by dividing this value by 4,275 (95 cells x 45 stimuli). We also performed this analysis using a shared set of 40 textures with SC and S2/PV responses, and the multiple comparisons correction was then set at 3800 comparisons in S2/PV (95 cells x 40 stimuli) and 5640 comparisons in SC (141 cells x 40 stimuli).

Selection of 'texture' cells: We identified those cells that were modulated by texture by performing a 1-way analysis of variance (ANOVA) of texture-evoked firing rates to 45 textures across repeats. Significance thresholds ($p < 0.05$) were Bonferroni corrected for multiple comparisons (95 cells x 45 stimuli).

Selection of 'decision' cells: Similar to above, we identified decision-modulated cells by performing a 1-way ANOVA on firing rates during the final 400 ms of the second stimulus periods on trials during which the monkey indicated "same" vs those in which he indicated "different". Significance thresholds ($p < 0.05$) were Bonferroni corrected for multiple comparisons (95 cells x 2 decisions).

Sliding window ANOVA: We performed the same analysis described above (1-way ANOVA with significance thresholds corrected for multiple comparisons) for firing rates calculated across 400 ms windows. We performed this analysis every 25 ms to identify the time-varying proportion of neurons that respond to texture, trial type, and the animal's decision.

Sparseness Index: The sparseness index (I_{SP}) is a measure of uniformity of responses to a variety of stimuli. First, we calculate the mean firing rate of a given cell to each texture (across 5 repeats). We then calculate the cell's I_{SP} as the squared average of responses divided by the average of squared responses:

$$I_{SP} = [\Sigma_{t=1,n}\left(\frac{\mu_t}{n}\right)]^2 \,/\, [\Sigma_{t=1,n}(\frac{{\mu_t}^2}{n})],$$

where n = 40 or 45 textures and μ_t = the mean response to texture t.

Selectivity Index: The selectivity index (I_{SE}) is a measure of the range between a neuron's response to its most and least preferred stimuli. We first calculate the mean firing rate of a given cell to each texture (across 5 repeats). We then take the difference between the cell's maximum and minimum texture-evoked response and divide the difference by a sum of the cell's maximum and minimum responses:

$$I_{SE} = \mu_{t\,max} - \mu_{t\,min} / \mu_{t\,max} + \mu_{t\,min},$$

where $\mu_{t\,max}$ = a cell's maximum mean texture-evoked response and $\mu_{t\,min}$ = a cell's minimum mean texture-evoked response.

Principal components analysis: We performed a principal components analysis of population texture response with each neuron as a feature and each texture as an observation (40 textures, 95 S2/PV cells) using the Matlab pca() function. We also performed a principal components analysis on a subset of 27 S2/PV 'texture' cells' responses as well as for 141 SC cells' responses. Briefly, we first calculated each cell's mean response across repetitions to each texture presented during the final 400 ms of the first stimulus period. We then computed the principal component eigenvalues and each texture's principal component scores. To compare these principal component projections to roughness ratings, we performed a simple linear regression of mean roughness ratings onto principal component scores and determined the correlation coefficient (r) and squared this value to find the coefficient of determination (R^2).

Rate classification: We set out to classify textures from each single cell's response to all 45 stimuli. In brief, we performed a cross-validated nearest-neighbor classifier on Euclidian distances between texture-evoked firing rates. We first calculated the cell's mean response to each texture across 4/5 repeats. We then computed the Euclidian distance between a test repeat to one texture and every response in the training vector. We repeated this for every texture and every repeat, and we calculated classification performance as the percentage of time the smallest distance in the vector was that of the same texture that was presented during the test repeat.

Population LDA classification: In order to assess population responses to texture, we implemented linear discriminant analysis to classify texture using Matlab's fitcdiscr() function. We

performed LDA classification for increasing population sizes by randomly sampling without replacement from our full or texture-modulated cells. We trained our LDA model on individual responses in 4/5 repeats and we tested the model's accuracy on a fifth, left-out repeat. For each population size, we performed 10 iterations in order to find a mean classification performance across different samples of cells.

LDA improvement: To test how often a given cell would increase classification performance in a small population of cells, we randomly sampled 4 cells without replacement from our population, excluding the cell of interest. We calculated classification performance using these 4 cells, and we repeated the process with the same cells and the cell of interest. We repeated this process 100 times, sampling randomly from the population, to identify the fraction of samples in which the added cell improved classification.

Sliding window classification: In addition to training/testing LDA classifiers on stead-state texture responses during the final 400 ms of the first stimulus period, we tested the extent to which the neural response throughout the trial period was informative about texture, trial type, and the animal's decision. To do this, we trained and tested LDA classifiers (as described above) on the firing rate over a 400 ms window in 10 ms increments from 800 ms before the stimulus touched the fingertip until 1 s after the second stimulus ended. To classify texture, class labels were unique to each stimulus, and we split the analysis between same trials and different trials to exclude the effect of differences between the physical swath of texture. For classification of trial type, class labels were applied based on whether the trial was a "same" trial or a "different" trial and included observations from all textures across all repeats. For classification of the animal's

decision, class labels were applied based on the animal's ultimate decision at the end of the trial. In this case, the model was trained on 80% of the trials and tested on 20%, rather than splitting the data by repeats. In order to keep chance performance at 50%, an equal number of "same" and "different" choice observations were used to train the model and to test the model.

Basic statistics: For a variety of analyses, two-sample, unpaired, 1-tailed t-tests were used to assess differences between SC and S2/PV responses. Significance thresholds of $p<0.05$ were always Bonferroni corrected for multiple comparisons.

3.6 | APPENDIX: CHAPTER THREE SUPPLEMENTAL FIGURES

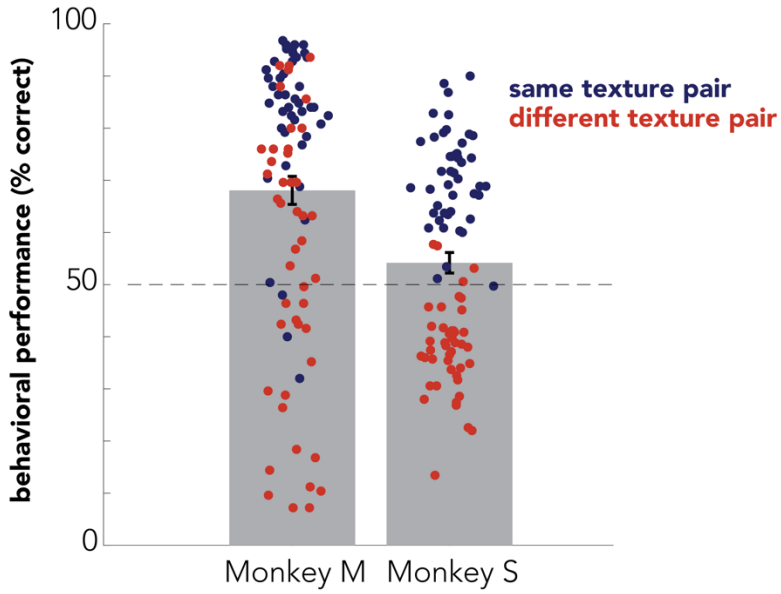

Supplemental Figure S.3.1: Average behavioral performance of each animal. Average performance on this task differed between animals (Monkey M: 68%, Monkey S: 54%). Performance also differed for stimulus pairs, but both monkeys were rarely incorrect on "same" trials (blue). Each point denotes one texture pair. Texture pairs were the same for both monkeys. Task performance was averaged all sessions during which neural responses were recorded.

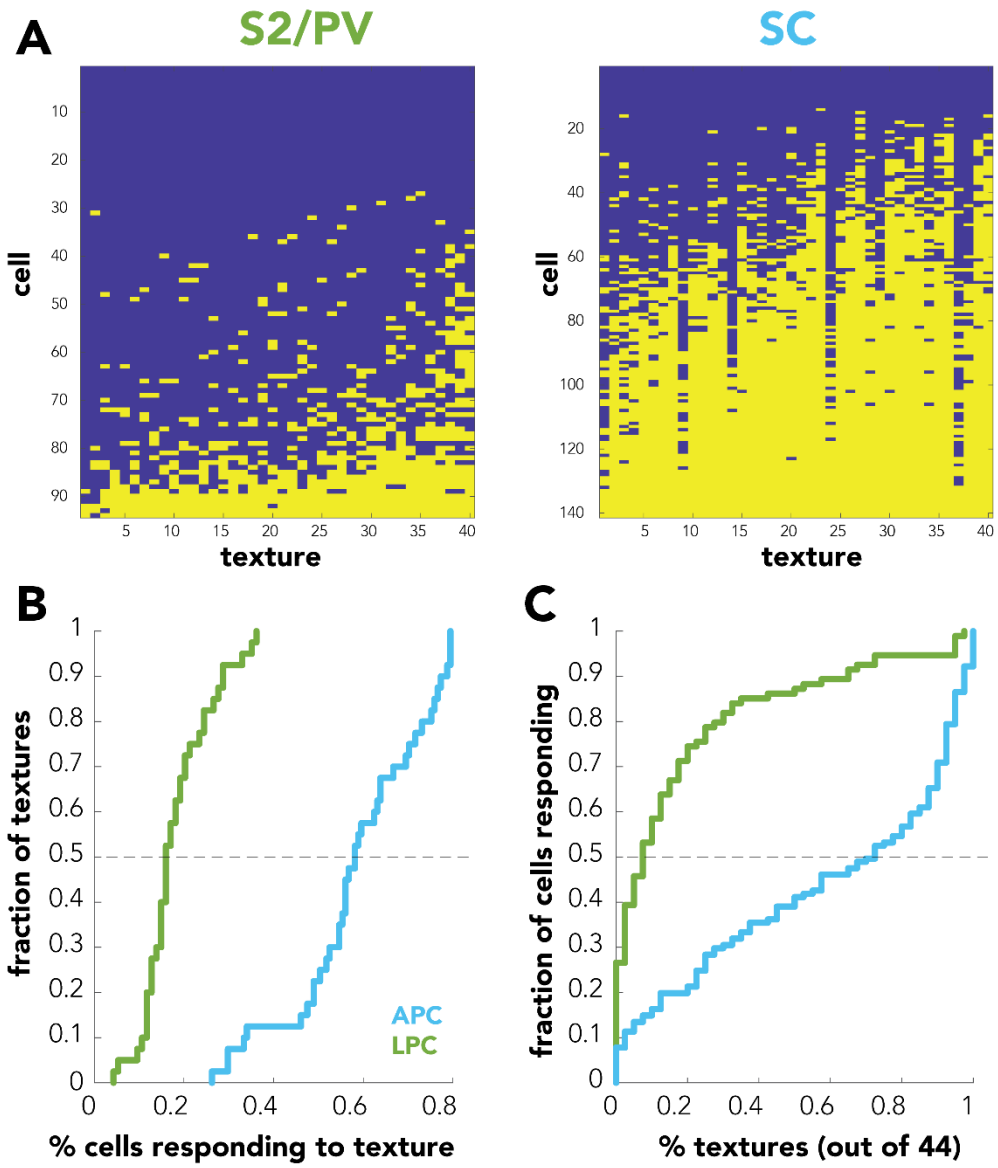

Supplemental Figure S.3.2: Texture responsiveness across individual cortical cells in S2/PV and SC. (A) Heatmap showing textures (n = 40) for each cell that evoke a significant above-baseline response (permutation test). Yellow squares denote above-baseline responses. Textures are sorted by the proportion of cells responding in S2/PV (increasing from left to right). (B)

Cumulative distributions of textures the evoke a response in increasing proportions of cells. (C) Cumulative distributions of SC an S2/PV cells responding to increasing proportions of texture.

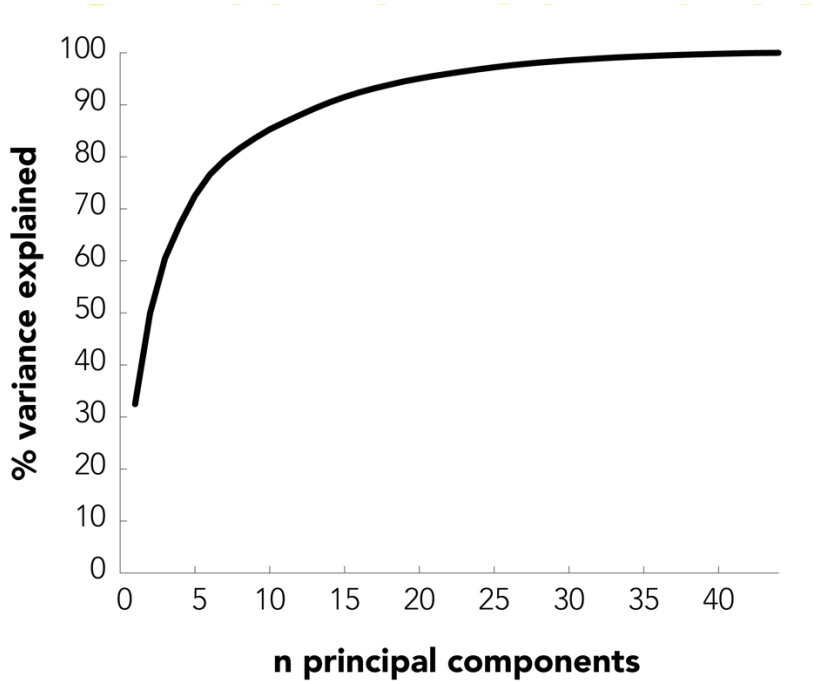

Supplemental Figure S.3.3: Cumulative scree plot of prinicipal components of the population S2/PV texture response. Variance explained by each principal component determined by a PCA of the full S2/PV texture response of 95 features (neurons) to 44 observations (textures).

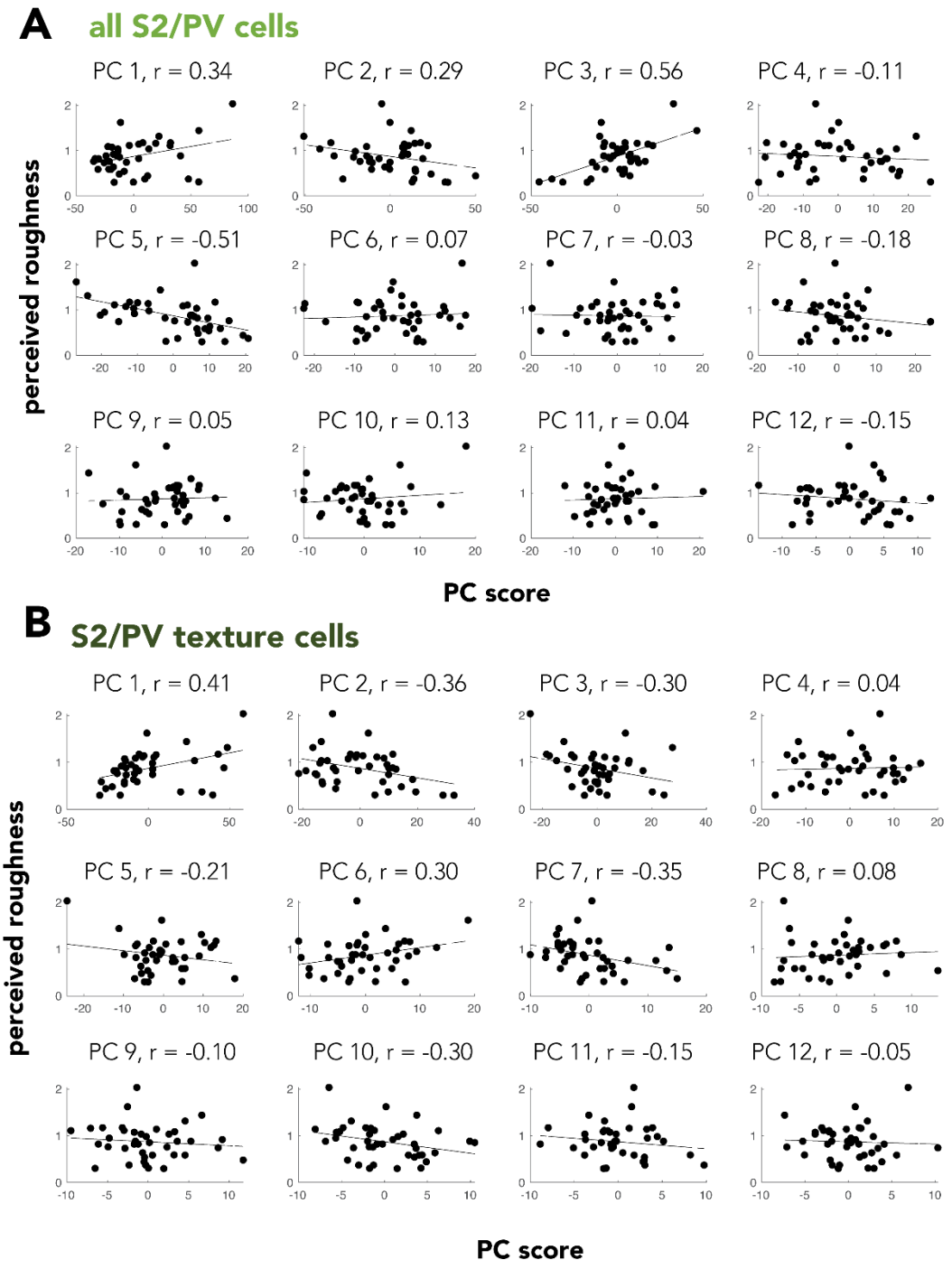

Supplemental Figure S.3.4: S2/PV responses are not correlated with perceived roughness of texture. We regressed perceived roughness onto principal component scores for each texture

(each point). Titles of each subplot list the correlation coefficient of the best linear fit of roughness and a given principal component's texture scores. Principal components (PC) were determined from the responses of (A) all 95 S2/PV cells and (B) 27 texture-modulated S2/PV cells.

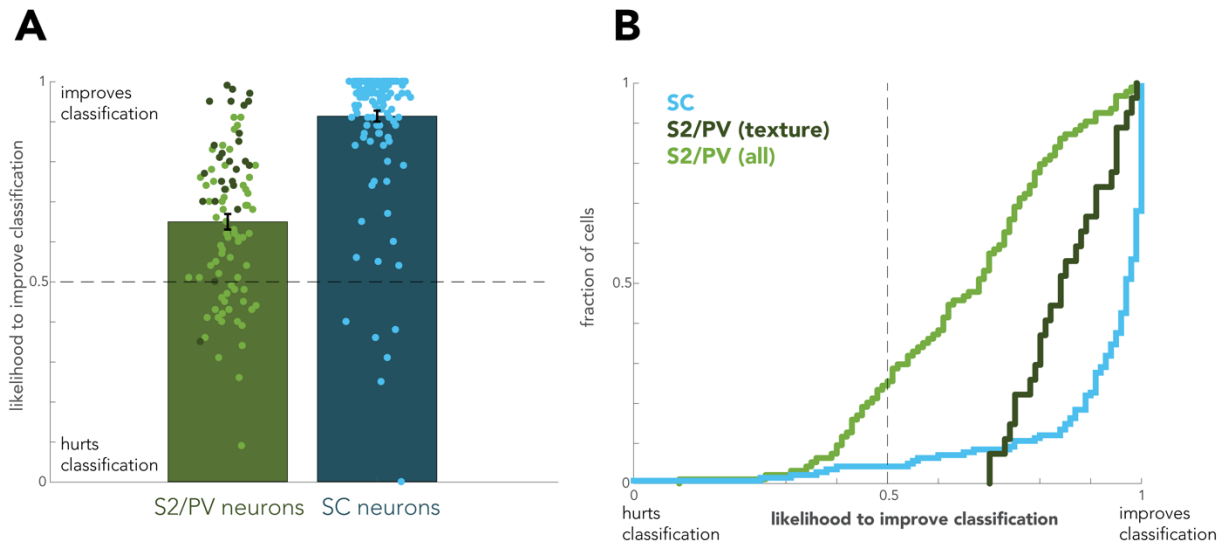

Supplemental Figure S.3.5: Contributions of single cells in population classification. (A) We performed LDA classification of texture in small populations of 4 randomly sampled cells from either S2/PV or SC. We then calculated the fraction of 100 independent sampled populations for which classification improved when the cell of interest (denoted as individual circles) was added to create a population of 5 cells. Likelihoods above 0.5 increase are more likely to improve classification performance than hurt it. (B) Cumulative distributions of SC, S2/PV, and S2/PV texture cells to improve classification performance.

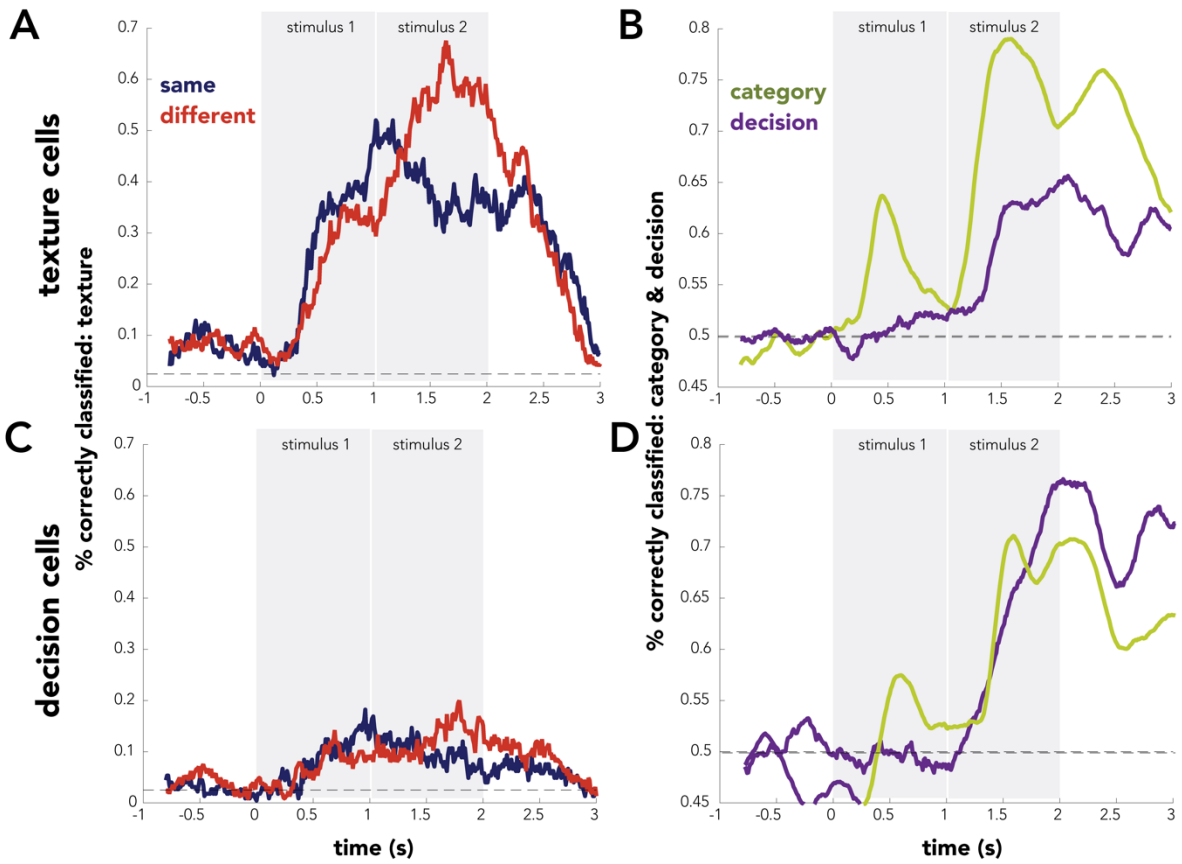

Supplemental Figure S.3.6: Classification of texture, trial type, and decision among texture-modulated and decision-modulated subpopulations of cells. (A,C) LDA population classification of 45 textures (chance = 2.2%). At each timepoint, the LDA classifier is trained on the mean firing rate responses of all either 27 texture-modulated cells (A) or 7 decision-modulated cells (C) in S2/PV over the previous 400 ms. (B,D) LDA population classification of trial type (same vs different trial, green line, chance = 50%) and decision (animal choice of same or different, purple line, chance = 50%). For each LDA model, either 27 texture-modulated cells (B) or 7 decision-modulated cells (D) were included as features in the model.

3.7 | REFERENCES

Arcizet, F., Jouffrais, C., & Girard, P. (2008). Natural textures classification in area V4 of the macaque monkey. *Experimental Brain Research*, *189*(1), 109–120. https://doi.org/10.1007/s00221-008-1406-9

Blake, D. T., Hsiao, S. S., & Johnson, K. O. (1997). Neural Coding Mechanisms in Tactile Pattern Recognition: The Relative Contributions of Slowly and Rapidly Adapting Mechanoreceptors to Perceived Roughness. *Journal of Neuroscience*, *17*(19), 7480–7489. https://doi.org/10.1523/JNEUROSCI.17-19-07480.1997

Burton, H., Sinclair, R. J., Hong, S.-Y., K.C. J.R. PRuett, J., & Whang. (1997). Tactile-spatial and cross-modal attention effects in the second somatosensory and 7b cortical areas of rhesus monkeys. *Somatosensory & Motor Research*, *14*(4), 237–267. https://doi.org/10.1080/08990229770971

Chalk, M., Marre, O., & Tkačik, G. (2018). Toward a unified theory of efficient, predictive, and sparse coding. *Proceedings of the National Academy of Sciences*, *115*(1), 186–191. https://doi.org/10.1073/pnas.1711114115

Chapman, C. E., & Meftah, E.-M. (2005). Independent controls of attentional influences in primary and secondary somatosensory cortex. *Journal of Neurophysiology*, *94*(6), 4094–4107. https://doi.org/10.1152/jn.00303.2005

Connor, C. E., & Johnson, K. O. (1992). Neural coding of tactile texture: Comparison of spatial and temporal mechanisms for roughness perception. *The Journal of Neuroscience: The Official Journal of the Society for Neuroscience*, *12*(9), 3414–3426.

Groen, I. I. A., Silson, E. H., & Baker, C. I. (2017). Contributions of low- and high-level properties to neural processing of visual scenes in the human brain. *Philosophical Transactions of the Royal Society B: Biological Sciences*, *372*(1714), 20160102. https://doi.org/10.1098/rstb.2016.0102

Hollins, M., Bensmaïa, S., Karlof, K., & Young, F. (2000). Individual differences in perceptual space for tactile textures: Evidence from multidimensional scaling. *Perception & Psychophysics*, *62*(8), 1534–1544. https://doi.org/10.3758/BF03212154

Jiang, W., Tremblay, F., & Chapman, C. E. (1997). Neuronal Encoding of Texture Changes in the Primary and the Secondary Somatosensory Cortical Areas of Monkeys During Passive Texture Discrimination. *Journal of Neurophysiology*, *77*(3), 1656–1662. https://doi.org/10.1152/jn.1997.77.3.1656

Krubitzer, L., Clarey, J., Tweedale, R., Elston, G., & Calford, M. (1995). A redefinition of somatosensory areas in the lateral sulcus of macaque monkeys. *The Journal of Neuroscience : The Official Journal of the Society for Neuroscience*, *15*, 3821–3839. https://doi.org/10.1523/JNEUROSCI.15-05-03821.1995

Lieber, J. D., & Bensmaia, S. J. (2019). High-dimensional representation of texture in somatosensory cortex of primates. *Proceedings of the National Academy of Sciences*, *116*(8), 3268–3277. https://doi.org/10.1073/pnas.1818501116

Lieber, J. D., & Bensmaia, S. J. (2020). Emergence of an Invariant Representation of Texture in Primate Somatosensory Cortex. *Cerebral Cortex*, *30*(5), 3228–3239. https://doi.org/10.1093/cercor/bhz305

Lieber, J. D., Xia, X., Weber, A. I., & Bensmaia, S. J. (2017). The neural code for tactile roughness in the somatosensory nerves. *Journal of Neurophysiology*, *118*(6), 3107–3117. https://doi.org/10.1152/jn.00374.2017

Long, K. H., Lieber, J. D., & Bensmaia, S. J. (2021). *Texture is encoded in precise temporal spiking patterns in primate somatosensory cortex* [Preprint]. Neuroscience. https://doi.org/10.1101/2021.04.11.439354

Meftah, E.-M., Shenasa, J., & Chapman, C. E. (2002). Effects of a Cross-Modal Manipulation of Attention on Somatosensory Cortical Neuronal Responses to Tactile Stimuli in the Monkey. *Journal of Neurophysiology*, *88*(6), 3133–3149. https://doi.org/10.1152/jn.00121.2002

Okazawa, G., Tajima, S., & Komatsu, H. (2017). Gradual Development of Visual Texture-Selective Properties Between Macaque Areas V2 and V4. *Cerebral Cortex*, *27*(10), 4867–4880. https://doi.org/10.1093/cercor/bhw282

Pruett, J. R., Sinclair, R. J., & Burton, H. (2000). Response Patterns in Second Somatosensory Cortex (SII) of Awake Monkeys to Passively Applied Tactile Gratings. *Journal of Neurophysiology*, *84*(2), 780–797. https://doi.org/10.1152/jn.2000.84.2.780

Rauschecker, J. P. (1998). Cortical processing of complex sounds. *Current Opinion in Neurobiology*, *8*(4), 516–521. https://doi.org/10.1016/S0959-4388(98)80040-8

Rolls, E. T., & Tovee, M. J. (1995). Sparseness of the neuronal representation of stimuli in the primate temporal visual cortex. *Journal of Neurophysiology*, *73*(2), 713–726. https://doi.org/10.1152/jn.1995.73.2.713

Romo, R., Hernández, A., Zainos, A., Lemus, L., & Brody, C. D. (2002). Neuronal correlates of decision-making in secondary somatosensory cortex. *Nature Neuroscience*, *5*(11), 1217–1225. https://doi.org/10.1038/nn950

Rossi-Pool, R., Zainos, A., Alvarez, M., Diaz-deLeon, G., & Romo, R. (2021). A continuum of invariant sensory and behavioral-context perceptual coding in secondary somatosensory cortex. *Nature Communications*, *12*(1), 2000. https://doi.org/10.1038/s41467-021-22321-x

Sinclair, R. J., & Burton, H. (1993). Neuronal activity in the second somatosensory cortex of monkeys (Macaca mulatta) during active touch of gratings. *Journal of Neurophysiology*, *70*(1), 331–350. https://doi.org/10.1152/jn.1993.70.1.331

Weber, A. I., Saal, H. P., Lieber, J. D., Cheng, J.-W., Manfredi, L. R., Dammann, J. F., & Bensmaia, S. J. (2013). Spatial and temporal codes mediate the tactile perception of natural textures. *Proceedings of the National Academy of Sciences*, *110*(42), 17107–17112. https://doi.org/10.1073/pnas.1305509110

Yamins, D. L. K., & DiCarlo, J. J. (2016). Using goal-driven deep learning models to understand sensory cortex. *Nature Neuroscience*, *19*(3), 356–365. https://doi.org/10.1038/nn.4244

Although this first examination of texture responses in LPC has been fruitful, we have only just begun to scratch the surface, and many questions remain.

First, one of the hallmark features of higher-order cortical areas is the development of robust, tolerant representations of stimuli. In the somatosensory system, our perceptual experience of texture does not vary with the speed at which we slide our hand across it, nor does it depend on the force we apply or which fingertip we use. However, responses in the peripheral nerve vary systematically across each of these parameters. In SC, invariance to speed begins to emerge, demonstrated by lower changes in firing rate across speeds. In S2/PV, we may expect to see even greater speed invariance emerge, as well as invariance to the location on the hand that a stimulus is presented. Receptive fields in SC are too small to give rise to this type of invariance, but in S2/PV, receptive fields often include multiple fingertips. One remaining question is how similar neural response responses are when textures are presented to different fingertips, both within the receptive field of an individual S2/PV cell?

Second, LPC responses contain informative signals about texture, trial-type, and the animal's decision. To what degree are they multiplexed in individual cells? To the extent that there is mixed selectivity in individual LPC cells, how do these representations develop as an animal learns a particular task? Are "decision" cells always "decision" cells, or are some LPC cells co-opted for particular tasks as an animal learns? This question requires methods that are beyond those we currently have at our disposal, as chronic recordings in the upper bank of the lateral sulcus have never been performed. So, instead, in our current (and growing) dataset, we will

apply a demixed principal components analysis to evaluate the time-varying components of the response that relate to the each of these factors (texture, category, decision). This may allow for further examination of the particular subspaces of the population response that encode texture features, allowing for better characterization of what aspects of texture, if not roughness, drive these responses. We can also assess these subspaces over time, as we record from each animal over the course of many months.

Third, we see preliminary evidence of enhanced responses to suedes, furs, and metal textures in S2/PV, relative to what we'd predict from SC responses. These particular textures are likely of special relevance to laboratory macaque. Higher-order visual areas show preferential responses to naturalistic stimuli – is this same phenomenon true in the somatosensory pathway?

Fourth, we have collected a small dataset of responses in anterior parietal cortex in one monkey performing the same-different task. SC responses are less modulated by task-structure and task-relevance of stimuli than are those in S2/PV, but in order to fairly compare texture responses in SC and S2/PV, we will assess SC responses during the same-different task used here.

And fifth, there is evidence of differences in response properties across anatomical locations of cells within S2/PV. There are no reliable mapping techniques to differentiate these areas from responses alone. Instead, we will perform histology on both hemispheres of one monkey to identify the location (S2 or PV) of electrode penetrations (marked with electrolytic lesions) based on cytoarchitectonic criteria and evaluate the degree to which texture representations differ across areas.

CHAPTER 5 | CONCLUSIONS

This body of work focused on two major gaps in our understanding of sensory coding in somatosensory cortex. First, we find that precise temporal patterning in a subpopulation of cells in SC is informative about texture, and a combination of rate and timing is best for prediction perceptual features of texture. And second, we find that cells in S2/PV convey information about texture, but this representation is sparser, higher-dimensional, and less driven by a shared response to low-level features. Altogether, these findings provide for a more holistic view of texture coding and how it evolves across various stages of cortical processing in the somatosensory neuraxis.